

# **Development and evaluation of a diverse dynamic global vegetation model based on plant functional tradeoffs**

Dissertation

zur Erlangung des Doktorgrades der Naturwissenschaften  
im Department Geowissenschaften der Universität Hamburg

vorgelegt von

**Ryan Pavlick**

aus Baltimore, Maryland

Hamburg, 2012

Als Dissertation angenommen vom Department Geowissenschaften  
der Universität Hamburg

auf Grund der Gutachten von Prof. Dr. Martin Claussen  
und Dr. Axel Kleidon

Hamburg, den 17 Apr 2011

Professor Dr. Jürgen Oßenbrügge  
Leiter des Departments für Geowissenschaften

# Abstract

Dynamic Global Vegetation Models (DGVMs) typically abstract the immense diversity of vegetation forms and functioning into a relatively small set of predefined semi-empirical Plant Functional Types (PFTs). There is growing evidence, however, from the field ecology community as well as from modelling studies that current PFT schemes may not adequately represent the observed variations in plant functional traits and their effect on ecosystem functioning. Also, these PFTs are defined *a priori* and their simulated distribution is often based on observed relationships between present-day climate and vegetation patterns. Climate model projections, however, point towards the possibility of regional climates without present-day analogs. This PhD study concerns the development, evaluation, and application of a novel global vegetation model, the Jena Diversity-DGVM, which seeks to overcome these deficits with a richer representation of functional diversity more closely based on first-principles.

JeDi-DGVM simulates the performance of a large number of randomly-generated plant growth strategies (PGSs), each defined by a set of 15 trait parameters which characterize various aspects of plant functioning including carbon allocation, ecophysiology and phenology. Each trait parameter is involved in one or more functional tradeoffs. These tradeoffs ultimately determine whether a PGS is able to survive under the climatic conditions in a given model grid cell and its performance relative to the other PGSs. The biogeochemical fluxes and land-surface properties of the individual PGSs are aggregated to the grid cell scale using a mass-based weighting scheme based on the ‘biomass-ratio hypothesis’.

Simulated global biogeochemical and biogeographical patterns are evaluated against a variety of field and satellite-based observations following a protocol established by the Carbon-Land Model Intercomparison Project. The land surface fluxes and vegetation structural properties are reasonably well simulated by JeDi-DGVM, and compare favorably with other state-of-the-art terrestrial biosphere models. This is despite the parameters describing the ecophysiological functioning and allometry of JeDi-DGVM plants evolving as a function of vegetation survival in a given climate, as opposed to typical approaches that assign land surface parameters for each PFT *a priori*.

## ABSTRACT

JeDi-DGVM simulations are run in two configurations to quantify how the representation of functional diversity influences the simulated magnitude and variability of water and carbon fluxes. In the first configuration, we simulate a diverse biosphere using a large number of plant growth strategies, allowing the modelled ecosystems to adapt through emergent changes in ecosystem composition. In the second configuration, we recreate a low diversity PFT-like representation of the terrestrial biosphere by aggregating the surviving growth strategies from the diverse simulation to a single community-weighted plant growth strategy per grid cell. In agreement with earlier biodiversity-ecosystem functioning studies, the diverse representation of terrestrial vegetation leads generally to higher productivity and water-use efficiency. The land surface fluxes in the diverse simulations show greater temporal stability and resilience to climatic perturbations. These results demonstrate a need for improving the representation of functional diversity in comprehensive Earth System models and add support for conserving biodiversity to maintain ecosystem services.

The JeDi-DGVM modelling approach developed in this thesis sets the foundation for future applications, in which the simulated vegetation response to global change has a greater ability to adapt through changes in ecosystem composition, having potentially wide-ranging implications for biosphere-atmosphere interactions under global change.

# Contents

<b>Abstract</b>	<b>i</b>
<b>1 Introduction</b>	<b>1</b>
1.1 Motivation . . . . .	1
1.2 Research objectives . . . . .	3
1.3 Thesis outline . . . . .	5
<b>2 The Jena Diversity-Dynamic Global Vegetation Model (JeDi-DGVM)</b>	<b>7</b>
2.1 Introduction . . . . .	7
2.2 Representation of Trade-offs . . . . .	10
2.3 Environmental selection . . . . .	11
2.4 Aggregation to ecosystem scale . . . . .	12
<b>3 Evaluating the broad-scale patterns of terrestrial biogeography and biogeochemistry</b>	<b>15</b>
3.1 Introduction . . . . .	15
3.2 Simulation setup . . . . .	15
3.3 Evaluation protocol . . . . .	16
3.4 Results and discussion . . . . .	22
3.4.1 Biodiversity patterns . . . . .	22
3.4.2 Phenology . . . . .	24
3.4.3 Global carbon stocks . . . . .	27
3.4.4 Gross Primary Productivity . . . . .	27
3.4.5 Net Primary Productivity . . . . .	33
3.4.6 Evapotranspiration . . . . .	34
3.4.7 Seasonal cycle of atmospheric CO <sub>2</sub> . . . . .	37
3.4.8 Net terrestrial carbon exchange . . . . .	39
3.4.9 Comparison with eddy covariance measurements . . . . .	41
3.4.10 Carbon stocks and flows in Amazonia . . . . .	42
3.4.11 Sensitivity to elevated atmospheric CO <sub>2</sub> . . . . .	43

## CONTENTS

3.5	Summary of model evaluation . . . . .	46
<b>4</b>	<b>Quantifying functional diversity-biospheric functioning relationships</b>	<b>49</b>
4.1	Introduction . . . . .	49
4.2	Methods . . . . .	53
4.2.1	Simulation setup . . . . .	53
4.2.2	Diversity measures . . . . .	56
4.3	Results . . . . .	59
4.3.1	Differences in mean productivity and evapotranspiration . . . . .	59
4.3.2	Differences in variability of productivity and evapotranspiration . . . . .	63
4.3.3	Differences in the resilience of the biosphere to climatic perturbation . . . . .	68
4.4	Discussion . . . . .	76
4.4.1	Diversity-Productivity . . . . .	76
4.4.2	Diversity-Variability . . . . .	77
4.4.3	Diversity-Resilience . . . . .	78
4.5	Summary of diversity-biospheric functioning relationships . . . . .	78
<b>5</b>	<b>Summary and outlook</b>	<b>81</b>
5.1	Summary . . . . .	81
5.2	Outlook . . . . .	82
5.2.1	Representation of tradeoffs . . . . .	82
5.2.2	Is everything everywhere? . . . . .	83
5.2.3	Aggregation scheme and competition . . . . .	84
5.2.4	Further evaluation . . . . .	85
5.2.5	Ongoing and potential applications . . . . .	86
<b>A</b>	<b>Jena Diversity-Dynamic Global Vegetation (JeDi-DGVM) Model Description</b>	<b>89</b>
A.1	Plant module overview . . . . .	89
A.2	Vegetation carbon pool dynamics . . . . .	91
A.3	Growing Conditions . . . . .	91
A.4	Germination . . . . .	93
A.5	Carbon allocation . . . . .	93
A.6	Turnover and Senescence . . . . .	94
A.7	Land Surface Parameters . . . . .	95
A.8	Net Primary Productivity . . . . .	97
A.9	Scaling from plant growth strategies to community-aggregated fluxes . . . . .	99
A.10	Soil Carbon . . . . .	100

<b>B Land Surface Module</b>	<b>103</b>
B.1 Water storage and runoff generation . . . . .	105
B.2 Potential evapotranspiration . . . . .	107
B.3 Actual evapotranspiration . . . . .	108
B.3.1 Sublimation from snow cover . . . . .	108
B.3.2 Evaporation from canopy interception reservoir . . . . .	108
B.3.3 Bare soil evaporation . . . . .	109
B.3.4 Transpiration . . . . .	109
B.4 Approximation of latent and sensible heat fluxes . . . . .	109
<b>C Model parameters and variables</b>	<b>111</b>
<b>Bibliography</b>	<b>119</b>
<b>Acknowledgments</b>	<b>141</b>



# Chapter 1

## Introduction

### 1.1 Motivation

Human activities are altering the terrestrial biosphere at a large scale and an alarming rate (Millennium Ecosystem Assessment 2005). The risks associated with these activities have led to the development of Dynamic Global Vegetation Models (DGVMs; e.g. Foley et al. 1996; Friend et al. 1997; Woodward et al. 1998; Cox 2001; Sitch et al. 2003). These mechanistic, process-based, numerical models simulate the large-scale dynamics of terrestrial ecosystems and have proven useful for testing hypotheses and making predictions regarding the responses of ecosystem structure and functioning to past and future environmental changes (see recent review by Quillet et al. 2010). DGVMs have also been embedded within comprehensive Earth System Models (ESMs) to capture biogeochemical (e.g. Cox et al. 2000) and biogeophysical (e.g. Foley et al. 2000) feedbacks between the terrestrial biosphere and the physical climate system. Intercomparison studies (Friedlingstein et al. 2006; Sitch et al. 2008), however, have revealed considerable divergence among the results of these models with respect to the fate of the terrestrial biosphere and its function as a driver of the global carbon cycle under projected scenarios of climate change. This divergence may be, at least in part, due to their coarse and differing treatment of plant functional diversity (Sitch et al. 2008; Harrison et al. 2010; Fisher et al. 2010b).

For reasons of computational efficiency as well as a lack of sufficient data and theory, global vegetation models typically represent the immense functional diversity of the over 300,000 documented plant species to a small number (typically between 4 and 20) of discrete Plant Functional Types (PFTs; Kattge et al. 2011) which are defined *a priori* before any simulations are run. In the context of DGVMs, PFTs represent broad biogeographical, morphological, and phenological aggregations (e.g. tropical broadleaf evergreen forest or boreal needleleaf deciduous forest) within which parameter values

are held spatially and temporally constant and responses to physical and biotic factors are assumed to be similar (Prentice et al. 2007). They have typically been classified subjectively using expert knowledge and their occurrence within a given model grid cell is based, either directly or indirectly, on semi-empirical bioclimatic limits, such as minimum or maximum annual temperature (e.g. Box 1996; Bonan et al. 2002; Sitch et al. 2003). Inductive approaches have also been proposed wherein PFTs are objectively classified by applying statistical techniques to large datasets of vegetation traits and climatic variables (e.g. Chapin et al. 1996; Wang and Price 2007). Regardless of approach, the PFT schemes used by current DGVMs have been criticized as *ad hoc* and as ignoring much of our growing knowledge of comparative plant ecology (Harrison et al. 2010).

In fact, the field ecology community has shown that for many plant traits there is a large amount of variation within PFTs, and that for several important traits, there is greater variation within PFTs than between PFTs (Wright et al. 2005; Reich et al. 2007; Kattge et al. 2011). This trait variation may play an important role for many ecosystem functions (Díaz and Cabido 2001; Westoby et al. 2002; Ackerly and Cornwell 2007) and for ecosystem resilience to environmental change (Díaz et al. 2006). Recent model-data assimilation studies using eddy covariance fluxes (Groenendijk et al. 2011) as well as other field and satellite-based observations (Alton 2011) provide confirmation that current PFT schemes are insufficient for representing the full variability of vegetation parameters necessary to accurately represent carbon cycle processes. A more theoretical study by Kleidon et al. (2007) demonstrated that using a small number of discrete vegetation classes in a coupled climate-vegetation model can lead to potentially unrealistic multiple steady-states when compared with a more continuous representation of vegetation. Others have contended that DGVMs may overestimate the negative effects of climate change by not accounting for potential shifts in ecosystem compositions towards species with traits more suited to the new conditions (Purves and Pacala 2008; Tilman et al. 2006). For example, some coupled climate-vegetation models (e.g. Cox et al. 2000) project an alarming dieback of the Amazon rainforest under plausible scenarios of continuing anthropogenic greenhouse gas emissions. The coarse representation of functional diversity in these models provided by current PFT schemes could be leading to an overestimation of the strength and abruptness of this response (Fisher et al. 2010b). Likewise, DGVMs might underestimate the positive effects of environmental changes on ecosystem performance, e.g. by ignoring warm-adapted species in typically temperature-limited regions (Loehle 1998). Therefore, while PFTs have been and will likely continue to be useful for many modelling applications, going forward we

will need new approaches that allow for a richer representation of functional diversity in DGVMs.

Many approaches have been proposed to meet the challenge of improving the representation of functional diversity in DGVMs (e.g. Wright et al. 2005; Reich et al. 2007; Kattge et al. 2009; Harrison et al. 2010). However, so far, most of these continue to rely on empirical relationships between observed plant traits and environmental (primarily climatic) factors. The utility of such correlational approaches for predicting the effects of global change on the terrestrial biosphere may be limited, as climate model projections point towards the possibility of novel climates without modern or paleo analogs (Jackson and Williams 2004; Williams and Jackson 2007). Other modellers have introduced schemes in which PFT parameters adapt to environmental conditions; e.g. with adaptive parameters related to leaf nitrogen (Zaehle and Friend 2010), allocation (Friedlingstein et al. 1999), and phenology (Scheiter and Higgins 2009). However, despite some interesting proposals (e.g. Falster et al. 2010; Van Bodegom et al. 2011), so far no DGVM has sought to mechanistically represent the full range of functional trait diversity within plant communities (i.e. at the sub-grid scale) using a trait-based tradeoff approach. Similar approaches have enabled significant progress in modelling the biogeographical and biogeochemical patterns of global marine ecosystems (Brugge-man and Kooijman 2007; Litchman et al. 2007; Follows et al. 2007; Dutkiewicz et al. 2009; Follows and Dutkiewicz 2011)

## 1.2 Research objectives

This thesis introduces a prototype for a new class of vegetation models that mechanistically resolves sub-grid scale trait variability using functional tradeoffs, the Jena Diversity DGVM (hereafter JeDi-DGVM). Just as the first generation of PFT-based DGVMs were built upon earlier PFT-based equilibrium biogeography models, JeDi-DGVM builds upon an equilibrium biogeography model (Kleidon and Mooney 2000, hereafter KM2000) based on the concept of functional tradeoffs and environmental filtering. JeDi-DGVM and KM2000 were inspired by the hypothesis ‘*Everything is everywhere, but the environment selects!*’ (Baas-Becking 1934; O’Malley 2007). This nearly century-old idea from marine microbiology postulates that all species (or in the case of JeDi-DGVM, combinations of trait parameter values) are, at least latently, present in all places, and that the relative abundances of those species are determined by the local environment based on selection pressures. Rather than simulating a hand-

ful PFTs, JeDi-DGVM simulates the performance of a large number of plant growth strategies, which are defined by a vector of 15 functional trait parameters. The trait parameter values determine plant behavior in terms of carbon allocation, ecophysiology, and phenology and are randomly selected from their complete theoretical or observed ranges. JeDi-DGVM is constructed such that each trait parameter is involved in one or more functional trade-offs (Bloom et al. 1985; Smith and Huston 1989; Hall et al. 1992; Westoby and Wright 2006). These tradeoffs ultimately determine which growth strategies are able to survive under the climatic conditions in a given grid cell as well as their relative biomasses.

KM2000 demonstrated that this bottom-up plant functional tradeoff approach is capable of reproducing the broad geographic distribution of plant species richness. More recently, their approach has provided mechanistic insight into other biogeographical phenomena including the global patterns of present-day biomes (Reu et al. 2010), community evenness and relative abundance distributions Kleidon et al. (2009), as well as possible mechanisms for biome shifts and biodiversity changes under scenarios of global warming (Reu et al. 2011). JeDi-DGVM extends the KM2000 modelling approach to a population-based model capable of representing the large-scale dynamics of terrestrial vegetation and associated biogeochemical fluxes by aggregating the fluxes from the many individual growth strategies following the ‘biomass-ratio’ hypothesis (Grime 1998).

The major objectives of this study are to:

- To introduce a novel approach to representing functional diversity in a dynamic global vegetation model, which is less coarse and less reliant on empirical bioclimatic relationships than previous PFT-based approaches.
- Evaluate if this modelling approach is able to capture the broad-scale present-day patterns of terrestrial biogeography and biogeochemical fluxes reasonably well and compare its performance with previous PFT-based models.
- Investigate how a vegetation model with more diverse representation of functional diversity behaves differently relative to a sparse PFT-like representation of diversity. Specifically, we ask:
  - Does a more diverse representation of the terrestrial biosphere lead to generally higher productivity and evapotranspiration? What modulates the geographic pattern of these relationship?
  - How does the representation of functional diversity influence the temporal

variability of these biogeochemical fluxes?

- Does a more diverse representation of the terrestrial biosphere lead to greater resilience of biospheric functioning to large climatic perturbations?

## 1.3 Thesis outline

The remainder of this thesis is structured as follows:

### Chapter 2

The second chapter introduces the novel aspects of the Jena Diversity-Dynamic Global Vegetation Model (JeDi-DGVM), including how functional diversity has been implemented via mechanistic trade-offs and how the resulting biogeochemical fluxes and land-surface properties associated with many plant growth strategies are aggregated to the ecosystem-scale.

### Chapter 3

In the third chapter, simulated patterns of terrestrial biogeography and biogeochemistry from JeDi-DGVM are evaluated against a variety of field and satellite-based observations. The model evaluation follows a systematic protocol established by the Carbon-Land Model Intercomparison Project (C-LAMP; Randerson et al. 2009). By following this protocol, it is possible to directly compare the bottom-up functional tradeoff approach of JeDi-DGVM with evaluation results for terrestrial biosphere models based on the dominant PFT paradigm.

### Chapter 4

In the fourth chapter, we use JeDi-DGVM to quantify how differing representations of functional diversity impact the simulated magnitude and variability of water and carbon fluxes.

### Chapter 5

The fifth chapter begins with a concluding summary of the main findings of this thesis. We then propose possible directions for further model development and model evaluation and we highlight a few ongoing and potential applications of JeDi-DGVM.

### Appendices

The appendices contain a detailed description of JeDi-DGVM and the coupled land-surface scheme.

## CHAPTER 1 INTRODUCTION

Parts of this thesis are published for <sup>1</sup> open discussion in *Biogeosciences Discussions*.

---

<sup>1</sup>Pavlick, R., Drewry, D. T., Bohn, K., Reu, B., and Kleidon, A.: The Jena Diversity-Dynamic Global Vegetation Model (JeDi-DGVM): a diverse approach to representing terrestrial biogeography and biogeochemistry based on plant functional trade-offs, *Biogeosciences Discuss.*, 9, 4627-4726, doi:10.5194/bgd-9-4627-2012, 2012

## Chapter 2

# The Jena Diversity-Dynamic Global Vegetation Model (JeDi-DGVM)

### 2.1 Introduction

JeDi-DGVM consists of a plant growth module that is coupled tightly to a land surface module. Both components contain parameterizations of ecophysiological and land surface processes that are common to many current global vegetation and land surface models. The main novelties in the vegetation component are (i) a mechanistic representation of functional trade-offs, which (ii) constrain a large number of plant growth strategies with trait parameter values randomly sampled from their complete theoretical/observed ranges, and (iii) the aggregation of the fluxes/properties associated with those growth strategies to grid-scale structure and function based on their relative abundances. . The following overview of the model focuses on describing the novel combination of these components and how they are implemented in the model, while the full description with the detailed parameterizations are described in the Appendices. A schematic diagram of the JeDi-DGVM modelling approach is shown in Fig. 2.1.

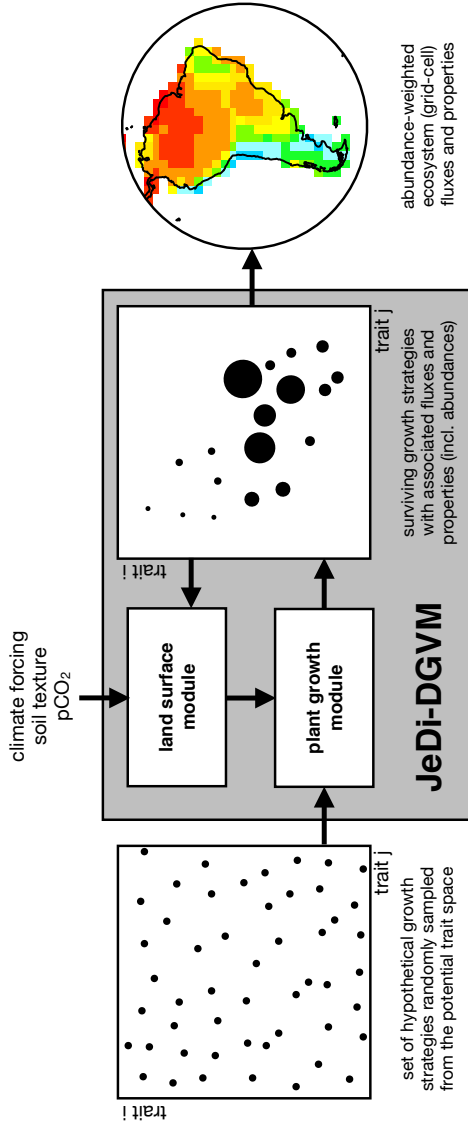


**Figure 2.1:** Schematic diagram of the JeDi-DGVM modelling approach. The model generates a large number of hypothetical plant growth strategies, each defined by 15 functional trait parameters that characterize plant behavior with regards to carbon allocation, phenology, and ecophysiology. The trait parameter values are randomly sampled from their full observed or theoretical ranges. The plant growth module simulates the development of the plant growth strategies (independently and in parallel) based on fundamental ecophysiological processes (e.g. photosynthesis, respiration, allocation, phenology, and turnover). The environmental conditions of each strategy are provided by the land surface module, which simulates canopy interception, infiltration, evaporation, root water uptake, and runoff using daily meteorological forcings of downwelling shortwave and longwave radiation, air temperature and precipitation. Land-surface parameters (e.g. leaf area index, surface albedo, and rooting depth) derived from the carbon pools and trait parameters of each plant growth strategy affect its simulated land-surface hydrology and, consequently, its net primary productivity (NPP), i.e. its supply of assimilates. Functional tradeoffs and the climatic conditions in each grid cell constrain the range and relative fitness of the surviving growth strategies (i.e. those that are able to maintain a positive balance of stored assimilates). The fluxes and properties of the surviving plant growth strategies are averaged, weighted by their relative biomasses, at each time step and grid cell to produce aggregated ecosystem-scale output variables. The aggregated litter fluxes form the input for an additional module (not shown) for simulating soil carbon dynamics and heterotrophic respiration.

## 2.2 Representation of Trade-offs

When we speak of terrestrial vegetation, we speak of a large number of plants of different species that differ to some extent in how they grow and respond to the environment. In fact, in a given environment there are potentially many different strategies by which individual plant species could grow and cope with the environment, with some ways being more beneficial to growth and reproductive success than other ways. Some plant species, for instance, grow and reproduce rapidly, such as grasses, while others, such as trees, grow slowly and it takes them a long time to reproduce. Some species allocate a greater proportion of their assimilates to leaves, thereby able to capture more of the incoming sunlight, while others allocate more to root growth and thereby being able to access more moisture within the soil. Some species react quickly to a change in environmental conditions, thereby potentially able to exploit more of the beneficial conditions for growth, while others are more conservative, thereby potentially avoiding damage by a turn to less favorable conditions.

To represent this flexibility of how to grow and reproduce in the model, many different plant growth strategies are simulated simultaneously using the same ecophysiological parameterizations under the same atmospheric forcing. The only part in which the plant growth strategies differ is in their values for fifteen functional trait parameters (Table C.2). These parameters control the amount of carbon from photosynthesis and storage allocated to six plant carbon pools (allocation), the response times to changes in environmental conditions and turnover times of the various carbon pools (phenology), and other aspects of ecophysiological functioning (e.g. leaf nitrogen concentration, which determines the balance between photosynthesis and respiration).

Each growth strategy is represented by six carbon pools representing leaves, fine roots, aboveground and belowground wood (stems and coarse roots), storage, and reproduction ('seeds'). These compartments are linked to the physical functioning of the land surface in terms of the absorption of solar radiation and soil moisture dynamics, which are simulated by the land surface module. For instance, leaf biomass is linked to the amount of absorbed solar radiation, and fine root biomass to the capability of a growth strategy to extract soil moisture from the rooting zone. Both of these examples have functional consequences: more absorbed radiation enhances the supply of energy for photosynthesis and evapotranspiration, and the amount of extracted soil water determines the water status of the plant and the supply of moisture for evapotranspiration. This coupled plant-land surface model is therefore capable of simulating the interaction between development of a plant growth strategy and land

surface functioning in a process-based manner.

Each trait parameter is associated with costs and benefits, leading to functional tradeoffs because no trait value (or set of trait values) can be optimal for plant fitness in all environments. For example, a particular growth strategy may allocate a relatively high fraction of carbon to fine roots, enhancing the rate at which it can extract moisture from the soil matrix. This may be beneficial in terms of higher productivity. However, it also comes with both real and potential costs. That growth strategy would incur the real metabolic costs of growth and maintenance respiration for the additional fine root biomass. A higher fractional allocation to fine roots also necessarily results in a lower fractional allocation to the other carbon pools (e.g. a lower allocation to the aboveground pools and thus a decreased ability to capture light). In a given environment, there will be some optimum allocation strategy that maximizes productivity. However, in environments with plentiful sunlight and soil moisture, a wide range of allocation strategies will perform close to the optimum. As the climate becomes harsher, the range of well-performing strategies will decrease.

## 2.3 Environmental selection

In order to implement the notion that ‘*everything is everywhere, but the environment selects*’, we test essentially the complete range of potential values for each of the 15 trait parameters. For some trait parameters, we sample values from the full mathematically possible range. For example, the trait parameters controlling the fractional allocation of carbon to the different plant carbon pools are only constrained such that together they sum to one. For other trait parameters (e.g. leaf nitrogen concentration), we sample values from observed ranges taken from literature. To effectively implement environmental selection, the model generates a large number of plant growth strategies using a quasi-random Latin Hypercube sampling algorithm (McKay et al. 1979). A 15-dimensional hypervolume representing the potential trait space is first divided into many equal subvolumes. A random point defining a plant growth strategy is then selected from each subvolume.

Each grid cell is seeded with a small amount of initial seed biomass for each plant growth strategy. The model mechanistically simulates the development of the plant growth strategies and their interactions with the coupled land surface module. Growth strategies which are able to maintain a positive balance of stored assimilates survive, passing through what Webb et al. (2010) refers to as a ‘mechanistic performance filter’.

As environmental conditions change, different strategies will respond in different ways, some may become more productive, others may no longer be able to cope with new conditions and die out. Strategies which were previously filtered out will again be given small amounts of seed carbon and may persist under the new conditions. This process allows the composition of the plant communities in each grid cell to adapt through time, without relying on *a priori* bioclimatic limits relating the presence or absence of a growth strategy to environmental variables. This mechanistic trial-and-error approach seems potentially better suited to simulate the response of the biosphere to climates without present-day analogs because even under new conditions fundamental functional tradeoffs that all plants face are unlikely to change.

## 2.4 Aggregation to ecosystem scale

Some mechanism is needed to aggregate the biogeochemical fluxes and vegetation properties of the potentially many surviving growth strategies within each grid cell. Most current DGVMs calculate grid-cell fluxes and properties as weighted averages across fractional coverages of PFTs. Of those models, the competition between PFTs for fractional area in a grid cell is typically computed implicitly based on moving averages of bioclimatic limits (Arora and Boer 2006). This approach is not suitable for JeDi-DGVM because its tradeoff-based framework does not rely on *a priori* bioclimatic limits. A few DGVMs (e.g. Cox 2001; Arora and Boer 2006) calculate PFT fractional coverages using a form of the Lotka–Volterra equations, in which the colonization rate of each of  $N$  PFTs is linked through a  $N$ -by- $N$  matrix of competition coefficients. For JeDi-DGVM, this Lotka–Volterra approach quickly becomes computationally burdensome as the size of the necessary competition matrix increases with the square of the potentially large number of tested growth strategies. The necessary competition coefficients are also difficult to determine theoretically (McGill et al. 2006).

Instead, JeDi-DGVM aggregates vegetation fluxes and properties to the grid-cell scale following the ‘*biomass–ratio*’ hypothesis (Grime 1998), which postulates that the immediate effects of the functional traits of a species are closely proportional to the relative contribution of that species to the total biomass of the community. Recent work (e.g. Garnier et al. 2004; Vile et al. 2006; Kazakou et al. 2006; Díaz et al. 2007; Quétier et al. 2007) supporting the ‘*biomass–ratio*’ hypothesis has shown strong statistical links between community-weighted functional traits (i.e. the mean trait values of all species in a community, weighted by their mass-based relative abundances) and

observed ecosystem functions (e.g. aboveground net primary productivity and litter decomposition). Others have combined the concept of community-weighted functional traits with the Maximum Entropy (MaxEnt) formalism from statistical mechanics to successfully make predictions, in the other direction, about the relative abundances of individual species within communities (e.g. Shipley et al. 2006b; Sonnier et al. 2010; Laughlin et al. 2011).

Here, rather than weighting the functional traits, JeDi-DGVM calculates ecosystem-scale variables by directly averaging the fluxes and properties across all surviving growth strategies, weighting the contribution of each strategy by its current biomass relative to the total biomass of all strategies within that grid cell (see Appendix A.9 for more details). The resulting ecosystem-scale variables are for the most part diagnostic and do not influence the development of the individual growth strategies or their environmental conditions. Although, the community-aggregated litter fluxes do form the input for a relatively simple soil carbon module, which then provides simulated estimates of heterotrophic respiration (see Appendix A.10). This implementation of the ‘biomass-ratio’ hypothesis assumes that interactions between plants, both competitive and facilitative, are weak and do not significantly alter plant survival or relative fitness. The potential implications of this assumption are discussed in Chapter 5.2.3. In principle, the trait parameters of the surviving growth strategies could also be aggregated, forming an additional testable output of the model. This is discussed further in Chapter 5.2.4.

## Chapter 3

# Evaluating the broad-scale patterns of terrestrial biogeography and biogeochemistry

### 3.1 Introduction

In this chapter, simulated patterns of terrestrial biogeography and biogeochemistry from JeDi-DGVM are evaluated against a variety of field and satellite-based observations. The model evaluation follows a systematic protocol established by the Carbon-Land Model Intercomparison Project (C-LAMP; Randerson et al. 2009). By following this protocol, we are also able to directly compare the bottom-up functional trade-off approach of JeDi-DGVM with evaluation results for terrestrial biosphere models based on the dominant PFT paradigm. We also evaluate the simulated biogeographical patterns of functional richness and relative abundances to illustrate the parsimonious nature of a functional trade-off approach to dynamic global vegetation modelling, i.e. it can provide more types of testable outputs with fewer inputs.

### 3.2 Simulation setup

In our simulation setup, we followed the experimental protocol from C-LAMP (Randerson et al. 2009) to facilitate comparison with other terrestrial biogeochemistry models. JeDi-DGVM was run with 2000 randomly-sampled plant growth strategies on a global grid at a spatial resolution of approximately  $2.8^\circ$  by  $2.8^\circ$  resolution, covering all land areas except Antarctica. The model was forced at a daily time step with downward shortwave and longwave radiation, precipitation, and near-surface air temperature from

an improved NCEP/NCAR atmospheric reanalysis dataset (Qian et al. 2006). We looped the first 25 years of the reanalysis dataset (1948-1972) with a fixed, preindustrial atmospheric CO<sub>2</sub> concentration until the vegetation and soil carbon pools reached a quasi-steady state ( $\sim 3500$  years). After this spinup simulation, a transient simulation was run for years 1798-2004 using prescribed global atmospheric CO<sub>2</sub> concentrations from the C4MIP reconstruction of Friedlingstein et al. (2006). This transient simulation was forced by the same climate forcing as the spinup run for years 1798-1947 and by the full reanalysis dataset for years 1948-2004. We ran an additional experiment to compare the response of JeDi-DGVM to a sudden increase in atmospheric CO<sub>2</sub> with results from the Free-Air CO<sub>2</sub> Enrichment (FACE) experiments (Norby et al. 2005). This FACE experiment simulation was similar to the transient simulation described above but with the atmospheric CO<sub>2</sub> concentration set to 550 ppm for years 1997-2004. We deviated from the C-LAMP experimental protocol by allowing the vegetation to evolve dynamically through the simulations, rather than prescribing the pre-industrial land cover dataset. The aspects of the C-LAMP protocol related to N deposition were not considered as a nitrogen cycle has not yet been implemented in JeDi-DGVM.

### 3.3 Evaluation protocol

We evaluated the performance of the JeDi-DGVM against multiple observational datasets using a set of systematic metrics developed for the C-LAMP (Randerson et al. 2009). As computed, each C-LAMP metric falls somewhere between zero and one and is then scaled by a numerical weight to produce a score. The weights are based on subjective estimates of a metric’s uncertainty, considering both the measurement precision of the observations and the scaling mismatch between the model and observations. Further details about each metric and the justifications behind their particular numerical weighting are described in Randerson et al. (2009). The metrics, their weights, along with the resulting scores for JeDi-DGVM are summarized in Table 3.1. The scores for two terrestrial biogeochemistry models based on the PFT concept, CLM-CN (Thornton et al. 2007) and CLM-CASA’ (Fung et al. 2005; Doney et al. 2006), are also shown for comparison (both were previously evaluated in Randerson et al. 2009). Below, we provide a brief summary of the datasets and scoring methods. The results of the evaluation are described in the following section.

**Table 3.1:** Summary of the evaluation metrics and scores. Each metric (Column 1) is associated with a possible score (Column 3) based on a subjective assessment of its level of uncertainty and model-data scale mismatch. Each metric is broken in to metric components (Column 2) with associated sub-scores (Column 4). Scores are presented for JeDi-DGVM (this paper) and, for comparison, CLM-CN and CLM-CASA' (previously evaluated in Randerson et al. 2009). The total score for each model (out of a possible score of 100) is presented at the bottom. MODIS, MODerate Resolution Imaging Spectroradiometer; EMDI, Ecosystem Model Data Intercomparison

Metric	Metric components	Score	Sub-score	JeDi-DGVM	CASA'	CN
Leaf Area Index		15		13.4	13.5	12.0
	MODIS phase		6	5.0	5.1	4.2
	MODIS maximum		5	4.7	4.6	4.3
	MODIS mean		4	3.7	3.8	3.5
Net Primary Productivity		10		8.4	8.0	8.2
	EMDI observations		2	1.5	1.5	1.6
	EMDI histogram		4	3.4	3.0	3.4
	MODIS spatial pattern		2	1.6	1.6	1.4
	MODIS zonal means		2	1.9	1.9	1.8
CO <sub>2</sub> seasonal cycle comparison with Globalview phase and amplitude		15		11.8	10.4	7.7
	60-90N		6	4.9	4.1	2.8
	30-60N		6	4.5	4.2	3.2
	EQ-30N		3	2.5	2.1	1.7
Carbon and energy fluxes from Ameriflux		30		18.3	17.2	16.6
	Net ecosystem exchange		6	2.6	2.5	2.1
	Gross primary productivity		6	3.5	3.4	3.5
	Latent heat		9	6.6	6.4	6.4
	Sensible heat		9	5.6	4.9	4.7
Carbon stocks and transient dynamics		30		16.3	16.7	13.8
	Aboveground biomass in the Amazon basin		10	6.7	5.3	5.0
	NPP stimulation from elevated CO <sub>2</sub>		10	6.9	7.9	4.1
	Interannual variability of terrestrial carbon fluxes		5	2.7	3.6	3.0
	Fire variability		5	0.0	0.0	1.7
Total		100	68.2	65.7	58.4	

### Phenology

We compared the simulated leaf area index (LAI) values against observations from the MODerate resolution Imaging Spectroradiometer (MODIS) (Myneni et al. 2002; Zhao et al. 2005, MOD15A2 Collection 4). We consider three phenology metrics, the timing of maximum LAI, the maximum monthly LAI, and the annual mean LAI. All three metrics used monthly mean LAI observations and modelled estimates from years 2000 to 2004. The LAI phase metric was computed at each grid cell as the offset in months between the observed and simulated maximum LAI values, normalized by the maximum possible offset (6 months), and finally, averaged across biomes. The maximum and annual mean LAI metrics  $M$  were computed using the equation:

$$M = 1 - \frac{\sum_{i=1}^n \frac{|m_i - o_i|}{m_i + o_i}}{n} \quad (3.1)$$

where  $m_i$  is the simulated LAI at the grid cell corresponding to the satellite observation ( $o_i$ ) and  $n$  is the number of model grid cells in each biome. Global means for these metrics were computed by averaging  $M$  across different biome types.

### Global patterns of productivity and evapotranspiration

Modelled estimates of net primary productivity (NPP) are compared against a compilation of field-based observations from the Ecosystem Model Data Intercomparison (EMDI) (Olson et al. 2001) and remote sensing-based estimates extracted from the MODIS MOD17A3 Collection 4.5 product (Heinsch et al. 2006; Zhao et al. 2005, 2006). We compared the mean annual NPP as simulated by JeDi-DGVM for years 1975-2000 with the EMDI observations on a point-by-point basis of each observation site to the corresponding model grid cell using Eq. 3.1 described above. As a second NPP metric, we used Eq. 3.1 again with the modeled and observed values averaged into discrete precipitation bins of 400mm per year. For the third and fourth NPP metrics, we computed the square of the Pearson coefficient of determination ( $r^2$ ) between the mean annual MODIS and modelled NPP (for years 2000-2004) for all non-glaciated land grid cells and for the zonal means.

In addition to the NPP metrics from the C-LAMP protocol, we also evaluated JeDi-DGVM against spatially-explicit, data-driven estimates of evapotranspiration (ET; Jung et al. 2010) and gross primary productivity (GPP; Beer et al. 2010). The estimate of ET (Jung et al. 2010) was compiled by upscaling FLUXNET site measurements

with geospatial information from remote sensing and surface meteorological data using a model tree ensemble algorithm (Jung et al. 2009). It covers years 1982-2008, although here, we use only use model years 1982-2004 for the comparison due to the limitation of the meteorological forcing dataset. The estimate of GPP (Beer et al. 2010) was derived from five empirical models calibrated also against FLUXNET observations. It covers years 1998-2005, although here, we use only use model years 1998-2004 for the comparison.

### Seasonal cycle of atmospheric CO<sub>2</sub>

We simulated the annual cycle of atmospheric CO<sub>2</sub> by applying the atmospheric impulse response functions from the Atmospheric Tracer Transport Model Intercomparison Project (TRANSCOM) Phase 3 Level 2 experiments (Gurney et al. 2004) to the JeDi-DGVM net ecosystem exchange (NEE) fluxes. The monthly JeDi-DGVM NEE fluxes for years 1991-2000 were aggregated into the 11 TRANSCOM land basis regions. The aggregated NEE fluxes are multiplied by monthly response functions from Baker et al. (2006), yielding simulated atmospheric CO<sub>2</sub> time series for 57 observation stations around the globe. This process was repeated for all 13 TRANSCOM atmospheric transport models and the multi-model mean annual cycle was compared with observations from the GLOBALVIEW dataset (Masarie and Tans 1995). We computed the square of the Pearson correlation coefficient ( $r^2$ ) as a measure of phase and the ratio of modeled amplitude  $A_M$  to observed amplitude  $A_O$  as a measure of magnitude (see Eq. 3.2).

$$M = 1 - \left| \frac{A_M}{A_O} - 1 \right| \quad (3.2)$$

These two metrics were computed for three latitude bands in the northern hemisphere (EQ-30°N, 30-60°N, 60-90°N). All stations within each band were weighted equally. The scores from the mid and high latitude bands were given more weight due to the stronger annual signal and the relatively smaller contributions from oceanic and anthropogenic fluxes.

### Interannual variability in CO<sub>2</sub> fluxes

The same TRANSCOM response functions (Baker et al. 2006) and the GLOBALVIEW CO<sub>2</sub> measurements (Masarie and Tans 1995) described above were combined to obtain estimates of the interannual variability in the global terrestrial NEE fluxes for years

1988-2004. We compared these estimates with JeDi-DGVM, again incorporating information about the phase and magnitude. The phase agreement was evaluated by the coefficient of determination ( $r^2$ ) between the simulated global annual mean NEE fluxes and the TRANSCOM-based estimates. The magnitude of interannual variability was calculated using the standard deviation of the simulated and observation values as  $A_M$  and  $A_O$  in Eq. 3.2. The phase and magnitude metrics were then averaged together with equal weighting.

In their C-LAMP evaluation, Randerson et al. (2009) also evaluated the magnitude and pattern of simulated fire emissions against observations in the Global Fire Emissions Database version 2 (GFEDv2; van der Werf et al. 2006). We set the score for this metric to zero because JeDi-DGVM does not simulate fire emissions.

### **Eddy covariance measurements of energy and carbon**

We compared the simulated monthly mean surface energy and carbon fluxes against gap-filled L4 Ameriflux data (Falge et al. 2002; Heinsch et al. 2006; Stöckli et al. 2008). For each Ameriflux data-month, we sampled the corresponding model grid output. Then, we constructed an annual cycle of monthly means and using Eq. 3.1 computed metrics for NEE, GPP, and the fluxes of sensible and latent heat. All 74 tower sites were weighted equally.

### **Carbon stocks and flows in Amazonia**

We evaluated the simulated aboveground living biomass in Amazonia against the LBA-ECO LC-15 Amazon Basin Aboveground Live Biomass Distribution Map compiled by Saatchi et al. (2007). We used Eq. 3.1 to calculate the model-data agreement between the simulated aboveground live biomass and the observed biomass values at each grid cell within the Amazon Basin. The model output used for comparison was the sum of the simulated aboveground wood and leaf carbon pools for year 2000. Although, not part of the metric calculation, we also compared the model results with carbon budget observations from three mature forest ecosystems in Amazonia (Malhi et al. 2009).

### **Sensitivity of NPP to elevated CO<sub>2</sub> concentrations**

To evaluate the sensitivity of simulated NPP to elevated CO<sub>2</sub> concentrations, we performed a model experiment (described above in Chapter 3.2) to mimic the treatment

plots in FACE experiments. We calculated the mean percentage increase in NPP between the control and elevated CO<sub>2</sub> simulations for years 1997-2001. Using Eq. 3.1, we compared the simulated increases at four temperate forest grid cells with corresponding site-level average increases reported by Norby et al. (2005). We also report a global map of the simulated NPP response to a step change in CO<sub>2</sub> concentrations from ambient to 550 ppm.

### 3.4 Results and discussion

The Jena Diversity DGVM described in this paper presents a new approach to terrestrial biogeochemical modeling, in which the functional properties of the vegetation emerge as a result of reproductive success and productivity in a given climate. This contrasts with the standard approach to mechanistic land surface modeling that utilizes a set of fixed PFTs, whose pre-determined properties are specified by parameter values often determined from databases of observed plant trait values. In an effort to understand if a more diverse representation of the terrestrial biosphere can reasonably capture observed patterns of biophysical and biogeochemical states and fluxes, we contrast below the performance of the less constrained JeDi-DGVM approach against the performance of two previously evaluated land surface models.

#### 3.4.1 Biodiversity patterns

In contrast to standard DGVMs, the broad sampling across a multi-dimensional trait space allows JeDi-DGVM to provide insight into potential plant biodiversity through an examination of the simulated functional richness (the number of sampled plants that survive in a grid cell). The geographic pattern of simulated functional richness (Fig. 3.1a) is highly and significantly ( $r^2 = 0.71$ ) correlated with a map of vascular plant species richness derived from observations (Kreft and Jetz 2007). Out of the 2000 randomly-assembled plant growth strategies, 1411 growth strategies survived in at least one grid cell and the maximum value for a single grid cell was 1322 in western Amazonia. These fractions of surviving growth strategies are much higher than those reported by KM2000. This is likely attributable to the difference in the survival criterion. In the earlier model of KM2000, the criteria for survival was whether or not a growth strategy was able to produce more seed carbon over its lifetime than its initial amount of seed carbon. Here, the criterion for survival was simply whether or not a growth strategy was able to maintain a positive carbon balance. Nonetheless, JeDi-DGVM is still able

to reproduce the observed broad global pattern of plant diversity through mechanistic environmental filtering due to functional trade-offs, and without invoking historical, competitive, or other factors.

The mean relative abundance distributions for four richness classes (Fig. 3.2a) are similar in shape to left-skewed log-normal distributions commonly observed throughout nature (McGill et al. 2007). The left skewness means that rare species are greater in number than abundant ones, another commonly observed attribute, especially in tropical rainforests (Hubbell 1997). With increasing levels of functional richness, the mean as well as the variance of the relative abundance distribution successively shifts to lower values. We also see that there is not necessarily one optimal combination of trait parameters for obtaining high biomass in an environment, but often many differing growth strategies can reach similarly high levels of fitness (cf. Marks and Lechowicz 2006; Marks 2007). As the climate becomes less constraining, in terms of increasing availability of light and precipitation, the range of feasible plant growth strategies increases. The ranked abundances of growth strategies (Fig. 3.2b) clearly show that the simulated relative abundances become increasingly even with higher richness. This pattern is also evident when visually comparing the maps of simulated function richness (Fig. 3.1a) and community evenness (Fig. 3.1b). This simulated trend towards greater evenness in more productive regions qualitatively reproduces the observed trend in rank-abundance plots of forests that show a much steeper decline in abundance in boreal forests than in tropical rainforests (Hubbell 1979, 1997).

### 3.4.2 Phenology

For the C-LAMP phase metric, JeDi-DGVM received a score of 5.0 out of 6, performing comparably with the two other land surface models (CLM-CN and CLM-CASA') previously evaluated in Randerson et al. (2009). Fig. 3.3 shows the comparison between the simulated and observed month of maximum LAI. The simulated timing of peak LAI matched observations reasonably well in the moisture-limited grassland and savannah regions of South America, Africa, and Australia. There were two clear patterns of bias, however. First, like CLM-CN and CLM-CASA', JeDi-DGVM simulated maximum LAI occurring about one month later than the MODIS observations across much of the northern hemisphere. Second, in the MODIS dataset, leaf area follows the seasonality of incident solar radiation across large parts of the Amazon basin, peaking during the early to mid part of the dry season when radiation levels are high and deep-rooted vegetation still has access to sufficient moisture (Myneni et al. 2007). JeDi-DGVM

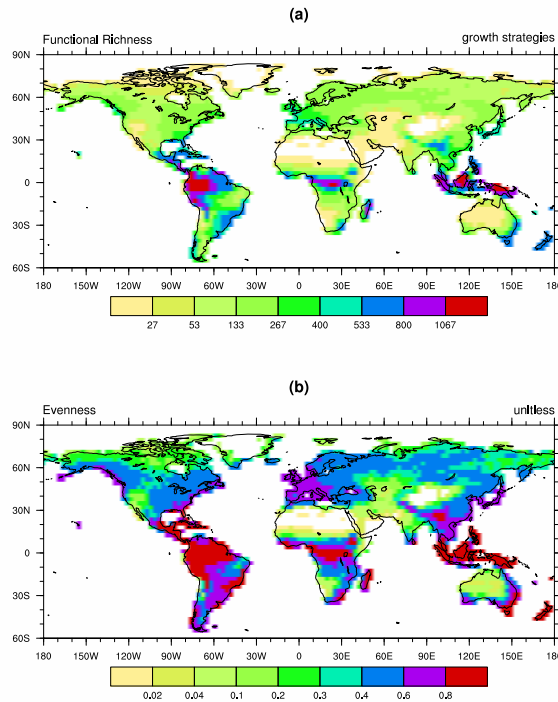


**Figure 3.1:** Geographic patterns of (a) richness and (b) community evenness as simulated by JeDi-DGVM. Richness is simply the number of surviving plant growth strategies in a grid cell out of the 2000 tested plant growth strategies. Community evenness is calculated as  $\frac{H'}{H_{\max}'}$  where  $H'$  is the Shannon entropy of the abundance distribution in a grid cell and  $H_{\max}'$  is the maximum possible value of  $H'$  if all growth strategies were equally abundant (Pielou 1966).

did not capture this opportunistic behavior, simulated peak LAI in the tropical moist forests of Amazonia, central Africa, and southeast Asia occurs during the rainy season. However, the issue of whether or not tropical forests green-up during dry periods is still not settled (Samanta et al. 2010; Asner and Alencar 2010).

The comparisons of simulated and observed maximum and mean LAI are shown in Figs. 3.4 and 3.5. Overall, JeDi-DGVM matched the observed values reasonably well, receiving scores of 3.7/4.0 (score/maximum score) and 4.7/5.0 for the mean and maximum LAI metrics, on par with the performances of CLM-CN and CLM-CASA'. The simulated mean LAI values were generally low relative to the observations across the boreal forest region. Also, both the simulated mean and maximum LAI were higher than observed values in several regions, particularly southeast Brazil, northeast India, the central United States, much of Europe, and eastern China. This may simply be

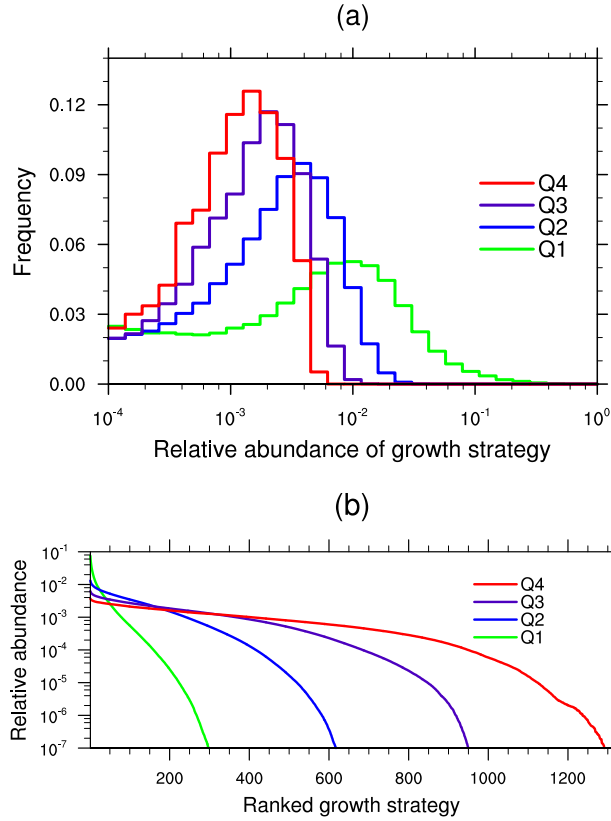


**Figure 3.2:** (a) Simulated relative abundance distributions of plant growth strategies for four richness quartiles. (b) Simulated relative abundance versus growth strategy rank for four richness quartiles. On the x-axis, growth strategies are ranked according to their abundances, which in turn are plotted on the y-axis. The relative abundance distributions are averaged over all grid points falling into four classes of functional richness: grid points with low richness (Q1;  $0 < D < 0.25$  of the maximum simulated richness level) to medium (Q2;  $0.25 < D < 0.50$ ), high (Q3;  $0.50 < D < 0.75$ ) and very high richness (Q4;  $0.75 < D < 1.00$ ), where the richness  $D$  is expressed in relation to the grid cell with maximum simulated value of functional richness

due to the fact that human land-use was not accounted for in the simulation set up and these regions are used extensively for agricultural purposes. These disparities could likewise indicate a need for reevaluation of the trade-off costs associated with root water uptake, i.e. the construction and maintenance costs of coarse and fine roots.

Overall, the performance of JeDi-DGVM in capturing observed global phenological patterns shows great promise in using less constrained approaches that allow the dynamics of the land surface to emerge from climatic constraints.

### 3.4 RESULTS AND DISCUSSION

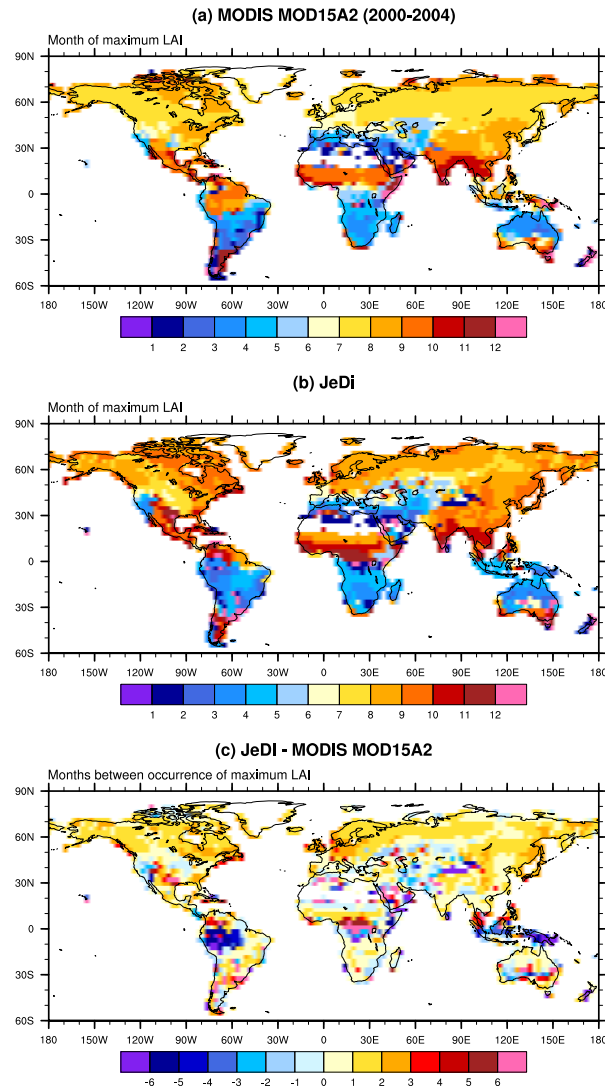


**Figure 3.3:** Mean month of maximum leaf area index for years 2000-2004 from (a) MODIS MOD15A2 Collection 4 LAI product (Myneni et al. 2002; Zhao et al. 2005); (b) as simulated by JeDi-DGVM; and (c) the lag in months between the occurrence of maximum LAI in the MODIS observations and the JeDi-DGVM model output.

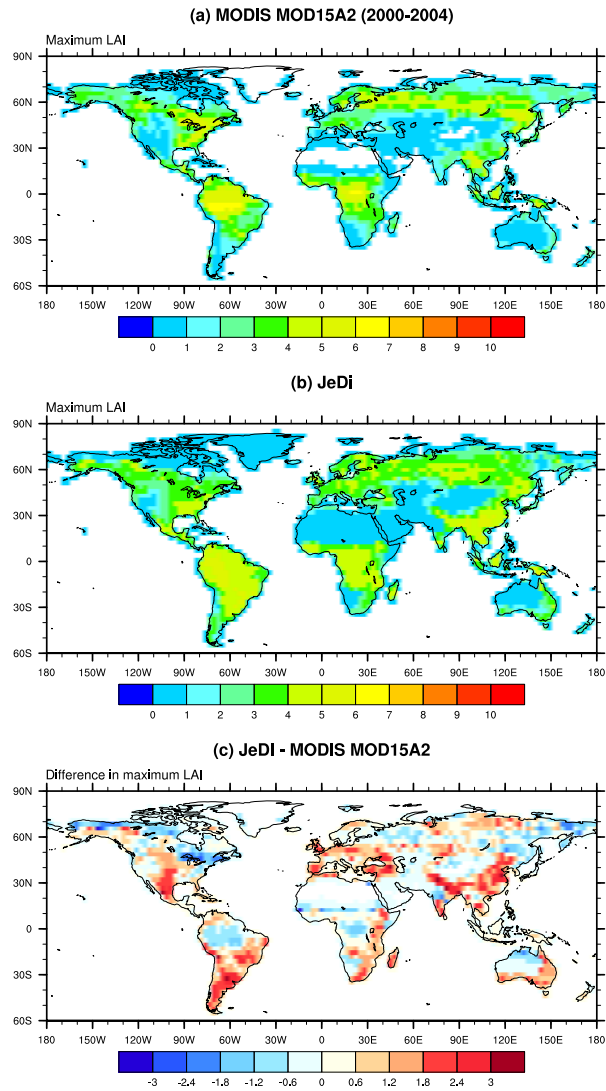


**Figure 3.4:** Mean intra-annual maximum leaf area index for years 2000-2004 from (a) MODIS MOD15A2 Collection 4 LAI product (Myneni et al. 2002; Zhao et al. 2005); (b) as simulated by JeDi-DGVM; and (c) the difference between the MODIS observations and the JeDi-DGVM model output.

### 3.4 RESULTS AND DISCUSSION

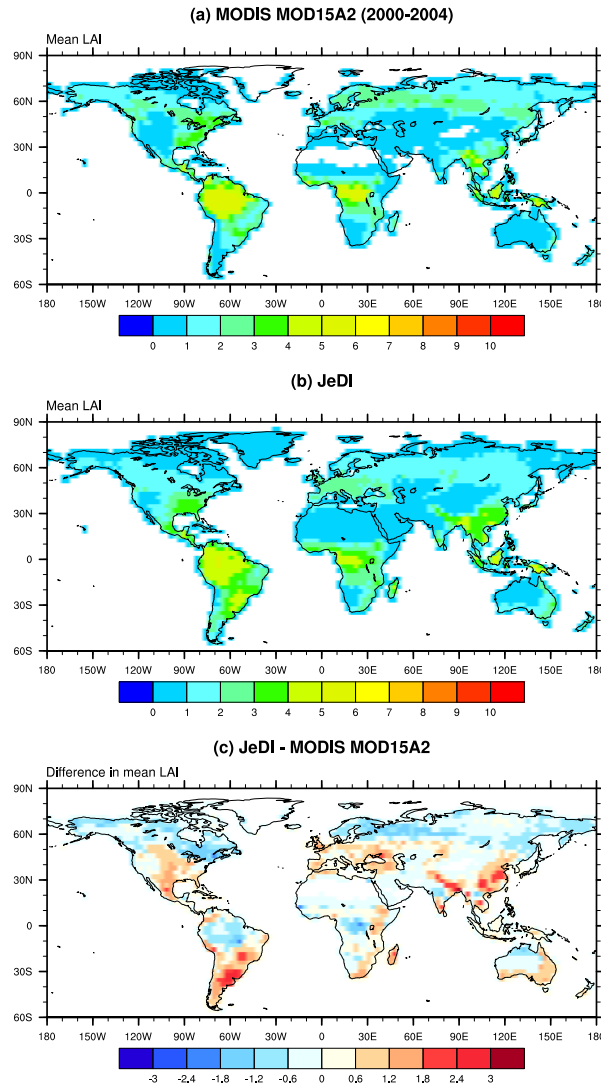


**Figure 3.5:** Mean leaf area index for years 2000-2004 from (a) MODIS MOD15A2 Collection 4 LAI product (Myneni et al. 2002; Zhao et al. 2005); (b) as simulated by JeDi-DGVM; and (c) the difference between the MODIS observations and the JeDi-DGVM model output.

### 3.4.3 Global carbon stocks

JeDi-DGVM simulated global stocks of vegetation, soil, and litter carbon of 637 PgC, 1904 PgC, and 208 PgC, respectively. These values are averages over the simulation period 1980-2004. The vegetation carbon stock simulated by JeDi-DGVM falls within the range of reported values from several PFT-based DGVM studies (500-950 PgC; Cramer et al. 2001; Sitch et al. 2003; Krinner et al. 2005; Zaehle et al. 2010) and estimates from global carbon inventories (385-650 PgC; Houghton et al. 2009). Likewise, the modelled estimate for litter carbon is close to the estimate based on carbon inventories (300 PgC) reported in Houghton et al. (2009). The simulated soil carbon stock also falls within previous inventory-based estimates (Houghton et al. 2009, 1200-3000 PgC;).

### 3.4.4 Gross Primary Productivity

JeDi-DGVM simulated a mean global terrestrial GPP of 138 PgC year<sup>-1</sup>, which is higher than the data-driven estimate of 123 ± 8 PgC year<sup>-1</sup> from Beer et al. (2010), but within the range of uncertainty (118 ± 26 PgC year<sup>-1</sup>) of a recent estimate from a processed-based model forced with remote sensing observations (Ryu et al. 2011). The zonally-averaged simulated GPP shows close agreement ( $r^2 = 0.89$ ) with the median estimate from Beer et al. (2010), falling within or near the range of uncertainty across most latitudes (Fig. 3.6a). JeDi-DGVM performed comparably with five PFT-based biosphere models evaluated in that study in reproducing the latitudinal pattern of GPP. Averaging zonally hides some offsetting regional biases, however. For instance, simulated productivity in Amazonia is about 25% lower than observation-based estimates, but productivity is overestimated throughout most of the Asian tropics (Fig. 3.7). Overall though, the broad spatial pattern of GPP is reasonably well captured by JeDi-DGVM ( $r^2 = 0.85$ ) when compared to the map of data-driven estimates from Beer et al. (2010).

### 3.4.5 Net Primary Productivity

JeDi-DGVM simulated a mean global terrestrial NPP of 79 PgC year<sup>-1</sup>, which is more than one standard deviation greater than the mean estimate from a recent meta-analysis of global NPP studies (56 ± 14 PgC year<sup>-1</sup>; Ito 2011). We hypothesize that this overestimation stems, in part, from the lack of nitrogen limitation within the model. Global

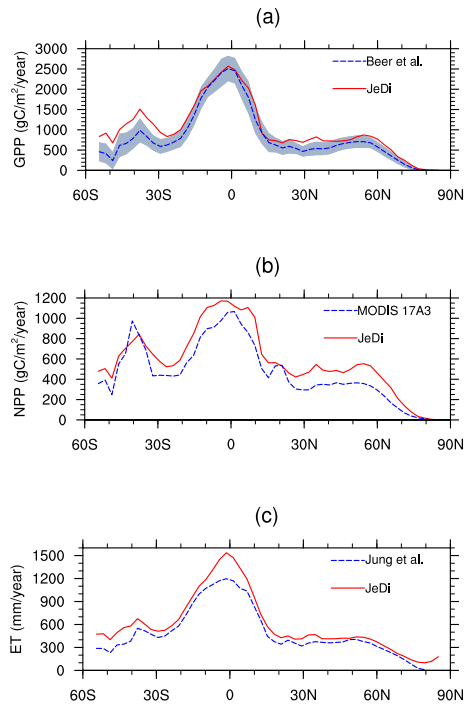


**Figure 3.6:** Comparison of mean annual zonally-averaged fluxes as simulated by JeDi-DGVM with (a) observation-based estimates of gross primary productivity (Beer et al. 2010); (b) net primary productivity from the MODIS MOD17A3 Collection 4.5 product (Heinsch et al. 2006; Zhao et al. 2005, 2006); and (c) observation-based estimates of evapotranspiration (Jung et al. 2010). The blue-shaded region in (a) represents the median absolute deviation of the five diagnostic models used in producing the observation-based estimate.

analyses of nutrient limitation studies (Elser et al. 2007; LeBauer and Treseder 2008) suggest that soil nitrogen availability and the energetic cost of nitrogen fixation and active ion uptake limit terrestrial productivity by about 20%. Adding a mechanistic representation of plant nitrogen acquisition based on plant energetic trade-offs (e.g. Fisher et al. 2010a) to future versions of JeDi-DGVM is critical, as it is thought that nitrogen availability will likely constrain the capacity of terrestrial ecosystems to continue taking up a large part of anthropogenic carbon emissions (Reich et al. 2006).

In a site-by-site comparison with field-based EMDI NPP observations (Fig. 3.8), JeDi-DGVM performed on par with CLM-CN and CLM-CASA' with a score of 1.5/2.0. JeDi-DGVM does relatively well in capturing the variability in NPP across the EMDI observation network (Fig. 3.8a), although it tends to overestimate NPP, particularly at intermediately productive sites. JeDi-DGVM also performed reasonably well and com-

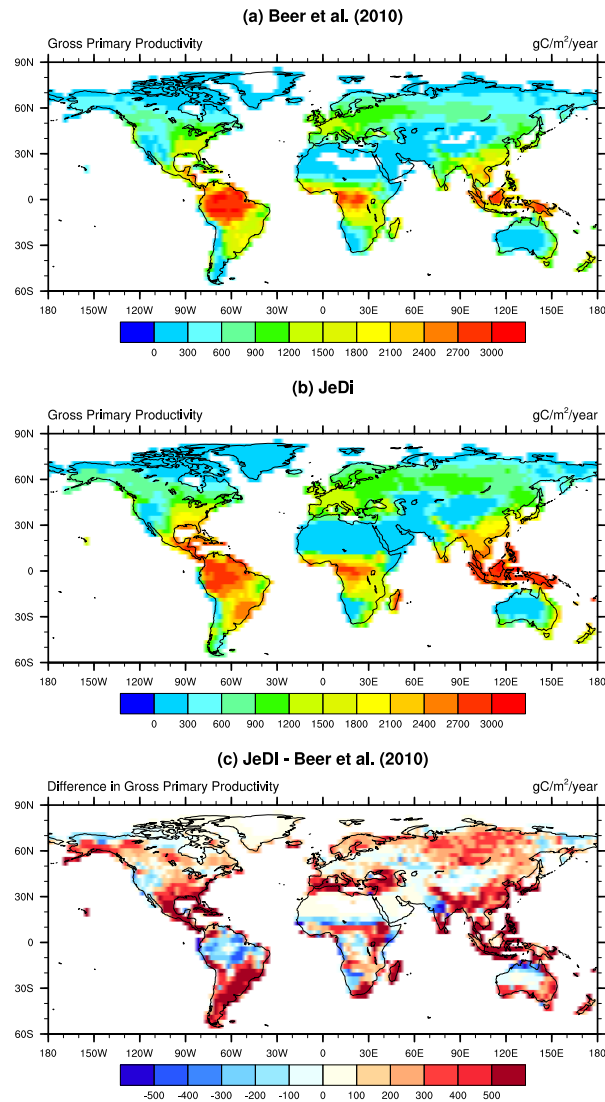


**Figure 3.7:** (a) Observation-based estimate of mean annual gross primary productivity for years 1998-2005 (Beer et al. 2010); (b) mean annual terrestrial gross primary productivity from JeDi-DGVM for years 1998-2004; and (c) the difference between the observation-based estimate and the JeDi-DGVM model output.

parably with the PFT-based models when the simulated NPP is binned by precipitation class (Fig. 3.8b). JeDi-DGVM underestimated NPP at the driest sites ( $< 400 \text{ mm yr}^{-1}$ ) and overestimated NPP at wetter sites.

For the two MODIS NPP metrics, JeDi-DGVM performed on par with CLM-CN and CLM-CASA', receiving scores of 1.6/2.0 (spatial pattern) and 1.9/2.0 (zonal means). The comparison with the MODIS NPP product reveals that JeDi-DGVM is able to capture the broad spatial patterns of NPP (Fig. 3.9). JeDi-DGVM prominently overestimates productivity, though, in the grassland regions of South America and the Sahel as well as the forested regions of the eastern United States, eastern China, and northern Eurasian. This high bias also emerges in the comparison with the zonally averaged MODIS NPP (Fig. 3.6b).

### 3.4.6 Evapotranspiration

JeDi-DGVM simulated a mean global terrestrial ET flux of  $82 \times 10^3 \text{ km}^3 \text{ year}^{-1}$ , which is higher than the observation-based estimate of  $65 \pm 3 \times 10^3 \text{ km}^3 \text{ year}^{-1}$  of Jung et al. (2010) but within the range of model-based estimates ( $60\text{--}85 \times 10^3 \text{ km}^3 \text{ year}^{-1}$ ) from the the Water Model Intercomparison Project (WaterMIP; Haddeland et al. 2011). Fig. 3.10 shows a spatial comparison of simulated mean annual ET and the observation-based estimates of Jung et al. (2010). Overall, the model performed reasonably well ( $r^2 = 0.78$ ) in reproducing the global pattern of ET. The zonal averages, however, show a strong positive bias in the equatorial tropics (Fig. 3.6c;  $r^2 = 0.80$ ). Further analysis revealed that some of this model bias is attributable to an overestimation of canopy interception, especially in tropical forests. Adjusting the parameterizations related to canopy interception and canopy storage capacity has improved model performance for other DGVMs (Bonan and Levis 2006; Liang and Xie 2008).

### 3.4.7 Seasonal cycle of atmospheric $\text{CO}_2$

JeDi-DGVM captured the general temporal pattern ( $r = 0.84 \pm 0.04$ ,  $0.83 \pm 0.08$ ,  $0.80 \pm 0.15$ ) of a spring drawdown of atmospheric  $\text{CO}_2$  in the northern hemisphere followed by an autumnal rise. However, there is a phase offset at many stations with the simulated spring drawdown occurring about one to two months later than observations. This offset may be due to the late leaf expansion mentioned above (Fig. 3.3) or to limitations stemming from the simple nature of heterotrophic respiration scheme. JeDi-DGVM overestimated the seasonal amplitude of atmospheric  $\text{CO}_2$  in the northern

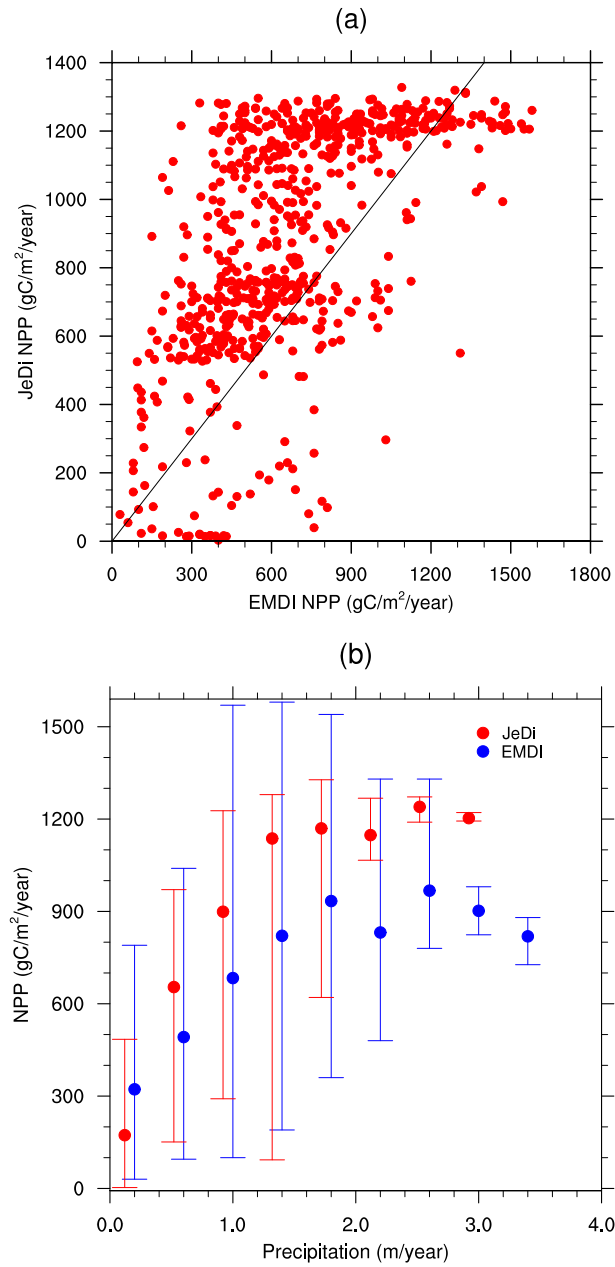


**Figure 3.8:** Comparison of net primary productivity between JeDi-DGVM model output (mean over years 1975-2000) and 933 site observations from the Ecosystem Model Data Intercomparison Initiative (EMDI) class B dataset (Olson et al. 2001). Shown as (a) scatterplot where the red dots represent matched pairs of model grid cells and observation sites and the black line is a 1:1 line; and (b) the same but normalized by precipitation (binned in to 400 mm yr<sup>-1</sup> increments)

### 3.4 RESULTS AND DISCUSSION

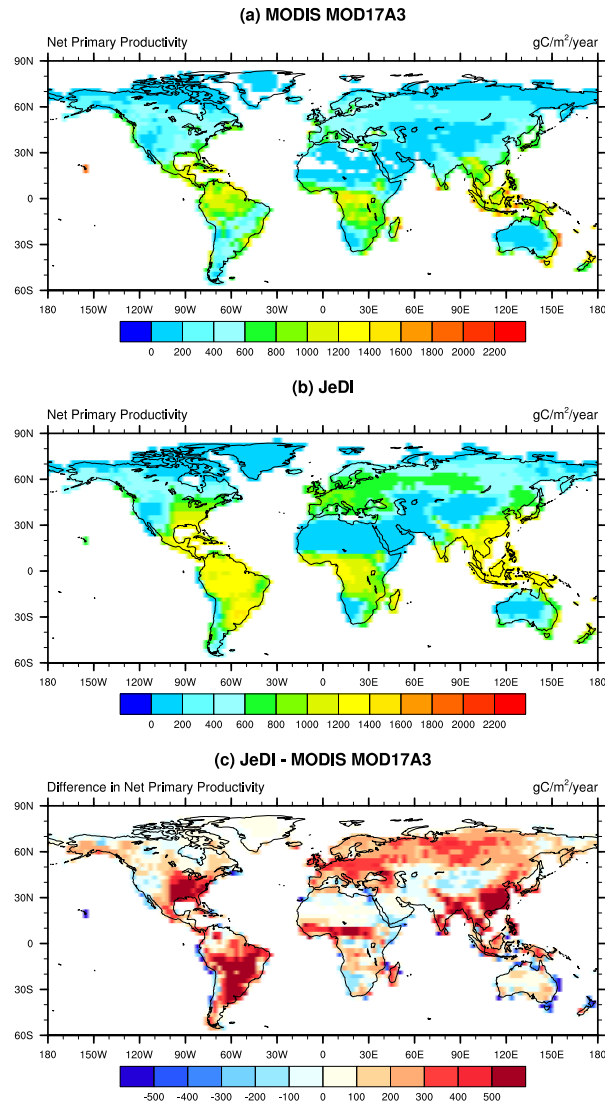


**Figure 3.9:** Mean annual net primary productivity for years 2000-2004 from (a) MODIS MOD17A3 Collection 4.5 product (Heinsch et al. 2006; Zhao et al. 2005, 2006); (b) as simulated by JeDi-DGVM; and (c) the difference between the MODIS product and the JeDi-DGVM model output.

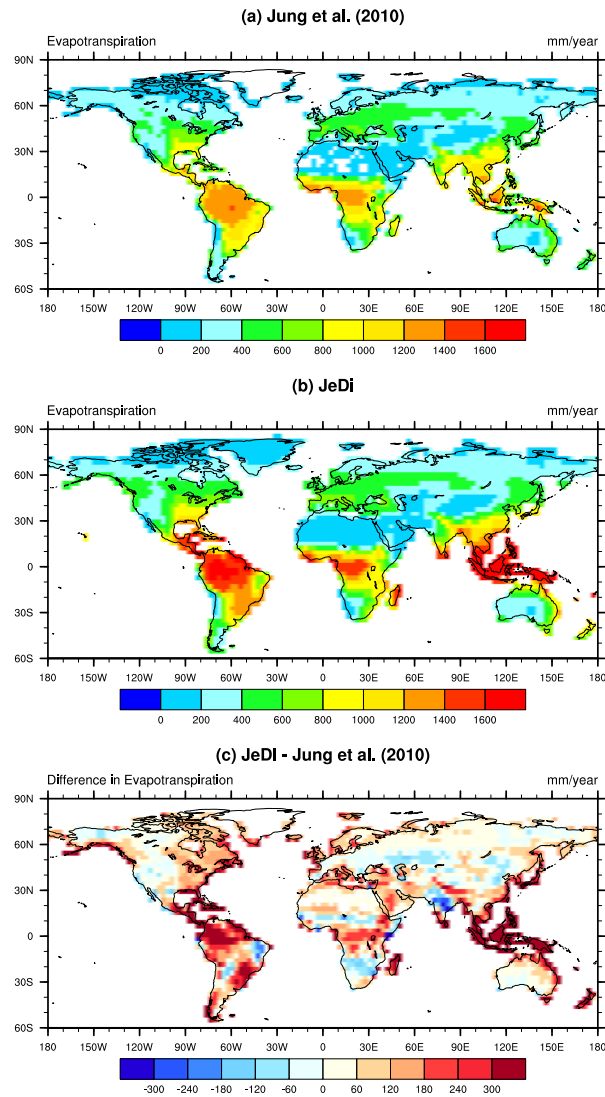


**Figure 3.10:** (a) Observation-based estimate of mean annual evapotranspiration for years 1982-2008 (Jung et al. 2010); (b) mean annual gross primary productivity as simulated by JeDi-DGVM for years 1982-2004; and (c) the difference between the observation-based estimate and the JeDi-DGVM model output.

hemisphere, particularly in the middle and high latitude bands. The ratios of simulated to observed amplitudes were  $1.23 \pm 0.08$ ,  $1.33 \pm 0.26$ , and  $1.10 \pm 0.16$ , for the high, middle, and equatorial latitude bands, respectively. This overestimation in seasonal amplitude is directly attributable to the overestimation of NPP in those regions. Fig. 3.11 illustrates the reasonably good agreement between the simulated seasonal CO<sub>2</sub> cycle and GLOBALVIEW measurements at a high latitude (Point Barrow, Alaska, United States), a mid-latitude (Niwot Ridge, Colorado, United States), and an equatorial station (Mauna Loa, Hawaii, United States). The results for all GLOBALVIEW stations considered here are summarized in a Taylor diagram (Taylor 2001) in Fig. 3.12.

Overall, JeDi-DGVM performed better than CLM-CN and CLM-CASA' on this metric with a combined score of 11.8/15.0. It scored better than both PFT-based models on the measure of amplitude agreement and fell between the scores of those models on the measure of phase agreement.

### 3.4.8 Net terrestrial carbon exchange

The net terrestrial carbon sink simulated by JeDi-DGVM is compatible with decadal budgets of the global carbon cycle given the uncertainties regarding the oceanic and anthropogenic fluxes. For the 1980s, JeDi-DGVM simulated a global terrestrial carbon flux of  $-2.89 \text{ PgC yr}^{-1}$  (negative values indicate a net uptake of carbon by the terrestrial biosphere), which lies within the range of uncertainty from the IPCC ( $-3.8$  to  $0.3 \text{ PgC yr}^{-1}$ ; Denman et al. 2007). In agreement with the IPCC carbon budgets, JeDi-DGVM simulated a larger carbon sink in the 1990s ( $-3.35 \text{ PgC yr}^{-1}$ ), which also lies within the IPCC range of  $-4.3$  to  $-1.0 \text{ PgC yr}^{-1}$  (Denman et al. 2007). The model estimates presented here suggest a stronger land carbon sink than previous DGVM studies ( $1.2$ - $2.75 \text{ PgC}$ ; Sitch et al. 2008; Randerson et al. 2009).

JeDi-DGVM captured the magnitude of interannual variability of terrestrial NEE quite well ( $\sigma = 0.94 \text{ Pg yr}^{-1}$ ) when compared to the TRANSCOM-derived estimates ( $\sigma = 1.04 \text{ PgC yr}^{-1}$ ) or the period 1988-2004. The model results are also moderately correlated ( $r = 0.42$ ;  $p < 0.05$ ) with the year-to-year TRANSCOM anomalies. The simulated anomalies fell within one standard deviation of the multi-model TRANSCOM mean in 12 of the 17 years.

The model captured the strong positive anomaly associated with the 1998 El Niño event, but not the similarly strong anomaly in 1997. The rapid growth rate of atmospheric CO<sub>2</sub> in 1997 has been linked with large peat and forest fires in the Asian

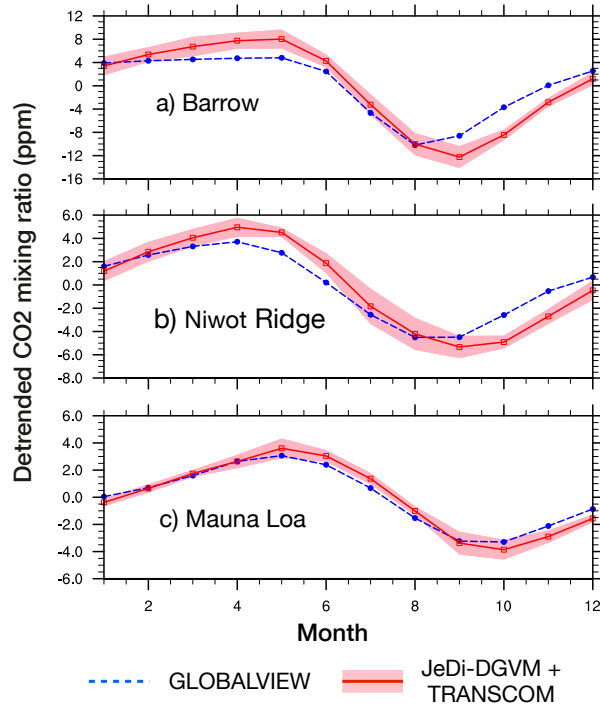


**Figure 3.11:** Mean seasonal cycle of atmospheric CO<sub>2</sub> at (a) Barrow, Alaska (71 °N), (b) Niwot Ridge, Colorado (40 °N), (c) Mauna Loa, Hawaii (20 °N) for years 1991-2000. The dashed blue lines represent the observations from the GLOBALVIEW dataset (Masarie and Tans 1995). The JeDi-DGVM estimates were obtained by combining the simulated NEE fluxes with the monthly impulse response functions (Gurney et al. 2004) of the 13 TRANSCOM atmospheric tracer transport models. The red line represents the mean of the model estimates. The light red shaded region represents one standard deviation around the multimodel mean.

tropics (Page et al. 2002; van der Werf et al. 2008). Incorporating mechanistic representations of fire (e.g. Thonicke et al. 2008) and peat dynamics (e.g. Kleinen et al. 2012) in JeDi-DGVM may improve performance on this metric.

JeDi-DGVM was also not able to capture the negative anomaly in 1992-1993. This drawdown has been associated with climate impacts from the Mount Pinatubo eruption, including an increase in diffuse radiation due to elevated stratospheric aerosol loads (Gu et al. 2003; Mercado et al. 2009). A more detailed canopy radiation transfer model (e.g. Drewry et al. 2010) would be required to appropriately capture the effects of diffuse light on vegetation productivity. If the two years strongly affected by the Pinatubo eruption (1992-1993) are excluded, the model time series is highly correlated ( $r = 0.63$ ;  $p < 0.01$ ) with the interannual TRANSCOM anomalies.

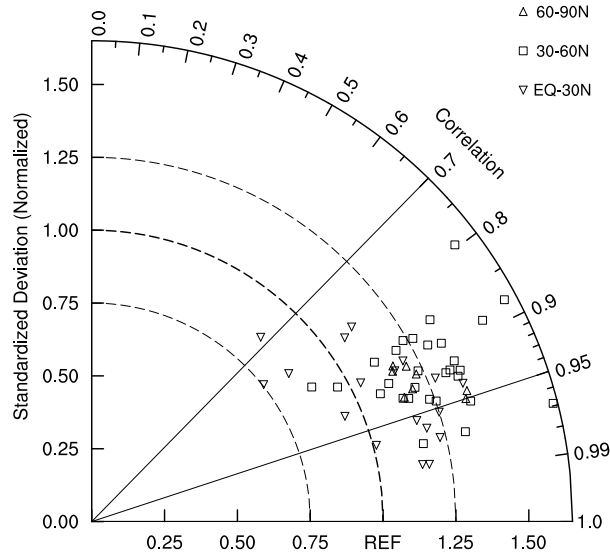


**Figure 3.12:** Taylor diagram comparing the simulated mean annual cycle of atmospheric CO<sub>2</sub> for years 1991-2000 to GLOBALVIEW observations at 57 stations in the Northern Hemisphere. The annual cycle of atmospheric CO<sub>2</sub> was computed by applying TRANSCOM impulse response functions (Gurney et al. 2004) to the monthly NEE fluxes simulated by JeDi-DGVM.

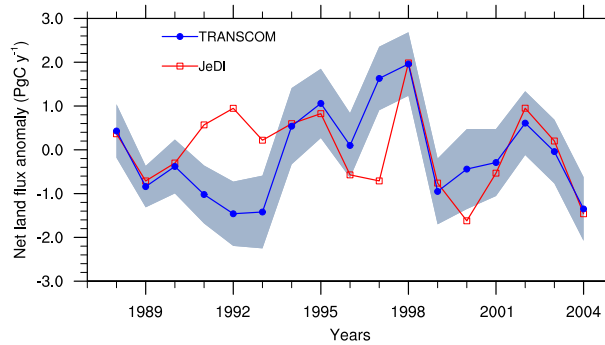


**Figure 3.13:** Comparison of the interannual variability in the global land net ecosystem exchange fluxes from the JeDi-DGVM to the TRANSCOM atmospheric model inversion estimates (Baker et al. 2006) for years 1988-2004. The red line represents the JeDi-DGVM flux anomalies from the long-term mean. The blue line represents the mean of the 13 models from the TRANSCOM experiment after removing the seasonal cycle and the long-term mean for each model. The light blue shaded region represents 1 standard deviation around the TRANSCOM multimodel mean.

### 3.4.9 Comparison with eddy covariance measurements

In the comparison with the Ameriflux observations, JeDi-DGVM performed comparably to CLM-CASA' and CLM-CN, both in terms of metric scores and overall patterns of bias. Seasonal variation in NEE was often lower in the JeDi-DGVM results than in the flux tower observations. And, although not always present, many sites showed a phase offset of one to two months delay. This is consistent with the model biases described above for the seasonal CO<sub>2</sub> cycle and phenology. At many of the temperate forest sites, JeDi-DGVM overestimated the length of the growing season (i.e. GPP was higher than observed in the spring and autumn) and underestimated GPP during the summer peak. Like CLM-CASA' and CLM-CN, JeDi-DGVM captured the seasonal pattern of latent heat fluxes (subscore 6.6/9.0) more accurately than that of sensible heat (5.6/9.0). JeDi-DGVM significantly overestimated the sensible heat fluxes at many sites, indicating the need for a more sophisticated treatment of canopy energy balance (e.g. Drewry et al. 2010).

### 3.4.10 Carbon stocks and flows in Amazonia

JeDi-DGVM performed reasonably well in matching the spatial pattern of aboveground living biomass density in South America (Fig. 3.14,  $r = 0.83$ ). Within the Amazon basin, JeDi-DGVM simulated a total aboveground biomass of 59 Pg C, slightly lower than the total of  $69 \pm 7$  PgC estimated from observations by Saatchi et al. (2007). We attribute some of the overestimation of biomass around the perimeter of the Amazon basin and further south in the Paraná basin to a lack of human land-use and fire as model processes/drivers. The underestimation of aboveground biomass in the central Amazon basin may be related to the lack of competitive interactions between plant growth strategies. More specifically the competition for light, which if incorporated in the model might favor plant growth strategies that invest proportionally more carbon towards growing woody stems. The implications of the current 'biomass-ratio' aggregation scheme and the current lack of resource competition within JeDi-DGVM are discussed further in Chapter 5.2.3.

The carbon allocation and storage scheme in JeDi-DGVM provides a basis for contrasting model estimates of carbon pools against carbon budget observations from three mature forest ecosystems in Amazonia synthesized by Malhi et al. (2009). This comparison is summarized in Fig. 3.15. Despite differences between GPP simulated by JeDi-DGVM ( $2474 \text{ gC m}^{-2} \text{ yr}^{-1}$ ) and observed values ( $3330 \pm 420 \text{ gC m}^{-2} \text{ yr}^{-1}$ ; *Figueira*

et al. 2008; Malhi et al. 2009), we find that JeDi-DGVM performs well when contrasting Amazon carbon pool and allocation flux estimates. The simulated ratio of autotrophic respiration to GPP (52%) was slightly less than the range of the observations ( $65 \pm 10\%$ ). The fractions of NPP allocated to each plant carbon pool correspond quite well with the observed allocation patterns. The simulated turnover times for the woody pools (37 years) closely matches the the mean of the observations ( $40 \pm 4$  years) from Malhi et al. (2009). Other studies, however, have suggested much longer wood turnover times ( $\sim 90$  years) (Vieira et al. 2004; Figueira et al. 2008). The simulated stock of coarse woody debris ( $2421 \text{ gC m}^{-2}$ ) closely matches the range of observed values ( $2421 \pm 560 \text{ gC m}^{-2}$ ). The mean simulated soil carbon stock ( $23460 \text{ gC m}^{-2}$ ) for this region is significantly greater than the mean of the observations to 2 m depth ( $14260 \pm 2728 \text{ gC m}^{-2}$ ; Malhi et al. 2009). However, Quesada et al. (2009) presents evidence for substantial carbon storage below that depth, including a soil carbon stock of  $22000 \text{ gC m}^{-2}$  to 3 m depth at the Tapajós site.

#### 3.4.11 Sensitivity to elevated atmospheric $\text{CO}_2$

Globally, simulated NPP increased by 18% during the first five years of simulated  $\text{CO}_2$  enrichment at 550ppm, exhibiting a large step change in the first year. Not surprisingly, simulated net terrestrial carbon uptake also quickly rose to  $15.03 \text{ PgC yr}^{-1}$  during that time. These values are similar to those exhibited by CLM-CASA' (17% and  $12.5 \text{ PgC yr}^{-1}$ ). During the same time period (1997-2001), mean NPP increased by  $15 \pm 1\%$  at the model grid cells corresponding to the four temperate forest FACE experiments reported in Norby et al. (2005). The observed increase at those sites was higher,  $27 \pm 2\%$ . The geographic variation of NPP enhancement (Fig. 3.16) is broadly similar to the pattern simulated by the global vegetation model LPJ-GUESS (Hickler et al. 2008), with the strongest enhancement occurring in tropical forest regions. JeDi-DGVM performed reasonably well on this metric with a score of 6.9/10. This was close to the performance of CLM-CASA' and significantly better than CLM-CN.

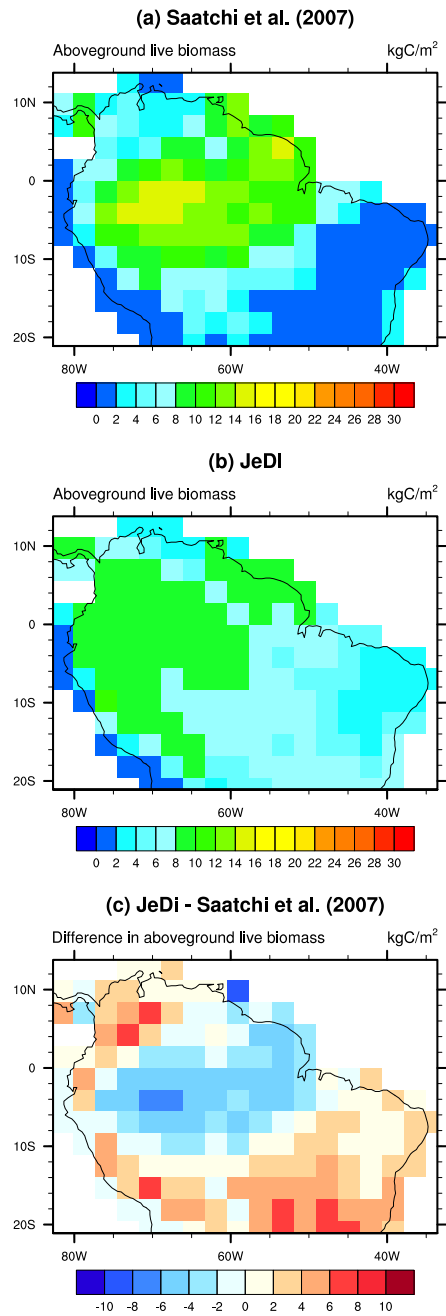


**Figure 3.14:** Aboveground live biomass in the Amazon basin from (a) observation-based estimates using plot measurements and remote sensing data (Saatchi et al. 2007); (b) as simulated by JeDi-DGVM at model year 2000; and (c) the difference between the observation-based estimates and the JeDi-DGVM model output.

### 3.4 RESULTS AND DISCUSSION

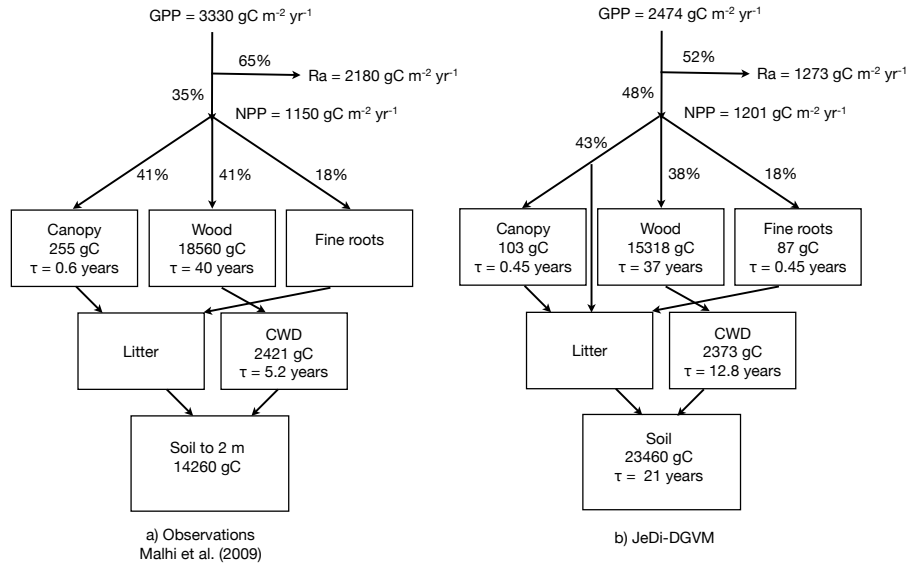


**Figure 3.15:** Carbon pools and fluxes in Amazonia from a) synthesis of observations (Malhi et al. 2009) and b) as simulated by JeDi-DGVM for years 1980-2004. GPP, gross primary productivity;  $R_a$ , autotrophic respiration; NPP, net primary productivity; CWD, coarse woody debris

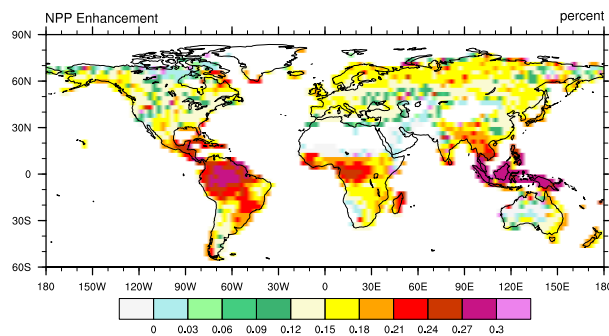


**Figure 3.16:** Geographic pattern of the simulated enhancement of net primary productivity (NPP) due to a step increase of atmospheric  $\text{CO}_2$  concentrations from ambient to 550 ppm. NPP values averaged over the period 1997-2001.

### 3.5 Summary of model evaluation

Overall, JeDi-DGVM received a score of 68.2 (out of 100 possible), exceeding the scores of the two PFT-based models (CLM-CASA'; 65.7 and CLM-CN; 58.4) evaluated in Randerston et al. (2009). The scores of the individual metrics are summarized in Table 3.1. JeDi-DGVM matched or exceeded the performance of at least one of the other models on almost every metric. The two exceptions were the comparisons with estimates of interannual terrestrial carbon exchange and fire emissions. The results of this evaluation imply that that the bottom-up functional trade-off approach of JeDi-DGVM, linked with an aggregation mechanism based on the 'biomass-ratio' hypothesis, is capable of simulating the broad-scale patterns of terrestrial biogeochemistry at least as well as two other state-of-the-art terrestrial biosphere models based on the dominant PFT paradigm. We have also shown that unlike PFT-based DGVMs, JeDi-DGVM is able to mechanistically represent the large-scale biogeographical patterns of plant species richness, community evenness, and relative abundance distributions, opening avenues to explore the impacts of future climate variability on terrestrial ecosystem composition and function in a much less constrained way than has been previously performed.

## Chapter 4

# Quantifying functional diversity-biospheric functioning relationships

### 4.1 Introduction

Ecologists have long suspected that plant functional diversity influences the magnitude and variability of ecosystem functioning. This thinking is well illustrated by a passage from Charles Darwin's unfinished manuscript *Natural Selection*, which was later edited and published nearly 100 years after his death (Darwin 1987):

We may . . . assert that a greater absolute amount of life can be supported; . . . when life is developed under many & widely different forms, than when under a few & allied forms; – the fairest measure of the amount of life, being probably the amount chemical composition within a given period. Imagine the case of an island, peopled with only three or four plants of the same order all well adapted to their conditions of life, & by three or four insects of the same order; the surface would no doubt be pretty well clothed with plants & there would many individuals of these species; . . . but assuredly there would seasons of the year, peculiar & intermediate stations, . . . which would not be well searched for food, & the amount of life would be consequently less, than if our island had been stocked with hundreds of forms, belonging to the most diversified orders.

Field and laboratory experiments in the last several decades have confirmed Darwin's thinking. Diversity manipulation experiments have shown that higher levels of functional diversity lead to higher ecosystem productivity (Cardinale et al. 2011; Hooper et al. 2005; Hector et al. 1999; Flombaum and Sala 2008) and lower temporal variability of ecosystem functioning (Tilman et al. 2006; Proulx et al. 2010; Ives and Carpenter

2007; Balvanera et al. 2006). There is a growing consensus in the ecological science community that human-induced biodiversity loss is a threat to the ecosystem services we rely upon and thus our well-being (Díaz et al. 2006). At the same time, the loss of species and, more importantly, the functional traits of those species is likely going to reduce the ability of ecosystems to adapt to environmental changes including ongoing global warming (Elmqvist et al. 2003). This ability of ecosystems to adapt to changes and to maintain their functioning in the face of those change is referred to as resilience (Peterson et al. 1998).

In many ways, current global vegetation models (Dynamic Global Vegetation Models, DGVMs) based on the PFT paradigm are simulating Darwin’s island. DGVMs reduce the immense functional diversity of terrestrial vegetation to handful of PFTs. Recent studies using trait data collected and compiled from all over the globe have shown that for several functional traits, there is greater variation within PFTs than between PFTs (Wright et al. 2005; Reich et al. 2007; Kattge et al. 2011). Current models, however, can only use a single parameter value to represent this large within-PFT variation. Model-data assimilation studies (Groenendijk et al. 2011; Alton 2011) have shown that the coarse representation of functional diversity provided by these PFT schemes is insufficient for representing the full variability of vegetation parameters necessary to accurately represent carbon cycle processes.

Based on the growing consensus regarding biodiversity-ecosystem functioning relationships, we can hypothesize that PFT-based models would underestimate productivity and overestimate the response of terrestrial ecosystems to climatic variability and change. In this chapter, we contrast the magnitude and variability of net primary productivity and evapotranspiration fluxes of diverse communities to those of a single, but representative PFT. This is accomplished by running a diverse JeDi-DGVM simulation with many plant growth strategies and where the community fluxes are aggregated from the different strategies (the Community Weighted Functioning, "CWF" approach in the following) and another simulation wherein the functional diversity is reduced. This reduction is accomplished by recreating something like a PFT by simulating only a single plant growth strategy at each grid cell characterized by the community-weighted functional trait parameters from the diverse simulation (the Community Weighted Trait "CWT" approach in the following). The major difference between the two approaches is that in the CWT approach, the community-weighted mean trait values are fixed at the start of the simulation. In the CWF approach of the diverse communities, the relative abundances of the growth strategies change throughout the simulation as the climate becomes relatively more or relatively less favorable for its particular set of trait

values.

The two model simulations are investigated to evaluate the role of diversity in ecosystem functioning. We focus on three different aspects with regard to the functioning. We hypothesize that the diverse representation of the terrestrial biosphere leads to a higher productivity in the climatic mean, to greater time stability, and to greater resilience to large climatic perturbations. In the CWF approach, altered climatic conditions would favor different trait combinations that are better suited to these conditions. If, for instance, conditions become wetter, then this would favor trait combinations that can exploit the greater availability of moisture, for instance by enhancing allocation to leaves rather than roots. This is schematically shown by the blue line in Fig. 4.1. Likewise, when conditions become drier, productivity is likely to be reduced. The extent of this reduction can, however, be partly compensated by trait combinations that can achieve a higher productivity at lower water availability (shown by the red curve in Fig. 4.1). In other words, the diverse ecosystem would be better able to exploit current climatic conditions as well as altered conditions due to climatic variability or change. In contrast, the CWT approach only captures the average trait composition of the mean climate, implying that the vegetation that this approach represents would likely be best suited and most productive under climatic mean conditions. Any deviation from the mean climate, for instance drier or wetter conditions due to climate variability or change, the resulting trait combination would likely not be most suitable to the altered conditions. This is schematically illustrated in Fig. 4.1 on the right.

To demonstrate the potential importance of vegetation diversity to climate, we also evaluate these simulations with respect to the differences in evapotranspiration.

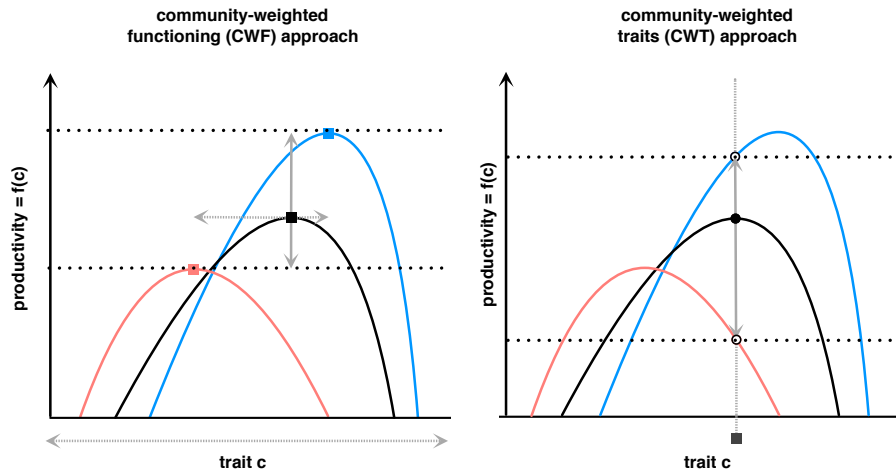


**Figure 4.1:** Conceptual diagram to illustrate the expected effect of diversity on productivity for altered climatic conditions. The left diagram shows the hypothesized outcome of a diverse community where the community fluxes are aggregated from the individual fluxes of the different trait combinations (the CWF approach). For present-day conditions (black curve), different trait values of a certain trait "c" are going to result in different values of the achieved productivity. As the trait combination that is most productive under current conditions is likely to be the most dominant as well, the community is likely to have a productivity near the maximum, as indicated by the black square. When the climatic conditions are altered to wetter or drier conditions (blue and red curves respectively), then the trait value that achieves highest productivity is likely to be different (as indicated by the blue and red squares). The right diagram shows the same reasoning but for the approach in which vegetation is represented by the community-weighted trait (CWT approach). Here, the community-weighted trait parameter would be fixed to the maximum for present-day conditions (black circle), and a change in climatic conditions is going to result in a reduced increase or greater decrease in productivity. Overall we would therefore expect lower productivity, less temporal stability, and lower ability to adapt in the CWT approach.

## 4.2 Methods

### 4.2.1 Simulation setup

We ran JeDi-DGVM with two different approaches for representing plant functional diversity, a community-weighted functioning (CWF) approach and a community-weighted traits (CWT) approach. The differences between the two approaches are described below. A schematic diagram illustrating the relationship between these two approaches is shown in Fig. 4.2.

We first ran JeDi-DGVM following the CWF approach, which is identical to the standard JeDi-DGVM approach for representing functional diversity described in Chapter 2. The development of two-thousand plant growth strategies were simulated indepen-

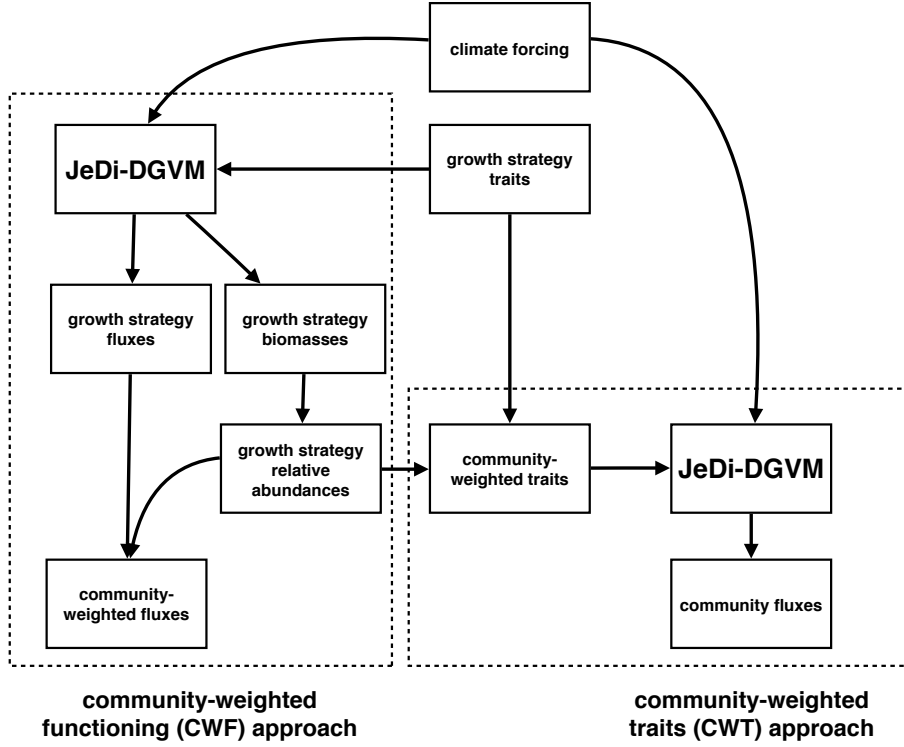


Figure 4.2: Schematic diagram of simulation set up.

dently and in parallel. Each growth strategy characterized by a vector of 15 functional trait parameters values ( $\mathbf{T}_k = [t_1, \dots, t_{15}]$ ), which determine its behavior in terms of carbon allocation, phenological response times, and other morphological and metabolic aspects. The trait values of each growth strategy were randomly-chosen from their complete theoretical or observed ranges as described in Chapter 2.3. In the CWF approach, diagnostic grid-cell scale variables are calculated at each timestep by averaging the fluxes and properties of all surviving plant growth strategies at that grid cell, weighting each its current mass-based relative abundances. The relative abundance  $p_{ij}$  (Eq. 4.1) of each surviving growth strategy  $i$  in a given grid cell  $j$  is proportional to its living biomass  $BM_{ij}$  at that grid cell relative to the sum of the living biomass of all surviving growth strategies  $S$  in that grid cell. The living biomass of a growth strategy being the sum of its leaf, fine root, woody, and storage carbon pools. Thus, the relative abundances within a plant community range between zero and one and the sum of the abundances is one.

$$p_{ij} = \frac{BM_{ij}}{\sum_{k=1}^S BM_{kj}} \quad (4.1)$$

Following Garnier et al. (2004), we refer to these diagnostic grid-cell scale variables as community-weighted fluxes (or properties). As an example, the  $NPP_{ij}$  of each growth strategy  $i$  at a grid cell  $j$  is a function of its traits parameter values  $\mathbf{T}_i$  and the environment forcing variables  $\mathbf{X}_j$ . The community-weighted NPP<sup>1</sup>  $\langle NPP_j \rangle$  for that grid cell is the sum of the NPP fluxes of all growth strategies  $S$  at that grid cell, weighting the contribution of each growth strategy by its mass-based relative abundance  $p_{i,j}$ :

$$\langle NPP_j \rangle = \sum_{i=1}^S p_{i,j} NPP_{ij} = \sum_{i=1}^S p_{i,j} f(\mathbf{T}_i, \mathbf{X}_j). \quad (4.2)$$

In the CWT approach, we use the time-averaged relative abundances  $\overline{p_{ij}}$  from the CWF simulation to calculate the community-weighted mean trait parameters ( $\langle \mathbf{T}_j \rangle = \sum_{i=1}^S \overline{p_{ij}} \mathbf{T}_i$ ) at each grid cell  $j$ . We then run JeDi-DGVM with just one plant growth strategy at each grid cell characterized by the community-weighted mean trait vector  $\langle \mathbf{T}_j \rangle$ . Continuing the example from above, the community NPP  $NPP_j$  in the CWT approach is a function of the community-weighted mean trait vector  $\langle \mathbf{T}_j \rangle$  from the the CWF approach and the same environment forcing variables  $\mathbf{X}_j$ :

$$NPP_j = f(\langle \mathbf{T}_j \rangle, \mathbf{X}_j) = f\left(\sum \overline{p_{ij}} \mathbf{T}_i, \mathbf{X}_j\right). \quad (4.3)$$

For both approaches, JeDi-DGVM was run on a global grid at a spatial resolution of approximately  $2.8^\circ$  by  $2.8^\circ$  resolution, covering all land areas except Antarctica. The model was forced at a daily time step with downward shortwave and longwave radiation, precipitation, and near-surface air temperature from an improved NCEP/NCAR atmospheric reanalysis dataset (Qian et al. 2006). The atmospheric  $\text{CO}_2$  concentration was fixed at 380 ppm throughout all simulations. We looped through the reanalysis dataset for 1000 years, allowing the vegetation carbon pools to reach a quasi-steady state. We used only the last 100 years of model output to evaluate the differences between the two approaches.

We also ran two additional 100 year perturbation simulations for both approaches to investigate the role of modelled functional diversity on ecosystem resilience to sudden climatic change. These perturbation simulations were branched from the end of the spin-up simulations described above. In the first perturbation, we reduced the precipitation at each time step by 50%. In the second perturbation, we added  $2^\circ$  C to the air

---

<sup>1</sup>We adopt chevron notation (e.g.  $\langle NPP_j \rangle$ ) to denote community-aggregated fluxes and properties.

temperature.

### 4.2.2 Diversity measures

We calculated three functional diversity measures for each grid cell of the CWF simulation. We use these diversity measures in the following section to help understand the differences between the CWT and CWF simulations.

The functional richness (FR) at each grid cell is derived from the number of surviving growth strategies (Fig. 4.3a). The FR is normalized by the maximum number of surviving PGSs in any of the grid cells. Here, survival is defined as maintaining a positive balance of stored assimilates. Thus, FR varies between zero for grid cells with no surviving PGSs and one at the grid cell (or grid cells) with the maximum number of growth strategies.

Functional evenness (FE) at each grid cell is calculated following the Pielou index (Pielou 1966), which is the the Shannon entropy of the relative abundances  $p_i$  of the  $S$  surviving growth strategies within that grid cell, normalized by the maximized possible Shannon entropy for that community (i.e. when all growth strategies are equally abundant). A map of simulated FE is shown in Fig. 4.3b.

$$FE = \frac{\sum_{i=1}^S p_i \ln p_i}{\ln S} \quad (4.4)$$

FE approaches zero as more and more plant biomass is found in only one or a few growth strategies. FE is set to zero when there is one or no surviving growth strategies. The Shannon entropy of a given community is basically a measure of uncertainty in predicting the relative abundances of the growth strategies that compose the relative abundance vector  $\mathbf{p} = (p_1, p_2, \dots, p_S)$ .

Functional dispersion (FD) is calculated as the weighted mean Euclidean distance of all growth strategies to the community-weighted centroid of all growth strategies in

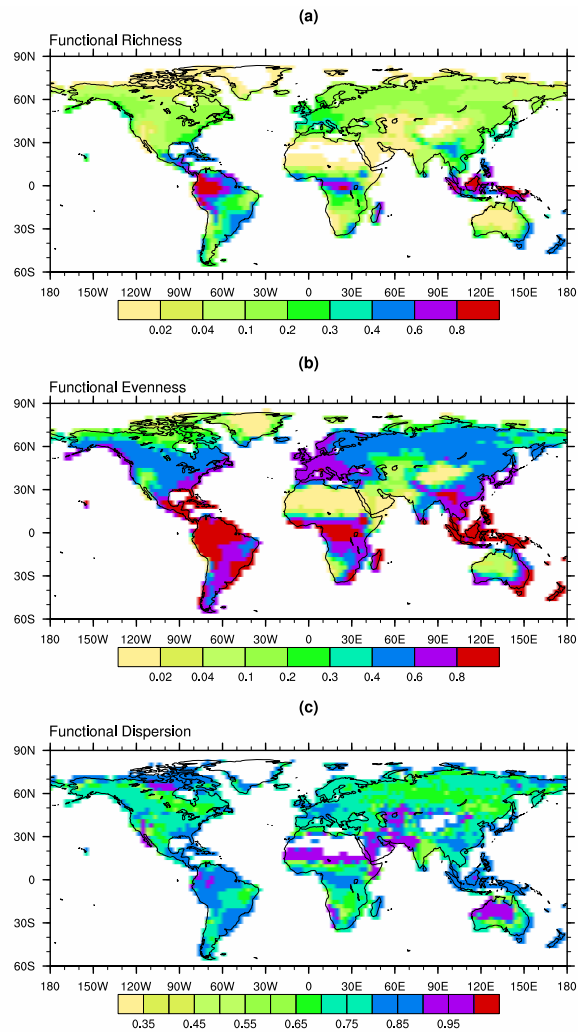


**Figure 4.3:** Simulated geographic patterns of a) functional richness (FR), b) functional evenness (FE), and c) functional dispersion (FD). Functional richness values are normalized by the maximum simulated FR value.

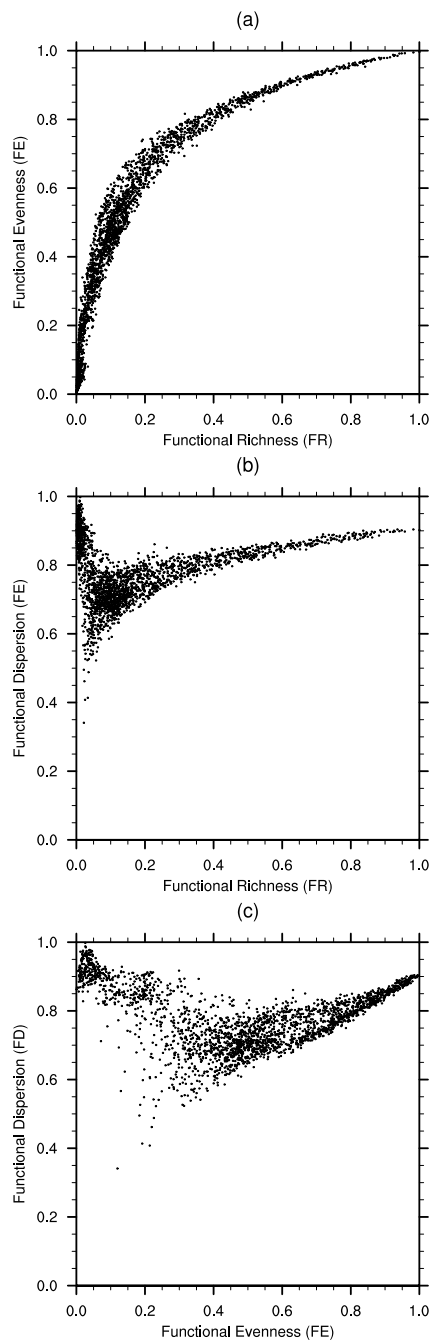


**Figure 4.4:** Simulated relationships between a) functional richness (FR) and functional evenness (FE), b) functional richness (FR) and functional dispersion (FD), and (c) functional evenness (FE) and functional dispersion (FD). Functional richness (FR) values are normalized by the maximum simulated FR value.

multidimensional trait space (4.3c):

$$z_i = \|\mathbf{T}_i - \langle \mathbf{T} \rangle\| = \sqrt{\sum_{k=1}^n (t_{ik} - \langle t_k \rangle)^2} \quad (4.5)$$

$$FD = \sum_{i=1}^S p_i z_i \quad (4.6)$$

$$(4.7)$$

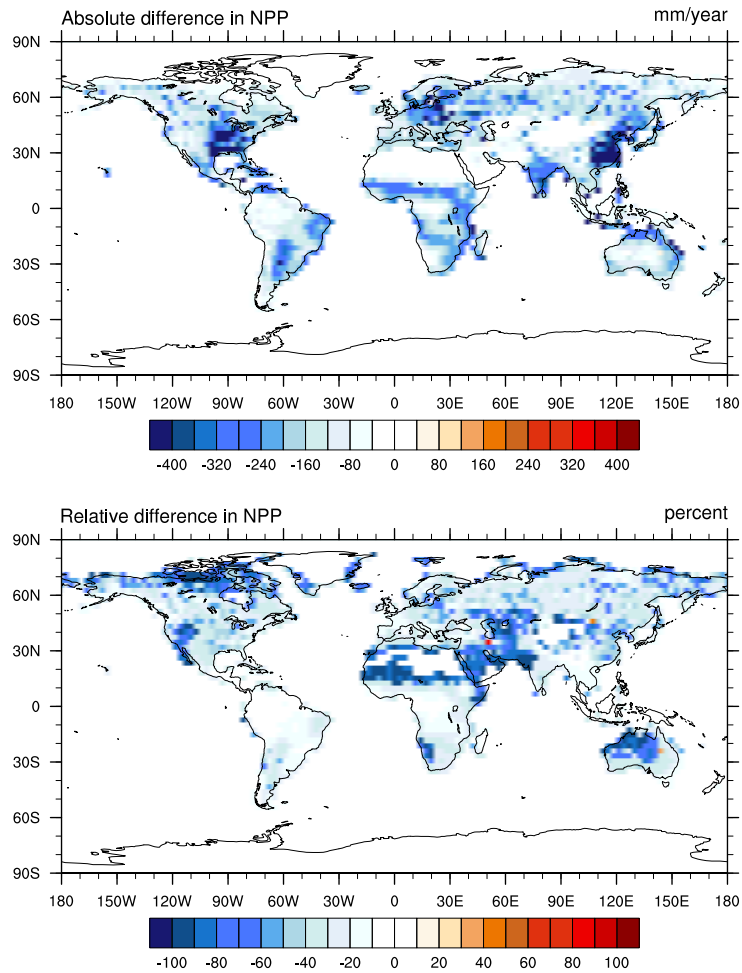
where  $p_i$  is the relative abundance of growth strategy  $i$ , and  $z_i$  is the distance of growth strategy  $i$  to the community-weighted centroid  $\langle \mathbf{T} \rangle$  (Laliberté and Legendre 2010). FD is low when the most abundant growth strategies (possibly the only surviving growth strategies) are all near the centroid. FD is highest when the community biomass is dominated by a few growth strategies that differ widely in their trait values.

## 4.3 Results

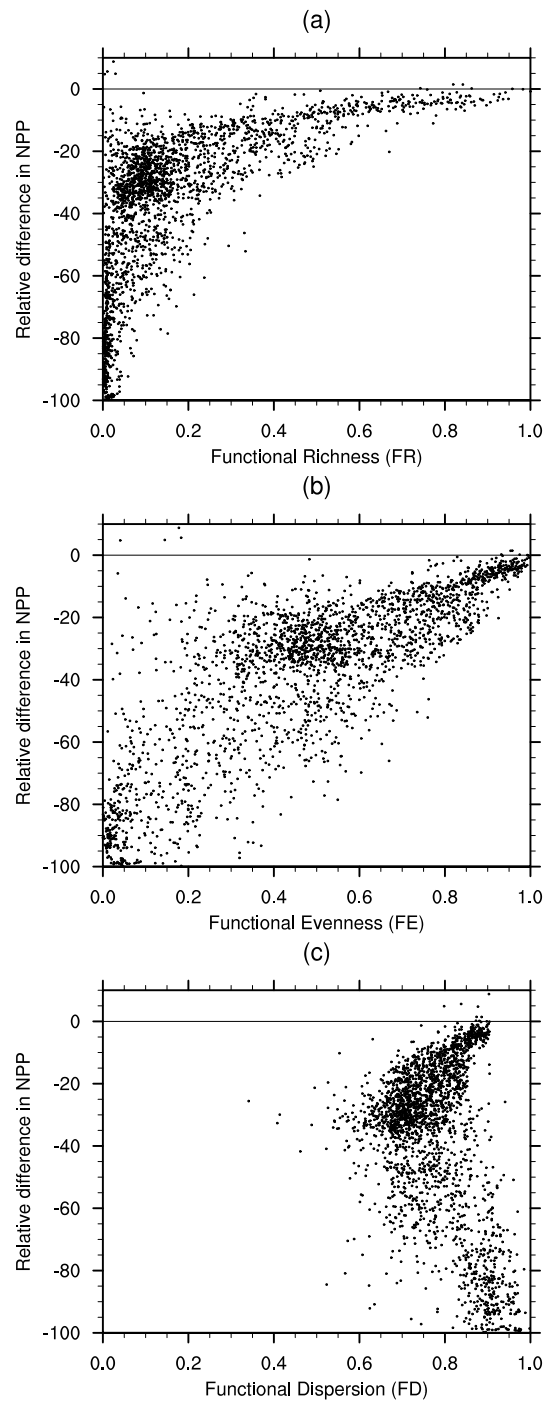
### 4.3.1 Differences in mean productivity and evapotranspiration

Fig. 4.5 shows the absolute difference (top) and relative difference (bottom) between the CWT and CWF simulations in mean NPP. The CWT simulation yielded lower NPP than the CWF simulation in nearly all regions, however, the magnitude of this decrease varies spatially. The relative difference in NPP varies nearly quite strongly with FR and FE (Figs. 4.6a and 4.6b), grid cells with more surviving growth strategies and strategies with more evenly distributed community biomass tend to have less difference in productivity between the CWT and the CWF approaches. The relative decrease in NPP is strongest in arid and arctic regions with high FD (Fig. 4.6c), i.e. regions where the distribution of community biomass is dominated by a few growth strategies with widely different in one or more trait parameter values. In fact, in some of these high FD grid cells, the CWT simulation shows no NPP, indicating that the growth strategy in the CWT simulation with community-weighted mean trait parameters from the CWF simulation is not able to survive. The absolute differences in productivity are most pronounced in the semi-arid tropical grassland and the temperate forests of eastern North America, Europe, and east Asia.

Fig. 4.7 shows the absolute differences (top) and relative differences (bottom) in the mean ET fluxes. Unlike the NPP fluxes, the ET fluxes in the CWT simulations



**Figure 4.5:** Geographic patterns of the (top) absolute and (bottom) relative differences between mean net primary productivity (NPP) as simulated by the community-weighted trait (CWT) and community-weighted functioning (CWF) approaches. These are the differences in the mean NPP averaged over the last 100 years of the simulations. The relative difference is calculated as the mean productivity of the CWT simulation minus the mean productivity of the CWF simulation, divided by the mean productivity of the CWF simulation.



**Figure 4.6:** The relative difference in percent between the mean net primary productivity (NPP) simulated by the community-weighted trait (CWT) and community-weighted functioning (CWF) approaches plotted against the three measures of functional diversity: a) functional richness (FR), b) functional evenness (FE), and c) functional dispersion (FD).

are generally higher than in the CWF simulations. However, the strength of these differences varies spatially and there are some regions where the ET flux is lower in the CWT simulations. Also, the magnitude of these differences in relative terms, however, is much less than for the NPP. For the ET fluxes, the patterns of absolute and relative difference between the two simulations are quite similar. The absolute differences are greatest in the tropics where the magnitude of the ET flux itself is highest. The greatest absolute differences are generally in the tropical forests, especially the seasonal dry forests of South America and southeast Asia, where the the land surface evapotranspires more than 100 mm per year more in the CWT simulation than in the CWF simulation. This corresponds to a relative increase of ET of about 10%. Larger relative differences approaching 20% are found in the more temperate regions of western Europe, New Zealand, and Chile.

The relationships between the relative differences in ET and the functional diversity metrics (Fig. 4.8) are weaker and less clear than those for the relative differences in NPP. There is a hump pattern in the relationships between the relative difference in ET and the FR and FE diversity metrics, with low or negative relative differences at the sites with the lowest FR and FE and the most pronounced relative difference at intermediate richness and evenness, and again a reversion towards no change in ET when approaching the grid cells with the highest FR and FE values. There is almost no difference between the two approaches in the ET fluxes in the aseasonal and constantly moist western Amazon basin, the region with the highest FR and FE values. Unlike with NPP, the ET fluxes were also quite similar between the two approaches in regions with the highest FD values.

#### 4.3.2 Differences in variability of productivity and evapotranspiration

Fig. 4.9 shows the relative differences between the CWT and CWF simulation in the interannual (top) and intraannual (bottom) variability of NPP. Fig. 4.10 shows the same relative differences for the ET fluxes. The variability of the NPP and ET fluxes, both interannual and intraannual, in the CWT simulation is generally higher than in CWF simulation, although the spatial patterns vary between the the two fluxes and the two measures of variability. There are no clear global relationships between the relative differences in NPP or ET variability and the three functional diversity metrics.

The largest relative differences in the interannual variability of NPP ( $> 200\%$  +) occur in the desert and arctic regions with high FD values, however, the temperate/boreal forests and non-tropical grasslands also see strong positive relative differences. There

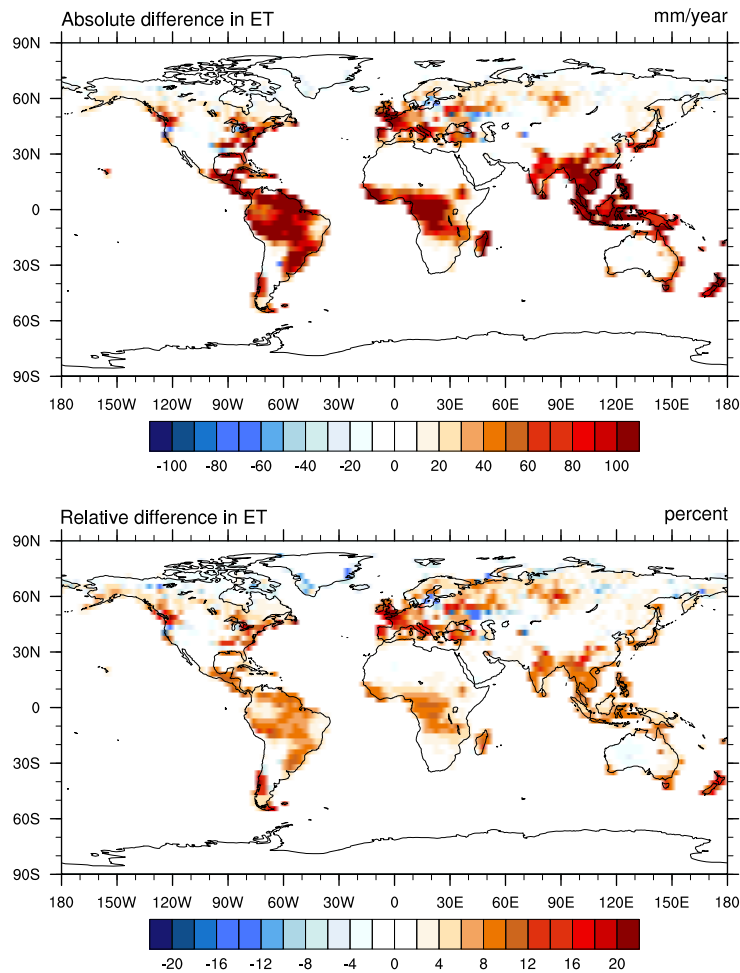


**Figure 4.7:** Geographic patterns of the a) absolute and b) relative differences between the mean evapotranspiration (ET) as simulated by the community-weighted trait (CWT) and community-weighted functioning (CWF) approaches.

is little difference between the CWT and CWF approach in the interannual variability of NPP in the tropical forests and grasslands of South America, Africa, and southeast Asia. That spatial pattern is somewhat reversed for the relative differences in the intraannual variability of NPP, with the greatest relative differences in the intraannual variability of NPP occurring in the seasonal dry forests in eastern Amazon basin, central Africa, and southeast Asia. The positive differences in intraannual variability of NPP are also smaller in the boreal and temperate forest regions of the northern hemisphere, and even negative in a few desert grid cells.

The interannual variability of ET is much greater in the CWT simulation than the

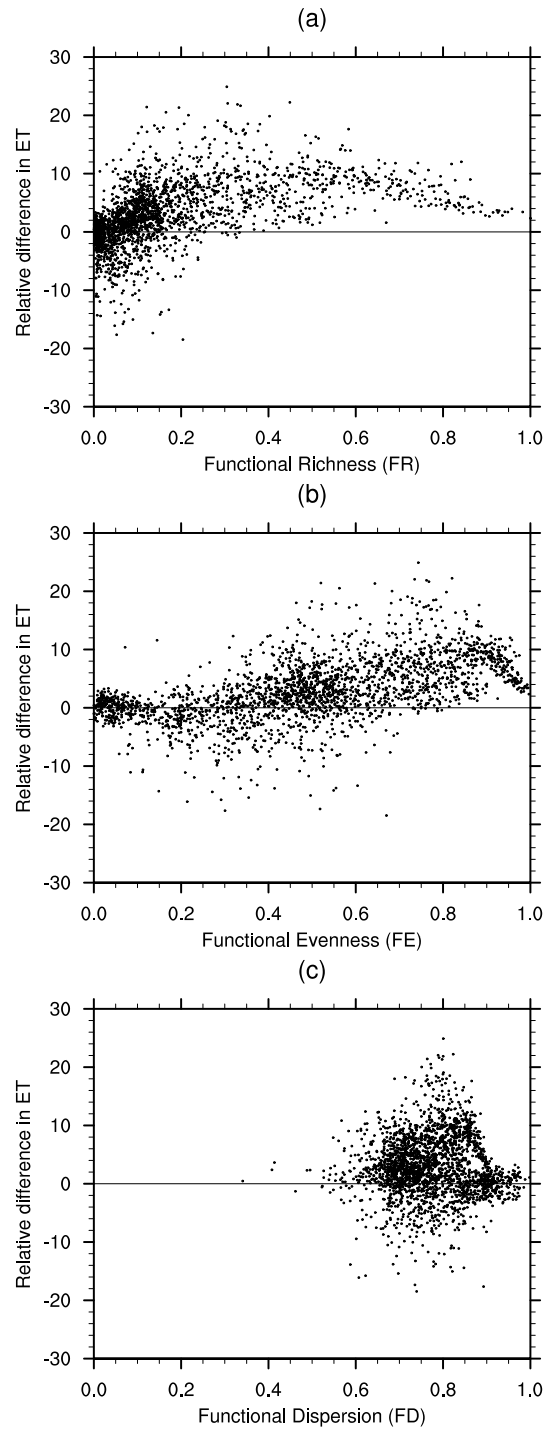


**Figure 4.8:** The relative difference in percent between the mean evapotranspiration (ET) simulated by the community-weighted trait (CWT) and community-weighted functioning (CWF) approaches plotted against the three measures of functional diversity: a) functional richness (FR), b) functional evenness (FE), and c) functional dispersion (FD).

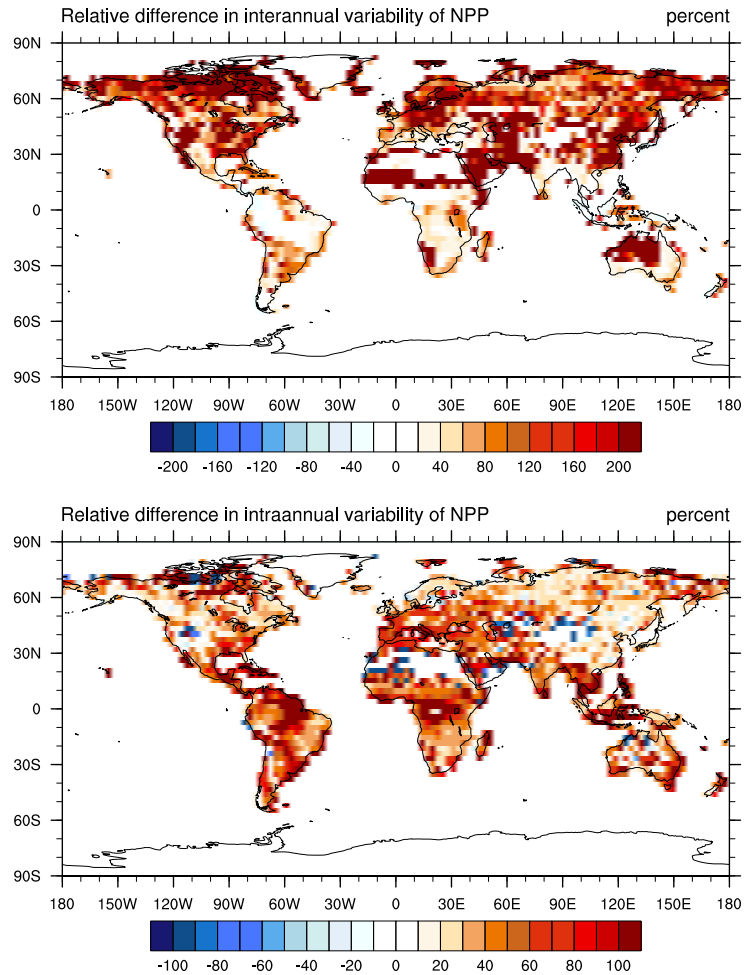


**Figure 4.9:** Geographic patterns of the relative differences the (top) interannual and (bottom) intraannual variability of net primary productivity (NPP) as simulated by the community-weighted trait (CWT) and community-weighted functioning (CWF) approaches. The interannual variability is calculated as the coefficient of variation (CV) of the yearly mean NPP values. The intraannual (or seasonal) variability is calculated as the CV of the multi-year monthly means, that is the CV of the vector of length 12 containing the mean NPP values across all Januaries, all Februaries, and so on.

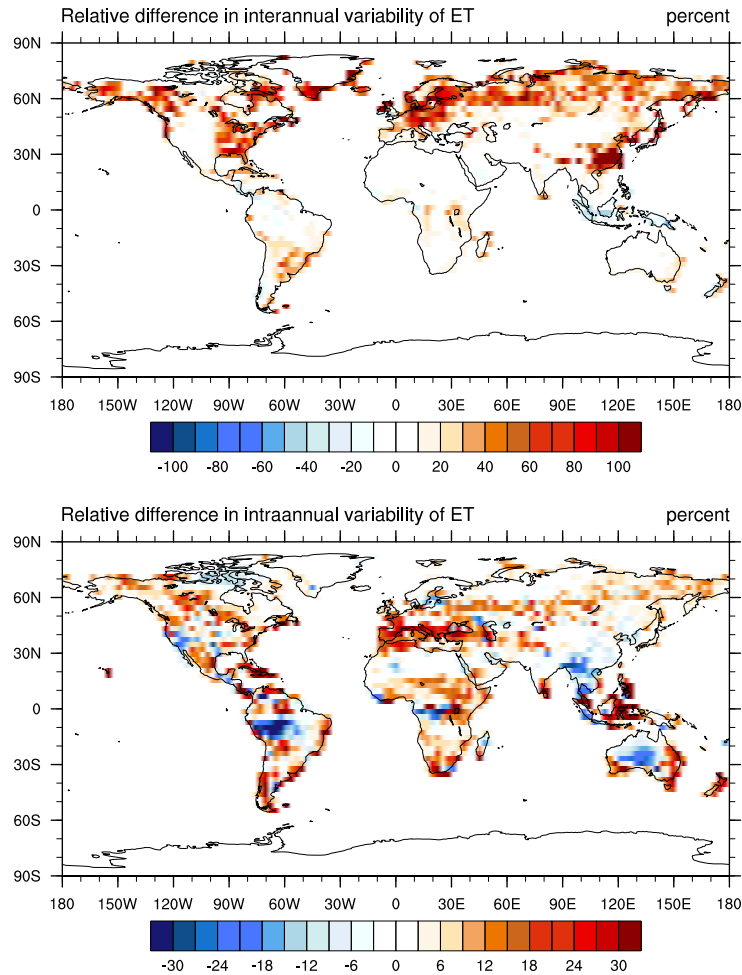


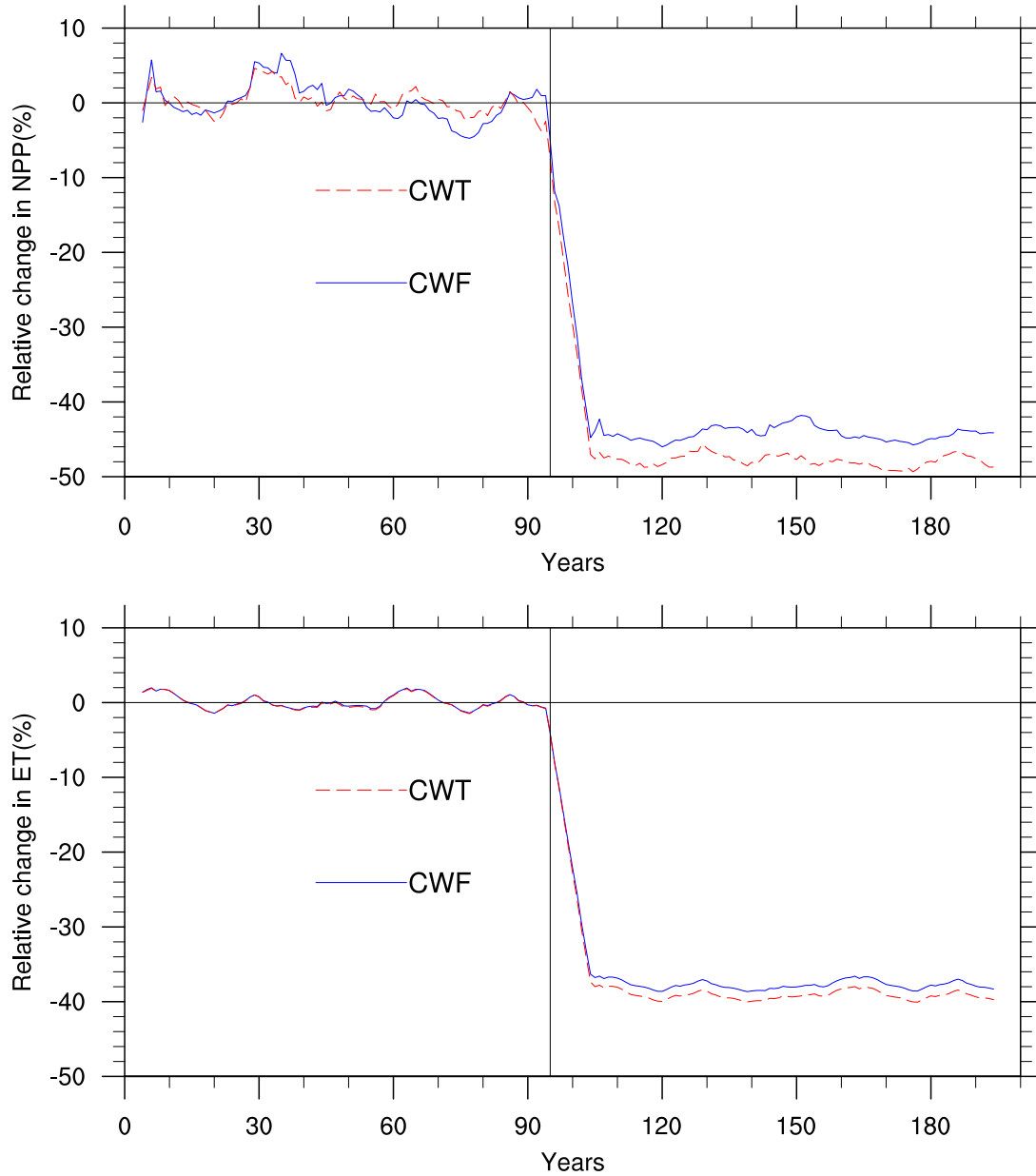
**Figure 4.10:** Geographic patterns of the relative differences the (top) interannual and (bottom) intraannual variability of evapotranspiration (ET) as simulated by the community-weighted trait (CWT) and community-weighted functioning (CWF) approaches. The interannual variability is calculated as the coefficient of variation (CV) of the yearly mean ET values. The intraannual (or seasonal) variability is calculated as the CV of the multi-year monthly means, that is the CV of the vector of length 12 containing the mean ET values across all Januaries, all Februaries, and so on.

CWF simulation throughout the temperate and boreal forest regions of North America and Eurasia, more than 100% greater in some grid cells. There is little difference in the interannual variability of ET in the tropics and arid region. The differences in the intraannual variability of ET are more mixed. In some regions, e.g. around the Mediterranean, the intraannual variability of ET is more than 25% greater in the CWT simulation, while in other regions, e.g. the southern part of Amazon basin, it is 25% less. There is no clear global trend relating the differences in the variability of ET and any of the three functional diversity measures.

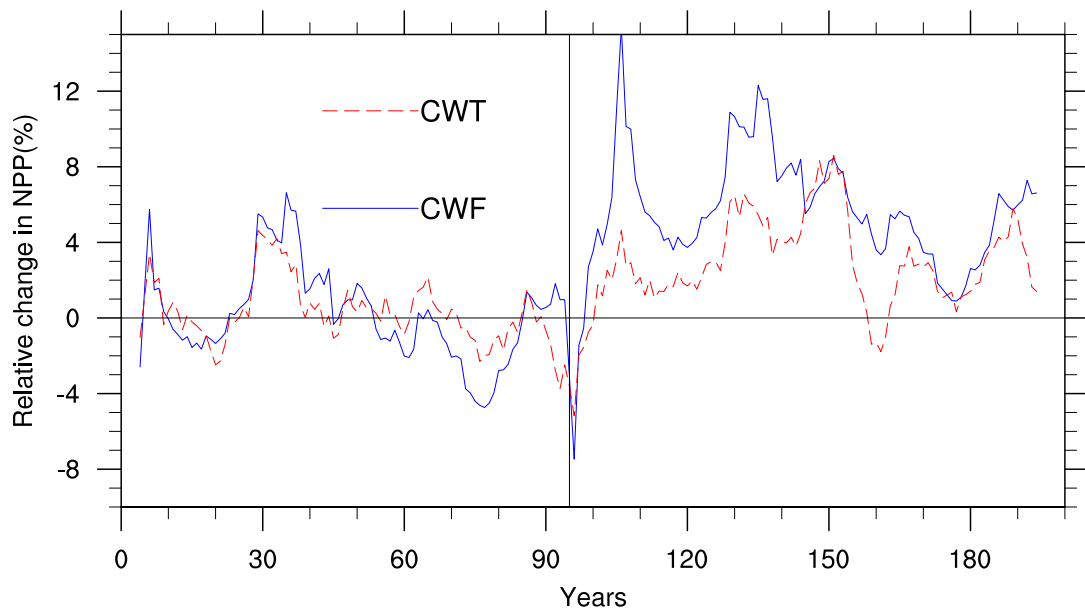
### 4.3.3 Differences in the resilience of the biosphere to climatic perturbation

Fig. 4.11 shows the simulated changes in global mean terrestrial NPP and ET over the course of the first perturbation experiment in which the precipitation forcing was reduced by 50%. The changes shown are relative to the long-term means of each flux prior to the imposing perturbation. Global mean NPP and ET fell significantly in both the CWT and CWF simulations after reducing the precipitation. The simulated fluxes associated with the diverse CWF simulation, however, were less affected by the perturbation than the sparse CWT simulation. The NPP and ET fluxes decreased across all regions (Fig. 4.13 and 4.14, although the magnitude of these decreases varied spatially. As one might expect, the semi-arid and arid regions showed the greatest response to the reduction in precipitation in both simulations. The smallest changes in both the CWT and CWF simulations are found in moist regions (e.g. tropical rainforest, boreal forests).

Fig. 4.12 shows the simulated change in global mean terrestrial NPP over the course of the second perturbation experiment in which a 2 degree warming was applied. Global mean There was little difference between the two approaches in the global mean change in ET after the warming perturbation. In the sparse PFT-like CWT simulation, the warming resulted in lower NPP throughout the tropics (Fig. 4.15a) and mixed results elsewhere. The diverse CWF simulation showed little change in NPP in the tropics (Fig. 4.15b) and consistently positive changes throughout colder regions. The changes in ET after the warming were relatively smaller (Fig. 4.16) than the changes in NPP in both simulations.



**Figure 4.11:** Relative change in terrestrial net primary productivity (NPP; top) and evapotranspiration (ET; bottom) from the mean of the control period as simulated by the community-weighted trait (CWT; red dashed line) and community-weighted functioning (CWF; blue solid line). The vertical black line denotes when the start of the simulated perturbation (50% decrease in precipitation). The horizontal black line denotes zero relative change. A 10 year running mean has been applied to both lines to improve clarity.



**Figure 4.12:** Relative change in terrestrial net primary productivity from the mean of the control period as simulated by the community-weighted trait (CWT; red dashed line) and community-weighted functioning (CWF; blue solid line). The vertical black line denotes when the start of the simulated perturbation ( $+2^{\circ}$  C warming). The horizontal black line denotes zero relative change. A 10 year running mean has been applied to both lines to improve the clarity.

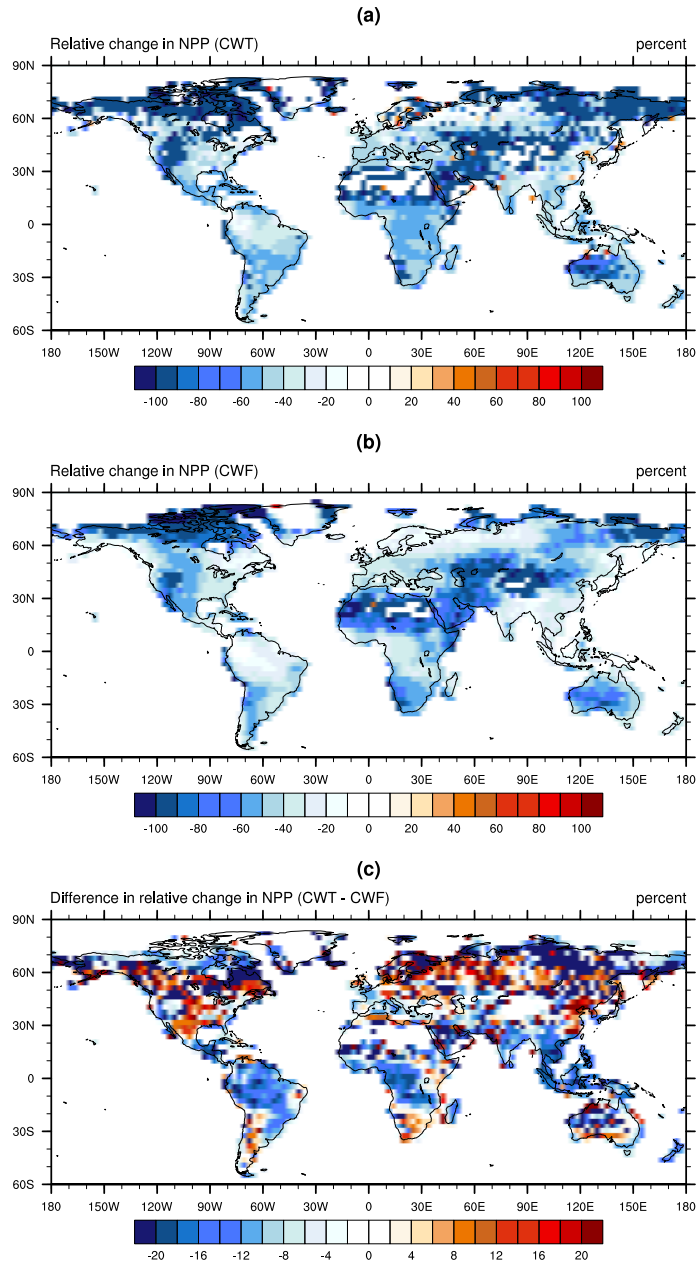


**Figure 4.13:** Relative change in net primary productivity (NPP) between the mean of the control period and the last 30 years of the 50% precipitation reduction perturbation experiment as simulated by the community-weighted trait (CWT; top) and community-weighted functioning (CWF; middle). The bottom plot shows the difference in relative change between the two approaches (CWT minus CWF).

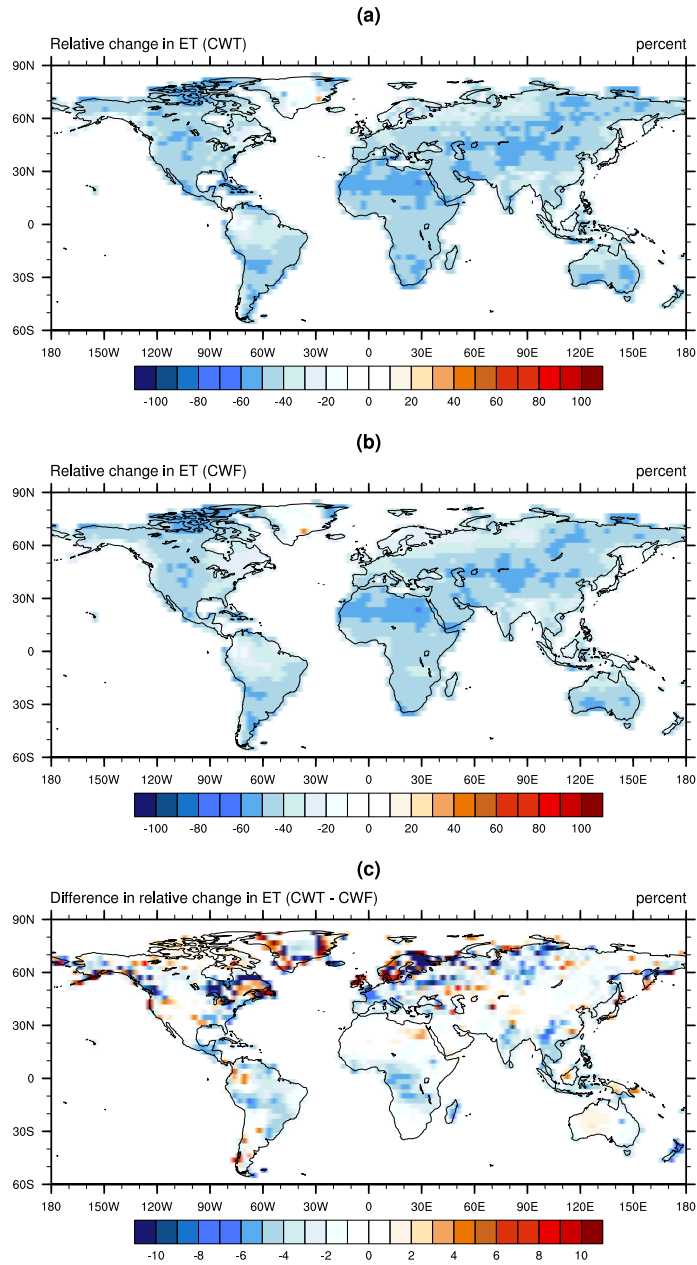


**Figure 4.14:** Relative change in evapotranspiration (ET) between the mean of the control period and the last 30 years of the 50% precipitation reduction perturbation experiment as simulated by the community-weighted trait (CWT; top) and community-weighted functioning (CWF; middle). The bottom plot shows the difference in relative change between the two approaches (CWT minus CWF).

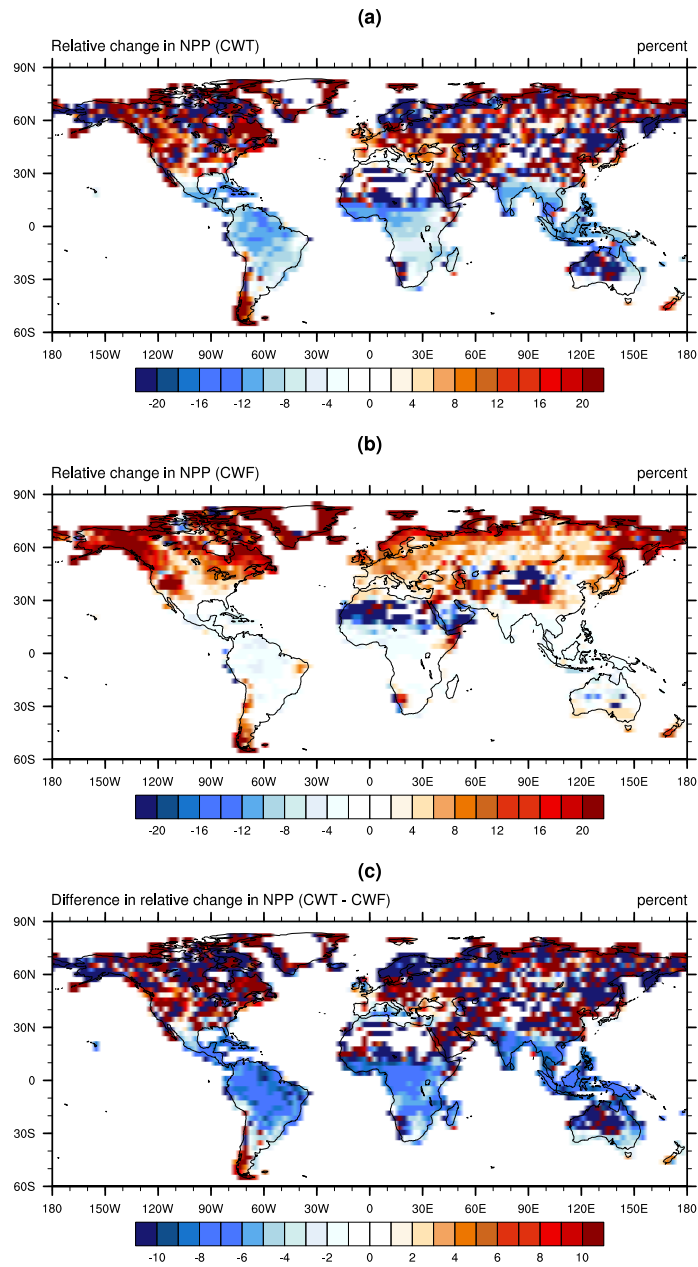


**Figure 4.15:** Relative change in net primary productivity (NPP) between the mean of the control period and the last 30 years of the  $+2^{\circ}\text{C}$  warming perturbation experiment as simulated by the community-weighted trait (CWT; top) and community-weighted functioning (CWF; middle). The bottom plot shows the difference in relative change between the two approaches (CWT minus CWF).

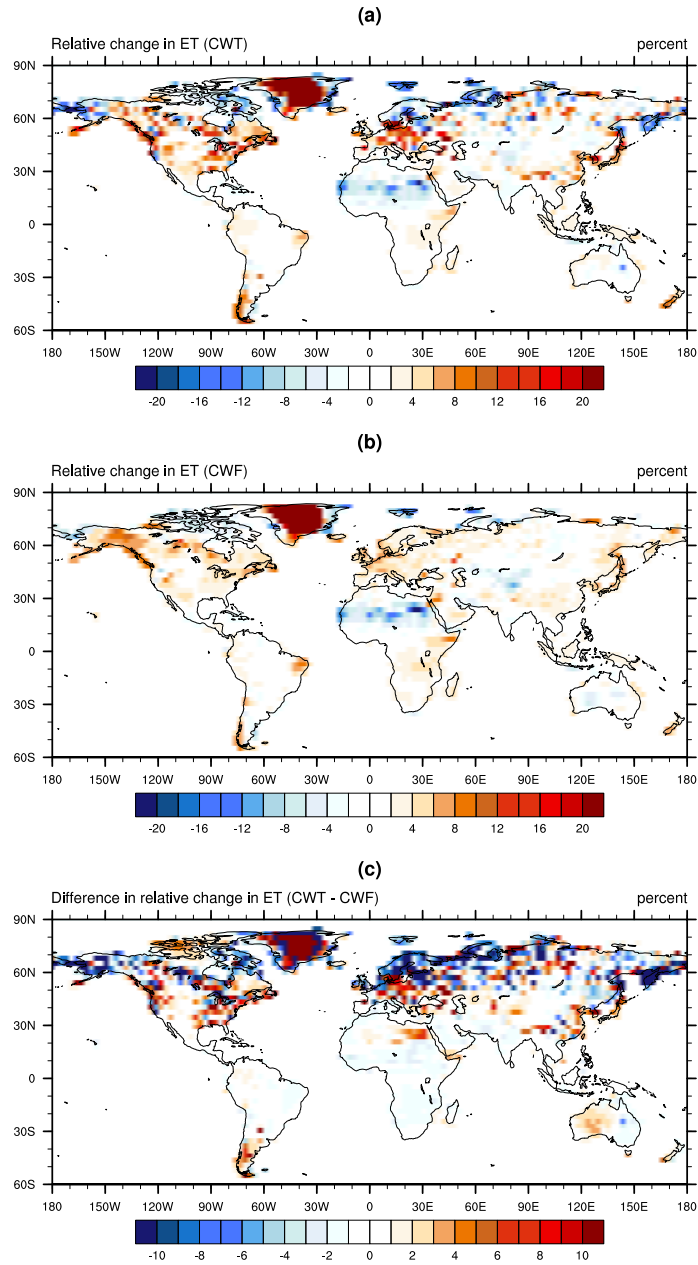


**Figure 4.16:** Relative change in evapotranspiration (ET) between the mean of the control period and the last 30 years of the  $+2^{\circ}\text{C}$  warming perturbation experiment as simulated by the community-weighted trait (CWT; top) and community-weighted functioning (CWF; middle). The bottom plot shows the difference in relative change between the two approaches (CWT minus CWF).

## 4.4 Discussion

This comparison of a diverse representation of functional diversity (CWF approach) and coarse representation of functional diversity (CWT approach) yielded three major results. The diverse approach resulted in (i) higher temporal mean vegetation productivity and water-use efficiency, (ii) a lower temporal variance of vegetation productivity and evapotranspiration, and (iii) a more adaptive response to climatic perturbations leading to more positive or less negative changes in productivity and evapotranspiration. These insights are consistent with the ecological understanding of diversity-ecosystem functioning relationships and are discussed in more detail in the following subsections.

### 4.4.1 Diversity-Productivity

The simulations showed that the diverse CWF approach yields higher temporal mean productivity. This is consistent to what we hypothesized in the introduction of this chapter (see Fig. 4.1). This effect of diversity on productivity is known as the diversity-productivity hypothesis in ecological theory. This result of the JeDi-DGVM is surprising to some extent because the model does not account for facilitation, i.e. the beneficial effects of one growth strategy on another.

We found that this productivity-enhancing effect was strongest in regions with the highest FD. These are regions where the distribution of community biomass is dominated by a few growth strategies which differ widely in one or more trait parameter values. With a greater productivity, the diverse simulations also exhibited a greater water-use efficiency (i.e. lower evapotranspiration flux relative to ecosystem productivity). This effect was strongest in tropical ecosystems. These results would imply that the coarse representation of functional diversity in current PFT-based DGVMs may lead to an underestimation of productivity and water-use efficiency.

### 4.4.2 Diversity-Variability

The simulations showed that the diverse CWF approach exhibits less temporal variation in both productivity and evapotranspiration. This is the case for interannual variations as well as seasonal variations within the year. This is again consistent to what we hypothesized in the introduction and with previous diversity-manipulation experiments (Tilman et al. 2006; Proulx et al. 2010; Allan et al. 2011) and models in theoretical ecology (Tilman et al. 1998; Naeem 1998; Doak et al. 1998; Yachi 1999).

To some extent, these results are mathematically inevitable due to the averaging and negative covariance effects. The growth strategy that does best in the mean climate, can not necessarily be the most productive during drier or wetter years. In the contrary, species that do better during wet periods, for instance by allocating more to leaf growth can not also do better during dry periods, when possibly a higher allocation to roots would be favorable. When growth strategies under altered conditions perform better, they gain more biomass, becoming more abundant and consequently, more heavily weighted in the aggregation of fluxes to the ecosystem-scale functioning. Thus, with a richer representation of functional diversity, the impact of climatic variability on ecosystem functioning will be reduced.

The strong effect of the representation of diversity on the evapotranspiration is likely to alter feedbacks between the vegetation and the atmosphere. The lower temporal variability in fluxes associated with the diverse approach would seem likely to stabilize vegetation fluxes under atmospheric variability, whereas the greater variability associated with the CWT approach could amplify these effects. This result supports the need for integrating a more diverse representation of functional diversity in to the land surface component of Earth System models.

#### 4.4.3 Diversity-Resilience

The productivity response of the diverse CWF simulation was generally less negative than the CWT simulation to drying perturbation experiment. The CWF simulation also exhibited generally more positive changes in productivity in response to the warming perturbation experiment. On the other hand, in the CWT simulation, the productivity decreased dramatically in some regions. This outcome is expected because the diverse representation allows for a shift in the dominance towards growth strategies with traits more suited to the altered conditions. This is also consistent with other two results described above. In a way this is the same result as the case of diversity-productivity effect, except that climatic variability is replaced by a climatic change.

This insight is specifically relevant for climate change research. For instance, the study by Cox et al. (2000) suggest an Amazon dieback under global warming scenarios. This result was obtained with a coarse representation of functional diversity with only a very few PFTs. Our results imply that with a more diverse representation of vegetation within an Earth system model would lead to less severe vegetation changes under climatic change. This would also support the importance of conserving functional diversity in ecosystems for them to maintain their ability to adapt to changing

conditions.

### **4.5 Summary of diversity-biospheric functioning relationships**

JeDi-DGVM simulations were run in two configurations to quantify how the representation of functional diversity influences the simulated magnitude and variability of water and carbon fluxes between the land surface and the atmosphere. In the first configuration, we simulated a diverse biosphere using a large number of plant growth strategies, allowing the modelled ecosystems to adapt through emergent changes in ecosystem composition. In the second configuration, we recreated a low diversity PFT-like representation of the terrestrial biosphere by aggregating the surviving growth strategies from the diverse simulation to a single community-weighted plant growth strategy per grid cell. In agreement with earlier biodiversity-ecosystem functioning studies, the diverse representation of terrestrial vegetation exhibited higher productivity and water-use efficiency in many regions. The land surface fluxes of productivity in the diverse simulations show greater temporal stability and resilience to climatic perturbations. The strength of these differences in magnitude and variability were modulated by the composition of the simulated ecosystems in the diverse simulations. In summary, these results support the notion that functional diversity plays a role in the functioning of the Earth System.

These results demonstrate a need for improving the representation of functional diversity in comprehensive Earth System models and add support for conserving biodiversity to maintain ecosystem services and land surface functioning.



# Chapter 5

## Summary and outlook

### 5.1 Summary

In this thesis, we introduced JeDi-DGVM as a prototype for a new class of dynamic global vegetation models with representation of functional diversity that are less coarse and less reliant on empirical bioclimatic relationships than previous PFT-based approaches. This is accomplished with (i) a mechanistic representation of functional trade-offs, which (ii) constrain a large number of plant growth strategies with trait parameter values randomly sampled from their complete theoretical/observed ranges, and (iii) the aggregation of the fluxes/properties associated with those growth strategies to grid-scale structure and function based on their relative abundances.

In a systematic evaluation of JeDi-DGVM in Chapter 3, we have shown that its bottom-up plant functional tradeoff approach together with a simple mass-based aggregation mechanism is able to capture the broad patterns of terrestrial biogeochemical fluxes and associated land surface properties reasonably well. The evaluation results compare favorably with two other state-of-the-art terrestrial biosphere models based on the presently dominant PFT paradigm. Additionally, we have shown that JeDi-DGVM is able to mechanistically reproduce the global-scale biogeographical patterns of plant species richness and community evenness. Because it is more closely based on first-principles, JeDi-DGVM requires less input data and is able to produce a wider range of testable outputs than earlier DGVMs based on the PFT concept.

We have also shown in Chapter 4, that when compared with a coarser representation of functional diversity, that the diverse JeDi-DGVM approach leads to a simulated terrestrial biosphere with higher productivity and water-use efficiency, greater stability in terms of its carbon and water fluxes, and greater resilience to climatic perturbations. These findings fit with previous theoretical and empirical work on biodiversity-

ecosystem functioning relationships. They highlight the need for improving the representation of functional diversity within the vegetation component of comprehensive Earth System models, but they also bolster support for conserving biodiversity to maintain biospheric functioning in a changing climate.

The JeDi-DGVM modelling approach developed in this thesis sets the foundation for future applications, in which the simulated vegetation response to global change has a greater ability to adapt through changes in ecosystem composition, having potentially wide-ranging implications for biosphere-atmosphere interactions under global change. In the next and last section of this thesis, we propose possible directions for further model development/evaluation and we highlight a few ongoing and potential applications of JeDi-DGVM.

## 5.2 Outlook

JeDi-DGVM introduces several elements novel to dynamic vegetation modeling, allowing for an explicit representation of functional diversity that can evolve temporally. As the current implementation represents an initial prototype from which refinements and added functionality will be made, we discuss below several key concepts that underlie the formulation of JeDi-DGVM, and which will likely result in the greatest impact on model improvement in future efforts. We also highlight several ongoing and potential applications of the model.

### 5.2.1 Representation of tradeoffs

JeDi-DGVM is a prototype meant to explore the potential utility of a trait-based functional tradeoff approach for transitioning the state-of-the-art of global vegetation modelling beyond the limitations of a set of fixed PFTs. One of the greatest potential advantages of this approach is that it does not constrain the vegetated land surface to be represented by a small set of functional types, but instead allows for a more continuous representation of vegetation types that can evolve as a function of climatic suitability. We demonstrate in this work that from this tradeoff-based approach a realistic representation of land surface biophysical form and function can emerge.

For this approach to be successful, several key requirements must be met, particularly (1) identification of the key tradeoffs that determine the ability of a plant to survive in a given environment, and (2) proper parameterization of the costs and benefits of

the traits associated with those tradeoffs. In this current implementation, JeDi-DGVM utilizes 15 functional parameters that characterize the behavior of a growth strategy in terms of its carbon allocation strategy, phenological dynamics, tissue turnover and the balance between respiration and photosynthesis. The positive performance of JeDi-DGVM in the C-LAMP evaluation lends credibility to this approach, and will motivate further evaluation of the critical plant traits and tradeoffs that determine the performance of the vegetated land surface. New information sources linking costs and benefits with observed traits, such as the TRY database (Kattge et al. 2011), will provide important constraints on future refinements of this approach.

### 5.2.2 Is everything everywhere?

JeDi-DGVM assumes that the distribution of plant growth strategies is able to adjust quickly to climatic changes, allowing all of the sampled plant growth strategies to emerge when a given climate anywhere on the globe becomes suitable. This can be stated through the ecological hypothesis of “Everything is everywhere, but the environment selects.” While this ecological hypothesis was originally formulated with respect to the biogeography of marine microbes, terrestrial plant species face considerable barriers to migration (e.g. mountain ranges, deserts, oceans). The timescales of terrestrial plant growth and dispersal also differ greatly from those of fast-lived marine microbes transported along ocean currents. A model-based study (Malcolm et al. 2002) showed that the preferred ranges of many plant species could shift tens to hundreds of kilometers over the next century due to anthropogenic greenhouse warming, making the issue of estimating migration rates, and the extent to which everything is truly everywhere, key to predicting future vegetation composition.

Despite the importance of this issue to the vegetation modelling community (Neilson et al. 2005), only one modelling group (Lee 2011) has introduced mechanistic migration processes in a DGVM. Lee (2011) attributes this partially to the difficulties associated with the considerable variation in seed dispersal rates within the PFTs used by the current generation of DGVMs. Incorporating aspects of seed dispersal in a functional tradeoff framework, through additional traits such as seed size, could help to constrain plant migration rates in climate change simulation experiments. Seed dispersal range, and consequently the rate of plant migration, is closely linked to seed size. Smaller seeds are more easily transported by the wind and animals than larger seeds (Ezoe 1998). On the other hand, larger seeds allow establishing plants to persist through longer periods of stress. Parameterizing the tradeoff between seed size and dispersal rates will be

challenging but possibly less so than modelling migration with a PFT-based scheme.

### 5.2.3 Aggregation scheme and competition

The aggregation of vegetation states and fluxes across the diversity represented in each computational grid cell is based on the ‘biomass-ratio’ hypothesis. This scheme determines the grid cell flux or state as an average across all surviving plant growth strategies in the grid cell, weighted by their respective biomass, imposing the implicit assumption that interaction between plant growth strategies is weak. For example, JeDi-DGVM does not currently account for shading of plant growth strategies that resemble understory plants by those that resemble dominant canopy trees. Likewise, the hydrologic conditions that a plant growth strategy experiences are not influenced by the other surviving plant growth strategies in its grid cell. Thus, understory plant growth strategies do not stand to benefit during periods of drought from the observed phenomena of hydraulic distribution, wherein deep-rooted plants redistribute soil water from lower soil layers (Lee et al. 2005; Prieto et al. 2012). These types of competitive and facilitative interactions are known to influence community-assembly processes at the local scale (Cavender-Bares et al. 2009), leading to trait divergence. However, at larger scales, including the spatial resolution of the simulation results presented here, trait selection and trait convergence due to environmental filtering have been shown to be the dominant community-assembly processes (Kraft et al. 2008; Swenson and Weiser 2010; Freschet et al. 2011; Kraft et al. 2011).

This ‘biomass-ratio’ aggregation scheme was chosen for its simplicity and its demonstrated effectiveness for making statistical predictions about community fluxes from trait abundance information at the field-scale (Garnier et al. 2004; Vile et al. 2006; Kazakou et al. 2006; Díaz et al. 2007; Quetier et al. 2007). However, the mechanistic tradeoff-based trait filtering framework of JeDi-DGVM does not preclude the integration of more sophisticated aggregation schemes. For example, Bohn et al. (2011) recently used JeDi-DGVM model output together with a simple population dynamics model DIVE (Dynamics and Interactions of VEgetation) to explore how seed competition, resource competition and environmental disturbance might influence community structure. In the future, the tradeoff-based modelling approach of the JeDi-DGVM could be directly integrated with the representation of population dynamics from the DIVE model or from other recent models (e.g. the Ecosystem Demography model; Moorcroft et al. 2001; Medvigy et al. 2009; Fisher et al. 2010b) which explicitly account for canopy height structure and age classes.

### 5.2.4 Further evaluation

In this thesis, we evaluated the feasibility of using the JeDi-DGVM modelling approach to simulate broad-scale patterns of terrestrial biogeochemistry and ecosystem properties. However, another key and unique test for this approach would be to directly compare the emergent patterns of simulated FT parameters with our growing knowledge about the geographic distribution of plant traits and their environmental co-variates. This information could come from trait databases (e.g. TRY; Kattge et al. 2011) or remote sensing products (e.g. canopy nitrogen observations; Ollinger et al. 2008). A further test would be to compare simulated shifts in FT parameters and allocation patterns with observed shifts in trait abundances from ecosystem manipulation experiments, e.g. irrigation (Axelsson and Axelsson 1986), CO<sub>2</sub> enhancement (Ainsworth and Long 2004), or throughfall exclusion (Fisher et al. 2007). These fine-scale comparisons would help further refine various aspects of the biogeochemical formulations and trade-offs incorporated into JeDi-DGVM, and give greater confidence in projections regarding the future fate of the terrestrial biosphere.

In Chapter 3.4.10, we briefly compared the simulated allocation of NPP to different plant carbon pools with carbon budget observations (Malhi et al. 2009) from three Amazonian forest ecosystems. This analysis should be expanded globally by comparing the the simulated patterns of carbon flows and stocks with observations from other existing datasets based on carbon inventories (Cannell 1982; Litton et al. 2007; Luysaert et al. 2007; Malhi et al. 2011). More specifically, one could look at how the simulated allocation patterns vary along environmental gradients (cf. Litton and Giardina 2008; Cornwell and Ackerly 2009). In this study we only examined at the community-weighted allocation fluxes. It would be equally interesting to explore how the simulated partitioning of NPP varies among surviving plant growth strategies within grid cells (cf. Ackerly and Cornwell 2007).

For instance, Wolf et al. (2011) and Malhi et al. (2011) found evidence that the strongest allocation trade-off was not between root and shoots, as has been commonly thought, but rather more specifically between allocation to fine roots and aboveground wood. This relationship is likely mediated between sites by hydrological conditions and within sites by the competitive dynamics between faster and slower growing trees. In principle, the functional tradeoff modelling approach of JeDi-DGVM should be able to capture both of these phenomena. However, it might require the introduction of further constraints related to disturbances (Bohn et al. 2011) and FT parameters related to wood economics and plant hydraulics (cf. Hickler et al. 2006; Chave et al. 2009; Falster

et al. 2010)

### 5.2.5 Ongoing and potential applications

The “bottom-up” functional tradeoff-based modelling framework presented here represents a step forward in the development of a comprehensive and predictive representation of the terrestrial biosphere for use in Earth System Models. By mechanistically simulating the full range and continuous nature of plant functional diversity, it will be possible to explore new areas of research including:

1. The JeDi-DGVM is currently participating in the Intersectoral Model Intercomparison Project. This initiative is seeking to make quantitative estimates regarding climate change impacts and their uncertainties across different sectors (e.g. agriculture, water, ecosystems, infrastructure and health) with multiple impact models. We hypothesize based on the results from Chapter 4, which showed the more flexible approach of JeDi led to greater productivity, stability, and resilience than a more coarse PFT-like representation of functional diversity, that JeDi-DGVM will simulate less severe biospheric impacts of projected climate change than the other participating DGVMs based on the PFT paradigm.
2. By coupling the JeDi-DGVM tradeoff-based approach with an optimization algorithm, it is possible to seek out those functional trait combinations that maximize a particular ecosystem service. For example, Drewry et al. (in prep), have used JeDi-DGVM to investigate the optimal set of trait parameters which maximize the allocation to seed biomass under the present-day climate of each model grid cell, allowing for estimates of the upper bound of realizable yields as a function of climatic constraint. One could also apply the same methodology with climate model projections to identify regions where the optimal crop traits shift in order to inform agricultural and food security policies. The same methodology could also easily be applied to many other ecosystem system services of interest (e.g. maximizing leaf biomass production for forage/fodder or belowground carbon allocation for carbon sequestration).
3. Climate model projections point towards the possibility of novel climates without present-day analogs (Jackson and Williams 2004; Williams and Jackson 2007). This causes difficulties for PFT-based modelling approaches because they often rely so heavily on bioclimatic relationships based on present-day empirical observations. Because JeDi-DGVM samples functional trait parameters from their

full theoretical or observed ranges, it may produce surviving growth strategies or compositions of growth strategies without present-day analogs (Reu et al., in review). Coupling JeDi-DGVM directly within an Earth System Model would allow for the exciting possibility of exploring where these no-analog vegetation compositions appear in climates that widely different from that of today. It would also be interesting to explore the role of functional diversity in moderating atmosphere-biosphere feedbacks. As an example, one could compare “online” and “offline” simulations to quantify the net effect of biodiversity on sustaining continental moisture recycling.



## Appendix A

# Jena Diversity-Dynamic Global Vegetation (JeDi-DGVM) Model Description

JeDi-DGVM builds upon the plant diversity model of KM2000, which itself took many model formulations from earlier land surface (Roeckner et al. 1996) and terrestrial biosphere models (e.g. Potter et al. 1993; Knorr and Heimann 1995; Kaduk and Heimann 1996). Here, the ecophysiological parameterizations have been kept relatively simple to keep the computational requirements manageable. This makes it possible to simulate many the development of many plant growth strategies in parallel across a global grid over long simulation periods within a reasonable timeframe on a single Linux workstation. That said, several of the formulations and parameter values, particularly with respect to the calculation of productivity and respiration, have been changed to improve the realism of the simulated fluxes. Also, whereas the KM2000 model simulated the life-cycle of individual generic plants from germination to death, the JeDi-DGVM introduces tissue turnover and thus simulates something closer to the mean of a population for each plant growth strategy. Finally, the most important new feature is the introduction of a scaling mechanism to aggregate the exchange fluxes and land-surface properties of many plant growth strategies to the community-level based on the ‘*biomass-ratio*’ hypothesis.

### A.1 Plant module overview

The plant module simulates the development of plant growth strategies based on the fundamental ecophysiological processes of photosynthesis, respiration, allocation, phenology, and reproduction. Plant development is coupled in a process-based manner to a land-surface hydrology module which simulates canopy interception, throughfall, infiltration, evaporation, root-water uptake, and surface runoff, using daily meteorological data.

logical forcing of downwelling shortwave and net longwave radiation, precipitation, and near-surface air temperature. The variables and parameters involved in the development of the plant growth strategies are summarized in Table C.1. The details of the land-surface module are described in Appendix B.

Each plant growth strategy is represented by six carbon tissue pools: stored assimilates  $C_A$ , leaves  $C_L$ , fine roots  $C_R$ , aboveground wood (branches and stems)  $C_{WL}$ , belowground wood (coarse roots)  $C_{WR}$ , and a reproductive (or ‘seed’) pool  $C_S$ . When growing conditions are favorable, carbon germinates from the ‘seed’ pool to the storage pool. The plant then begins to grow by allocating carbon from the storage pool to the various tissue pools. The tissue pools are also subject to turnover and senescence. The litter fluxes from these two processes serve as input to the soil carbon module. The sizes of the tissue pools influence the parameter values of the land-surface module, affecting both the absorption of solar radiation and the land-surface hydrology. For example, the absorption of solar radiation, which supplies the energy for photosynthesis and evapotranspiration, is proportional to leaf area index (LAI) which is derived from leaf biomass. Fine root biomass affects the maximum rate of water uptake from the rooting zone, influencing the plant’s water status and the supply of moisture for evapotranspiration. Likewise, the coarse root biomass of a plant determines the hydrologic depth of its rooting zone. The land-surface conditions in turn affect the net primary productivity (NPP), which forms the input to the storage pool. A plant growth strategy is considered to be alive as long as the carbon in the storage pool is greater than zero ( $C_A > 0$ ). The details of these processes are described in the following subsections.

The particular functioning of a plant growth strategy is defined by a set of 15 functional trait (FT) parameters ( $t_1 \dots t_{15}$ ). These FT parameters control the allocation of carbon from the storage pool to the other tissue pools, the tissue turnover rates, the phenological response to environmental conditions, and the ecophysiological balance between photosynthesis and respiration. All of the FT parameters range between zero and one. However, these ranges are often extended by using the FT parameters as either exponents or coefficients. Each FT parameter is associated with one or more functional tradeoffs. For instance, a higher allocation to fine roots enhances the rate at which a plant can extract moisture from the soil matrix, but this comes at the expense of allocation to the aboveground pools and thus a decreased ability to capture light for photosynthesis, as well as the metabolic cost of maintaining that biomass. The implementation of these tradeoffs are explained in further detail below. The descriptions of the FT parameters are summarized in Table C.2.

## A.2 Vegetation carbon pool dynamics

The following differential equations describe the dynamics of the vegetation carbon pools:

$$\begin{aligned}
\frac{dC_A}{dt} &= \text{NPP} + \text{GERM} - \sum C_A A_{\text{tissue}} (1 - c_{\text{RES,tissue}}) \\
\frac{dC_S}{dt} &= C_A A_S (1 - c_{\text{RES,S}}) - \text{GERM} - \frac{C_S}{\tau_S} \\
\frac{dC_L}{dt} &= C_A A_L (1 - c_{\text{RES,L}}) - \frac{C_L}{\tau_L} \\
\frac{dC_R}{dt} &= C_A A_R (1 - c_{\text{RES,R}}) - \frac{C_R}{\tau_R} \\
\frac{dC_{WL}}{dt} &= C_A A_{WL} (1 - c_{\text{RES,WL}}) - \frac{C_{WL}}{\tau_{WL}} \\
\frac{dC_{WR}}{dt} &= C_A A_{WR} (1 - c_{\text{RES,WR}}) - \frac{C_{WR}}{\tau_{WR}}
\end{aligned} \tag{A.1}$$

The details of the various terms are described below in the following subsections.

## A.3 Growing Conditions

The timing of plant growth and germination is controlled by environmental conditions, specifically, soil wetness  $f_W$  and near-surface air temperature  $T$ . Soil wetness  $f_W$  being defined as the ratio of moisture  $W$  stored in the rooting zone relative to the maximum storage capacity of the rooting zone  $W_{\text{MAX}}$ . FT parameters  $t_1$  and  $t_2$  in time constants  $\tau_W$  and  $\tau_T$  determine how quickly a plant responds to changes in the environmental

## APPENDIX A MODEL DESCRIPTION

conditions.

$$f_{\text{GROW},T}(t) = \frac{T + \tau_T f_{\text{GROW},T}(t - \Delta t)}{1 + \tau_T}$$

with  $\tau_T = 10^{4t_1-2}$

$$f_{\text{GROW},W}(t) = \frac{f_W + \tau_W f_{\text{GROW},W}(t - \Delta t)}{1 + \tau_W}$$

with  $f_W = \frac{W}{W_{\text{MAX}}}$  and  $\tau_W = 10^{4t_2-2}$  (A.2)

$$f_{\text{GROW},G}(t) = \frac{f_{W,\text{bare}} + \tau_W f_{\text{GROW},G}(t - \Delta t)}{1 + \tau_W}$$

with  $f_{W,\text{bare}} = \frac{W_{\text{bare}}}{W_{\text{MAX},0}}$

Values of FT parameters  $t_1$  and  $t_2$  near zero represent a short memory and thus a quick response to change, while larger values represent a longer memory and a slower response. For example, a plant with a low value of  $\tau_T$  would react almost immediately to a warm day in early spring, whereas a plant with a larger value would react only after several days or weeks of spring warmth. Likewise, a high value of  $\tau_W$  would lead a plant to continue to allocate carbon despite persisting drought conditions.

For germination, only the soil wetness of the top 50mm  $W_{\text{top}}$  (see Eq. B.16) relative to the storage capacity of bare non-vegetated soil is considered. Germination and growth only occur when both the temperature function  $f_{\text{GROW},T}$  is above a critical temperature  $T_{\text{crit}}$  and the relevant soil wetness condition,  $f_{\text{GROW},W}$  or  $f_{\text{GROW},G}$ , is greater than a critical value of 0.5. The critical temperature  $T_{\text{crit}}$  is a linear function of FT parameter  $t_3$  between  $-5^\circ\text{C}$  and  $10^\circ\text{C}$ .

$$f_{\text{GROW}} = \begin{cases} 0 & f_{\text{GROW},W} < 0.5 \text{ and } f_{\text{GROW},T} < T_{\text{crit}} \\ 1 & f_{\text{GROW},W} \geq 0.5 \text{ or } f_{\text{GROW},T} \geq T_{\text{crit}} \end{cases}$$

$$f_{\text{GERM}} = \begin{cases} 0 & f_{\text{GROW},G} < 0.5 \text{ and } f_{\text{GROW},T} < T_{\text{crit}} \\ 1 & f_{\text{GROW},G} \geq 0.5 \text{ or } f_{\text{GROW},T} \geq T_{\text{crit}} \end{cases} \quad (\text{A.3})$$

## A.4 Germination

Germination of carbon from the ‘seed’ pool  $C_S$  to the storage pool  $C_A$  occurs when germination conditions are favorable ( $f_{\text{GERM}} = 1$ ) and the ‘seed’ pool is not empty ( $C_S > 0$ ):

$$GERM = f_{\text{GERM}} \gamma_{\text{GERM}} \frac{C_S}{\max(p, k_{\text{GERM}})} \quad (\text{A.4})$$

with  $\gamma_{\text{GERM}} = 10^{4t_4-4}$ .

FT parameter  $t_4$  modulates the germination fraction  $\gamma_{\text{GERM}}$ , the fraction of ‘seed’ carbon  $C_S$  which can germinate to the storage pool  $C_A$  in a single daily time step (Cohen 1968; Alvarado and Bradford 2002). Values of  $t_4$  near zero result in a conservative strategy with only a small fraction of ‘seed’ carbon germinating to the storage pool per day when germination conditions are met ( $f_{\text{GERM}} = 1$ ). Higher values yield increasingly more opportunistic strategies. When germination conditions are favorable ( $f_{\text{GERM}} = 1$ ) and the ‘seed’ pool is ( $C_S = 0$ ), a small amount of initial carbon is added to the ‘seed’ pool to allow a growth strategy to begin growth. When this occurs, an equivalent amount of carbon is added to the community-aggregated gross primary productivity (see Appendix A.9) to maintain the conservation of mass in the grid-cell variables.

## A.5 Carbon allocation

Plants allocate carbon from the storage pool to growth when the growing conditions are favorable ( $f_{\text{GROW}} = 1$ ). Allocation to the ‘seed’ pool occurs when net primary productivity is greater than zero ( $f_{\text{SEED}} = 1$  when  $NPP > 0$ ). The amount of carbon allocated to each tissue pool is proportional to the size of the storage pool  $C_A$  and to the set of FT parameters,  $t_5 \dots t_{10}$ , which together form the plant’s carbon allocation

strategy:

$$\begin{aligned}
 A_S &= f_{\text{SEED}} \frac{t_5}{t_5 + t_6 + t_7 + t_8} \\
 A_L &= f_{\text{GROW}} (1 - t_9) \frac{t_6}{t_5 + t_6 + t_7 + t_8} \\
 A_R &= f_{\text{GROW}} (1 - t_{10}) \frac{t_7}{t_5 + t_6 + t_7 + t_8} \\
 A_{\text{WL}} &= f_{\text{GROW}} f_{\text{VEG}} t_9 \frac{t_6}{t_5 + t_6 + t_7 + t_8} \\
 A_{\text{WR}} &= f_{\text{GROW}} f_{\text{VEG}} t_{10} \frac{t_7}{t_5 + t_6 + t_7 + t_8}.
 \end{aligned} \tag{A.5}$$

The allocation fractions are mathematically constrained such that they sum to less than one ( $\sum A_{\text{tissue}} < 1$ ). The unallocated fraction ( $1 - \sum A_{\text{tissue}}$ ) remains in the storage pool  $C_A$  for future growth or maintenance respiration.

## A.6 Turnover and Senescence

The turnover times  $\tau_{\text{WL}}$  and  $\tau_{\text{WR}}$  of the woody tissue pools are defined as functions of FT parameter  $t_{11}$ :

$$\tau_{\text{WL}} = \tau_{\text{WR}} = 365 (79 t_{11} + 1) \tag{A.6}$$

Eq. A.6 yields a range of turnover times between 1 and 80 years. The base turnover time  $\tau_{\text{L},0}$  for the leaf and fine root pools is defined as a function of FT parameter  $t_{12}$ :

$$\tau_{\text{L},0} = \frac{365}{12} 10^{2.0 t_{12}}. \tag{A.7}$$

Eq. A.7 yields a range of turnover times log-distributed between 1 and 100 months, which covers the range of observations in the TRY database (Kattge et al. 2011). The turnover times for the ‘seed’ and storage pools are assumed constant across all plant growth strategies (see Table C.1).

Senescence is triggered when both NPP and the time-averaged net primary productivity  $f_{\text{NPP}}$  are negative, where:

$$\begin{aligned}
 f_{\text{NPP}}(t) &= \frac{NPP + \tau_{\text{NPP}} f_{\text{NPP}}(t - \Delta t)}{1 + \tau_{\text{NPP}}} \\
 &\text{with } \tau_{\text{NPP}} = 10^5 t_{13}^{-2}.
 \end{aligned} \tag{A.8}$$

$$f_{\text{SEN}} = \begin{cases} 0 & f_{\text{NPP}} \geq 0 \text{ or } \text{NPP} \geq 0 \\ 1 & f_{\text{NPP}} < 0 \text{ and } \text{NPP} < 0 \end{cases} \quad (\text{A.9})$$

FT parameter  $t_{13}$  in time constant  $\tau_{\text{NPP}}$  describes the memory to past NPP conditions. Values of  $t_{13}$  near zero represent a short persistence during periods of negative NPP, while values closer to one represent longer persistence. During periods of senescence, the turnover rates of the leaf and fine root pools increase proportional to a constant factor  $\tau_{\text{SEN}}$ . The relative magnitude of this increase is determined by FT parameter  $t_{14}$ :

$$\begin{aligned} \tau_{\text{L}} &= \left( \frac{1}{\tau_{\text{L},0}} + \frac{1}{\tau_{\text{SEN}}} f_{\text{SEN}} t_{14} \right)^{-1} \\ \tau_{\text{R}} &= \left( \frac{1}{\tau_{\text{L},0}} + \frac{1}{\tau_{\text{SEN}}} f_{\text{SEN}} (1 - t_{14}) \right)^{-1} \end{aligned} \quad (\text{A.10})$$

## A.7 Land Surface Parameters

The land-surface parameters (maximum plant available water storage in the rooting zone  $W_{\text{MAX}}$ , leaf area index  $LAI$ , potential supply rate for transpiration  $S$ , fractional vegetative cover  $f_{\text{VEG}}$ , fractional forest cover  $f_{\text{FOR}}$ , snow-free surface albedo  $a_{\text{ns}}$ , and the storage capacity of the canopy  $W_{\text{LMAX}}$ ) relate the development of a plant growth strategy to the coupled land-surface module which simulates its environmental conditions. The module itself is based on the land-surface component of the ECHAM4 atmospheric General Circulation Model (Roeckner et al. 1996) along with modifications introduced by KM2000 and is described in detail in Appendix B. These parameters are computed for each plant growth strategy from its carbon tissue pools and FT parameters:

$$\begin{aligned} LAI &= C_{\text{L}} SLA \\ f_{\text{VEG}} &= 1 - e^{-k LAI} \\ f_{\text{FOR}} &= 1 - e^{-c_{\text{FOR}} C_{\text{WL}}} \\ W_{\text{LMAX}} &= c_{\text{WLMAX}} LAI \\ a_{\text{ns}} &= f_{\text{VEG}} a_{\text{VEG}} + (1 - f_{\text{VEG}}) a_{\text{SOIL}} \\ W_{\text{max}} &= \max \left[ W_{\text{max},0}, c_{\text{PAW}} \sqrt{c_{\text{SRL}} C_{\text{WR}}} \right] \\ S &= c_{\text{SRU}} C_{\text{R}} f_{\text{W}} \end{aligned} \quad (\text{A.11})$$

## APPENDIX A MODEL DESCRIPTION

The land-surface parameters and their conversion constants are summarized in Table C.3.

The leaf area index  $LAI$  of a plant growth strategy is calculated as the product of its leaf biomass  $C_L$  and its specific leaf area  $SLA$ . The  $SLA$  of a plant growth strategy being estimated as a function of leaf lifespan using an empirical relationship derived by Reich et al. (1997), where  $\tau_{L_0}$  is the base leaf turnover rate from Eq. A.7.

$$SLA = 0.030 \left( \frac{365}{\tau_{L_0}} \right)^{-0.46} \quad (\text{A.12})$$

This establishes a trade-off such that a plant growth strategy falls along a spectrum between an evergreen strategy with thicker, long-lived leaves and a deciduous strategy with thinner, short-lived leaves (Reich et al. 1998; Westoby et al. 2002; Shipley et al. 2006a).

The leaf area index  $LAI$  is then used to determine both the fractional vegetation cover  $f_{\text{VEG}}$  according to the Lambert-Beer law (Monsi and Saeki 1953) and the water storage capacity of the canopy  $W_{LMAX}$ . The parameterization of the fractional forest cover  $f_{\text{FOR}}$  is taken as an analogy to the formulation used for vegetative cover  $f_{\text{VEG}}$ . The snow-free surface albedo  $a_{\text{ns}}$  is calculated as the mean of its canopy albedo  $a_{\text{VEG}}$  and the bare soil albedo  $a_{\text{SOIL}}$  (constant for all plant growth strategies), weighted by its fractional vegetation cover  $f_{\text{VEG}}$ . The canopy albedo  $a_{\text{VEG}}$  of a plant growth strategy is a linear function of the canopy nitrogen concentration  $[N_L]$  (Hollinger et al. 2010).

$$a_{\text{VEG}} = 3.216 [N_L] + 0.02 \quad (\text{A.13})$$

The formulations regarding root properties ( $W_{\text{MAX}}$  and  $S$ ) are obtained from first principles. The motivation for using a square-root relationship for the maximum plant available water storage in the rooting zone comes from the Shinozaki et al. (1964) pipe model. From the pipe model perspective, the root system is viewed as an assemblage of pipes which connect the root ends (the organs responsible for water absorption from the soil) with the leaves. If we assume a uniform density of root ends within the rooting zone, we obtain a square root relationship between the depth of the rooting zone and the total length of the coarse roots (given by the product of the coarse root biomass  $C_{\text{WR}}$  and an assumed constant specific root length parameter  $c_{\text{SRL}}$ ). The maximum plant available soil water storage  $W_{\text{MAX}}$  is then given by the product of this rooting zone depth and the unit plant available water capacity  $c_{\text{PAW}}$  (i.e. the difference between field capacity and permanent wilting point per unit depth) taken from a global

dataset (Dunne and Willmott 1996). Finally, we assume the potential supply rate for transpiration  $S$  is related to the fine root biomass  $C_R$  and soil wetness  $f_W$  via a constant specific root water uptake parameter  $c_{SRU}$ .

## A.8 Net Primary Productivity

The net primary productivity  $NPP$  of each plant growth strategy is computed as the difference between its gross primary productivity  $GPP$  and its autotrophic respiration flux  $RES_a$ .

$$NPP = GPP - RES_a \quad (\text{A.14})$$

The parameters and variables involved in the calculation of these fluxes are summarized in Table C.4.

$GPP$  is estimated using a big-leaf non-rectangular hyperbola approach (Johnson and Thornley 1984; Franklin 2007):

$$GPP = \frac{h}{2\theta} \left[ (\phi I_a + P_{\max}) - \sqrt{(\phi I_a + P_{\max})^2 - 4\theta\phi I_a P_{\max}} \right] \alpha_{\text{H}_2\text{O}} \quad (\text{A.15})$$

While more sophisticated and likely more accurate photosynthesis schemes are abundant, we chose to use this relatively simple approach for its computational expediency and to keep the number of necessary parameters low. Absorbed photosynthetically active radiation  $I_a$  is derived, following the Lambert-Beer law of light extinction, from the photosynthetically active radiation (assumed to be half of downward shortwave radiation) above the canopy  $I_0$  and the fractional coverage of vegetation (Monsi and Saeki 1953):

$$I_a = I_0 f_{\text{VEG}} \quad (\text{A.16})$$

The light-saturated canopy photosynthetic capacity  $P_{\max}$  of a plant growth strategy is estimated as a linear function of the canopy nitrogen concentration  $[N_L]$  following an empirical relationship proposed by Ollinger et al. (2008) assuming a foliar carbon content of  $0.48 \text{ gC gDM}^{-1}$ . Similar relationships between N content and photosynthetic capacity are well-documented at the leaf scale (Field and Mooney 1986; Reich et al. 1997; Wright et al. 2004).

$$P_{\max} = (59.2 \times 10^{-4} [N_L] + 1.1 \times 10^{-4}) \alpha_T \quad (\text{A.17})$$

$$[N_L] = 10^{t_{15}-2}$$

## APPENDIX A MODEL DESCRIPTION

The canopy nitrogen concentration  $[N_L]$  itself is a function of FT parameter  $t_{15}$  leading to a range of values log-distributed between 0.01 and 0.10  $\text{gN gC}^{-1}$ . The supply of nitrogen is not considered as a limiting factor. The curvature parameter  $\theta$  is assumed constant across all plant growth strategies. Daylength  $h$  is computed from the cosine of the solar zenith angle, which varies with season and latitude (Hartmann 1994). The quantum efficiency  $\phi$  and the factor  $\alpha_T$  modifying the light-saturated photosynthetic capacity are computed as functions of both air temperature and ambient  $\text{CO}_2$  concentrations following Cannell and Thornley (1998).

The moisture stress factor  $\alpha_{\text{H}_2\text{O}}$  is a function of the ratio between the potential supply rate for transpiration ( $S$ ) and the atmospheric demand for transpiration ( $D$ ; further details in Appendix B).

$$\alpha_{\text{H}_2\text{O}} = 1 - e^{-\frac{S}{D}} \quad (\text{A.18})$$

The autotrophic respiration  $RES_a$  of a plant growth strategy is calculated as the sum of its growth respiration  $RES_g$  and maintenance respiration  $RES_m$  fluxes (McCree 1970; Thornley 1970). Growth respiration consumes a fixed fraction  $c_{\text{RES,tissue}}$  of the carbon allocated from the storage pool  $C_A$  to the each tissue pool. These fractions are assumed to be constant across all plant growth strategies.

$$RES_g = C_A \sum (A_{\text{tissue}} c_{\text{RES,tissue}}). \quad (\text{A.19})$$

Following Ryan (1991), maintenance respiration  $RES_m$  is calculated based on the nitrogen content of each tissue, a specific respiration rate  $c_{\text{RES,N}}$  at  $20^\circ\text{C}$  and a  $Q_{10}$  temperature function.

$$RES_m = c_{\text{RES,N}} Q_{10,a}^{\left(\frac{T-20}{10}\right)} [N_L] [(C_L + C_R) + c_{\text{sapwood}} (C_{\text{WL}} + C_{\text{WR}})] \quad (\text{A.20})$$

The fine root nitrogen concentration  $[N_R]$  is assumed to be equal to the leaf nitrogen concentration  $[N_L]$  for all plant growth strategies. The fractions of sapwood carbon to woody carbon (0.05) and sapwood nitrogen to leaf nitrogen (0.10) are similarly assumed constant across all plant growth strategies and are accounted for by parameter  $c_{\text{sapwood}}$ . The ‘seed’ and storage carbon pools are not subject to maintenance respiration within the model, however, they do decay at a constant rate as described in Section A.6.

## A.9 Scaling from plant growth strategies to community-aggregated fluxes

JeDi-DGVM calculates community-aggregated fluxes and land surface properties assuming the ‘*biomass-ratio*’ hypothesis (Grime 1998), i.e. as the mean over the individual plant growth strategies weighted by their mass-based relative abundances. The instantaneous relative abundance  $p_{(i,j)}^*$  of a plant growth strategy  $i$  in a grid cell  $j$  is assumed to be proportional to its living biomass at that grid cell relative to the sum of the living biomass of all surviving growth strategies  $S$  in that grid cell. The living biomass  $C_{\text{tot}(i,j)}$  of a growth strategy being the sum of its leaf, fine root, woody and storage carbon pools ( $C_{\text{tot}(i,j)} = C_{\text{A}(i,j)} + C_{\text{L}(i,j)} + C_{\text{R}(i,j)} + C_{\text{WL}(i,j)} + C_{\text{WR}(i,j)}$ ).

$$\begin{aligned} p_{(i,j)}^* &= \frac{C_{\text{tot}(i,j)}}{\sum_{k=1}^S C_{\text{tot}(k,j)}} \\ \frac{dp_{(i,j)}}{dt} &= \frac{p_{(i,j)}^* - p_{(i,j)}}{\tau_p} \end{aligned} \quad (\text{A.21})$$

The relative abundance  $p_{(i,j)}$  used for the calculation of community-aggregated fluxes and properties relaxes towards the instantaneous relative abundance  $p_{(i,j)}^*$  at time scale  $\tau_p$  (= 365 days). This relaxation mechanism was necessary to alleviate numerical issues related to the conservation of mass. In the previous subsections describing the development of a individual plant growth strategies, we omitted this subscript notation to improve readability. Throughout the remainder of this appendix, we adopt chevron (angled bracket) notation to denote community-aggregated fluxes and properties. As an example, the community-aggregated gross primary productivity  $\langle GPP_j \rangle$  for a given grid cell  $j$  is equal to the sum of the GPP fluxes of all the plant growth strategies  $S$  in that grid cell weighted by their respective mass-based relative abundances.

$$\langle GPP_j \rangle = \sum_{i=1}^S p_{(i,j)} GPP_{(i,j)} \quad (\text{A.22})$$

## A.10 Soil Carbon

The soil carbon module in JeDi-DGVM is loosely based on the soil carbon component of the JSBACH land surface model (Raddatz et al. 2007; Thum et al. 2011). The parameters and variables of the soil carbon module are summarized in Table C.5. The following differential equations describe the dynamics of the three detritus carbon pools,

## APPENDIX A MODEL DESCRIPTION

fine litter carbon  $C_{\text{LIT}}$ , woody litter carbon  $C_{\text{CWD}}$ , and soil carbon  $C_{\text{SOIL}}$ :

$$\begin{aligned} \frac{dC_{\text{LIT}}}{dt} &= \langle LIT_{\text{L}} \rangle + \langle LIT_{\text{R}} \rangle + \langle LIT_{\text{A}} \rangle + \langle LIT_{\text{S}} \rangle - DEC_{\text{LIT}} \\ \frac{dC_{\text{CWD}}}{dt} &= \langle LIT_{\text{WL}} \rangle + \langle LIT_{\text{WR}} \rangle - DEC_{\text{CWD}} \\ \frac{dC_{\text{SOIL}}}{dt} &= (1 - c_{\text{lit} \gt \text{atm}}) DEC_{\text{LIT}} + (1 - c_{\text{cwd} \gt \text{atm}}) DEC_{\text{CWD}} - DEC_{\text{SOIL}} \end{aligned} \quad (\text{A.23})$$

The soil carbon dynamics are not computed separately for each plant growth strategy. Instead, carbon enters the two common litter pools through the community-aggregated litter fluxes  $\langle LIT_{\text{tissue}} \rangle$  from the turnover of the various vegetation tissue pools.

$$\begin{aligned} \langle LIT_{\text{tissue}} \rangle &= \sum_{k=1}^n \left( p_{(k)} \frac{C_{\text{tissue}(k)}}{\tau_{\text{tissue}(k)}} \right) + \sum_{k=1}^n (C_{\text{tissue}(k)} \max(0, -\Delta p_{(k)})) \\ \langle LIT_{\text{S}} \rangle &= \sum_{k=1}^n \frac{C_{\text{S}(k)}}{\tau_{\text{A}(k)}} \end{aligned} \quad (\text{A.24})$$

The second term in the calculation of  $\langle LIT_{\text{tissue}} \rangle$  is necessary to maintain the conservation of carbon when the relative abundance of a plant growth strategy decreases during the current time step. Likewise, the vegetation carbon pools (except the ‘seed’ pool  $C_{\text{S}}$ ) are scaled down when the relative abundance of a growth strategy increases during the current time step.

$$C_{\text{tissue}(t)} = C_{\text{tissue}(t-\Delta t)} \frac{p_{(t-\Delta t)}}{p_{(t-\Delta t)} + \max(0, \Delta p)} \quad (\text{A.25})$$

The decomposition fluxes  $DEC_x$  out of the detritus carbon pools are computed from the amount of carbon in that pool, a  $Q_{10}$  temperature response function, and a fixed turnover time for that pool at reference temperature 20°C. The value of 1.4 for the sensitivity of heterotrophic respiration to air temperature  $Q_{10,h}$  is taken from a recent global study of FLUXNET sites (Mahecha et al. 2010). Fixed fractions of the decomposition fluxes from the litter pools enter the common soil carbon pool.

$$DEC_x = Q_{10,h}^{\left(\frac{T-20}{10}\right)} \frac{C_x}{\tau_x} \quad (\text{A.26})$$

The heterotrophic respiration flux  $RES_h$  to the atmosphere is estimated as the sum of the fractions of the decomposition fluxes from the litter pools not entering the soil carbon pool and the decomposition flux out of the soil carbon pool.

$$RES_h = c_{\text{lit} \gt \text{atm}} DEC_{\text{LIT}} + c_{\text{cwd} \gt \text{atm}} DEC_{\text{CWD}} + DEC_{\text{SOIL}} \quad (\text{A.27})$$

## A.10 SOIL CARBON

Finally, the community-aggregated net ecosystem exchange  $NEE$  is calculated as the difference the heterotrophic respiration and the community-aggregated net primary productivity fluxes.

$$NEE = RES_h - \langle NPP \rangle \quad (\text{A.28})$$



## Appendix B

### Land Surface Module

The land-surface hydrology module of JeDi-DGVM is largely based on the land-surface component of the ECHAM4 atmospheric General Circulation Model (Roeckner et al. 1996) along with modifications introduced by KM2000. It consists of four budget equations for water stored in the vegetation canopy  $W_L$ , in the snow cover  $W_S$ , in the rooting zone  $W$ , and below the rooting zone  $W_{SUB}$ :

$$\begin{aligned}\frac{dW_L}{dt} &= P_{\text{rain}} - E_{\text{can}} - F_{\text{thfall}} & (\text{B.1}) \\ \frac{dW_S}{dt} &= P_{\text{snow}} - F_{\text{melt}} - E_{\text{snow}} \\ \frac{dW}{dt} &= F_{\text{thfall}} + F_{\text{melt}} - F_{\text{runoff}} - E_{\text{bare}} - E_{\text{trans}} - F_{\text{drain}} - F_{\Delta W_{\text{max}}} \\ \frac{dW_{SUB}}{dt} &= F_{\text{drain}} - F_{\text{subdrain}} + F_{\Delta W_{\text{max}}}\end{aligned}$$

The variables and parameters of the land-surface module are summarized in Tables C.6 and C.7. The module runs on a daily time step using forcing variables: precipitation flux ( $P$ ), near-surface air temperature ( $T$ ), and downward shortwave and longwave radiation fluxes ( $R_{\text{sw}\downarrow}$  and  $R_{\text{lw}\downarrow}$ ). The various flux terms of the budget equations are described below. A schematic diagram of the land-surface module is shown in Fig. B.1.

APPENDIX B LAND SURFACE MODULE

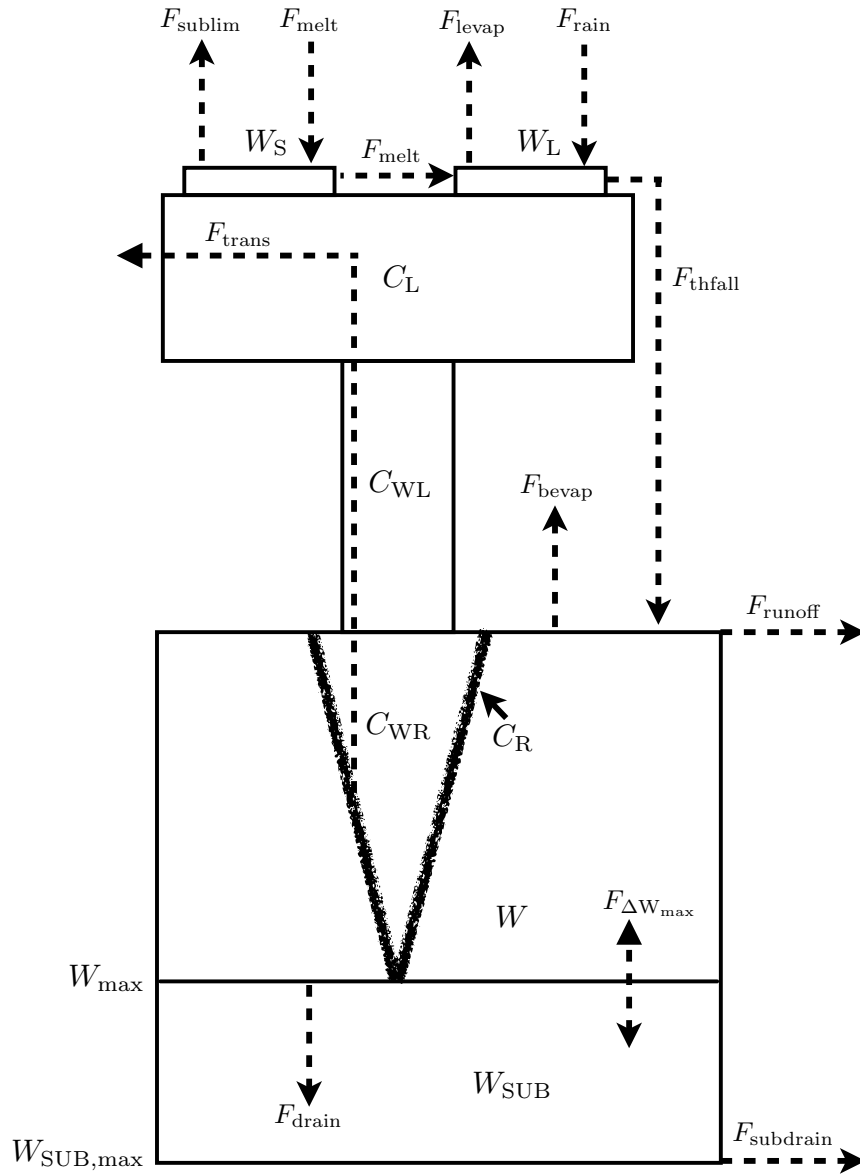


**Figure B.1:** Schematic diagram of the land-surface module. For symbols, see Tables C.1, C.3, C.6, and C.7.

## B.1 Water storage and runoff generation

The partitioning of precipitation between snow  $P_{\text{snow}}$  and rain  $P_{\text{rain}}$  depends on near-surface air temperature  $T$  following Wigmosta et al. (1994).

$$P_{\text{snow}} = \begin{cases} P & T \leq -1.1 \\ P \frac{3.3-T}{4.4} & -1.1 < T < 3.3 \\ 0 & T \geq 3.3 \end{cases} \quad (\text{B.2})$$

$$P_{\text{rain}} = P - P_{\text{snow}}$$

Rainfall is first intercepted in the canopy reservoir  $W_L$  up to a maximum storage capacity  $W_{L\text{max}}$  which depends on  $LAI$  (see Eq. A.11). If a precipitation event causes the water in the canopy reservoir to exceed its storage capacity, the excess water flows from the canopy reservoir to the rooting zone as throughfall  $F_{\text{thfall}}$ .

$$F_{\text{thfall}} = \max(0, W_L + P_{\text{rain}} - W_{L\text{max}}) \quad (\text{B.3})$$

Snowmelt  $F_{\text{melt}}$  is computed according to a day-degree formula using a melt rate of  $3.22 \text{ mm d}^{-1} \text{ }^\circ\text{C}^{-1}$  (Hagemann and Dümenil 1997).

$$F_{\text{melt}} = \begin{cases} 0 & T < 0 \\ \min(3.22 T, P_{\text{snow}} + W_S) & T \geq 0 \end{cases} \quad (\text{B.4})$$

Surface runoff  $F_{\text{runoff}}$  occurs when the throughfall or snowmelt fluxes cause the rooting zone reservoir to exceed its maximum capacity  $W_{\text{MAX}}$  (see Eq. A.11).

$$F_{\text{runoff}} = \begin{cases} F_{\text{thfall}} & T \leq 0 \\ \max(0, W + F_{\text{thfall}} + F_{\text{melt}} - W_{\text{max}}) & T > 0 \end{cases} \quad (\text{B.5})$$

When the air temperature drops below  $0 \text{ }^\circ\text{C}$ , the soil is assumed to be frozen, inhibiting infiltration, and the entire throughfall flux becomes surface runoff.

Drainage from the rooting zone  $F_{\text{drain}}$  supplies water to the sub-rooting zone and

## APPENDIX B LAND SURFACE MODULE

depends on the soil wetness ( $f_W = W/W_{\text{MAX}}$ ).

$$F_{\text{drain}} = \begin{cases} 0 & f_W \leq 0.05 \\ d_{\text{min}} f_W; & 0.05 < f_W < 0.9 \\ d_{\text{min}} f_W + (d_{\text{max}} - d_{\text{min}}) \left( \frac{f_W - 0.9}{1 - 0.9} \right)^d; & f_W \geq 0.9 \end{cases} \quad (\text{B.6})$$

When the rooting zone is between 5% and 90% of field capacity, it drains slowly ( $d_{\text{min}} = 0.24 \text{ mm d}^{-1}$ ) with a linear dependence on soil wetness. When the rooting zone nears saturation ( $f_W \geq 0.9$ ), the drainage rate quickly increases with increasing wetness towards its maximum drainage rate ( $d_{\text{max}} = 2.40 \text{ mm d}^{-1}$ ). Drainage from the rooting zone ceases when the soil wetness falls below 5%.

When the incoming drainage from the overlying rooting zone  $F_{\text{drain}}$  causes the sub-rooting zone to exceed its maximum capacity ( $W_{\text{SUB,max}}$ ), the excess flows out as sub-rooting zone drainage  $F_{\text{subdrain}}$ :

$$F_{\text{subdrain}} = \max(0, W_{\text{SUB}} + F_{\text{drain}} - (W_{\text{SUB,max}} - W_{\text{max}})) \quad (\text{B.7})$$

where  $W_{\text{SUB,max}}$  is maximum storage capacity of the entire soil column.

The flux term  $F_{\Delta W_{\text{max}}}$  accounts for changes in the depth of the rooting zone  $W_{\text{MAX}}$  (see Eq. A.11) due to the balance between carbon allocation to coarse root growth and the loss of coarse root biomass via turnover.

$$F_{\Delta W_{\text{max}}} = \begin{cases} \Delta W_{\text{max}} \cdot \frac{W_{\text{SUB}}}{W_{\text{SUB,max}} - W_{\text{max}}} & \Delta W_{\text{max}} < 0 \\ \Delta W_{\text{max}} \cdot \frac{W}{W_{\text{max}}} & \Delta W_{\text{max}} > 0 \end{cases} \quad (\text{B.8})$$

Coarse root growth (i.e. an increase in the depth of the rooting zone  $W_{\text{MAX}}$ ) leads to a virtual flow of water from the sub-rooting zone to the rooting zone. Likewise, a decrease in the depth of rooting zone due to coarse root turnover leads to a virtual flow of water from the rooting zone to the sub-rooting zone.

## B.2 Potential evapotranspiration

The fractional snow area  $f_{\text{SNOW}}$  depends on the amount of water in the snow cover  $W_{\text{S}}$ :

$$f_{\text{SNOW}} = \min\left(1, \frac{W_{\text{S}}}{W_{\text{Scrit}}}\right) \quad (\text{B.9})$$

where  $W_{\text{S,crit}}$  is the critical snow depth (water-equivalent). Following Robock (1980), the albedo of snow  $a_{\text{s}}$  depends on air temperature  $T$  and the fractional forest cover  $f_{\text{FOR}}$  (see Eq. A.11).

$$a_{\text{s}} = \begin{cases} 0 & T \geq 0 \\ a_{\text{s,max}} - (a_{\text{s,max}} - a_{\text{s,min}}) \frac{T+10}{10} & -10 < T < 0 \\ 1 & T \leq -10 \end{cases} \quad (\text{B.10})$$

$$a_{\text{s,min}} = 0.3 f_{\text{FOR}} + 0.4 (1 - f_{\text{FOR}})$$

$$a_{\text{s,max}} = 0.4 f_{\text{FOR}} + 0.8 (1 - f_{\text{FOR}})$$

The potential evapotranspiration fluxes for the snow-covered and snow-free fractions are estimated using the Priestley-Taylor equation (Priestley and Taylor 1972) from the net radiation fluxes described below, the slope of the saturation-vapor pressure curve  $\epsilon$  at air temperature  $T$ , the psychrometric constant  $\Gamma$ , the latent heat of vaporization  $\lambda$ , and the Priestley-Taylor coefficient  $\alpha_p$ .

$$D_{\text{s}} = \alpha_p \frac{\epsilon(T)}{\epsilon(T) + \Gamma} \frac{R_{\text{net,s}}}{\lambda}$$

$$D_{\text{ns}} = \alpha_p \frac{\epsilon(T)}{\epsilon(T) + \Gamma} \frac{R_{\text{net,ns}}}{\lambda} \quad (\text{B.11})$$

The net radiative energy available for evaporative processes  $R_{\text{net}}$  is calculated separately for the snow-covered and snow-free fractions from the downward shortwave  $R_{\text{sw}\downarrow}$  and net longwave  $R_{\text{lw}}$  radiation fluxes, daylength  $h$ , and the albedo of the respective fraction ( $a_{\text{s}}$  and  $a_{\text{ns}}$ ).

$$R_{\text{net,s}} = f_{\text{SNOW}} 86400 \left( R_{\text{sw}\downarrow} (1 - a_{\text{s}}) + \frac{h}{86400} R_{\text{lw}} \right)$$

$$R_{\text{net,ns}} = (1 - f_{\text{SNOW}}) 86400 \left( R_{\text{sw}\downarrow} (1 - a_{\text{ns}}) + \frac{h}{86400} R_{\text{lw}} \right) \quad (\text{B.12})$$

Net longwave radiation  $R_{lw}$  is the sum of the downward longwave radiation forcing  $R_{lw\downarrow}$  and upward longwave radiation  $R_{lw\uparrow}$  estimated from the near-surface air temperature in Kelvin ( $T_K = T + 273.16$ ) using the Stefan-Boltzmann equation:

$$R_{lw\uparrow} = \epsilon\sigma T_K^4 \quad (\text{B.13})$$

where  $\epsilon$  is the average emissivity of land surfaces (Brutsaert 1982) and  $\sigma$  is the Stefan-Boltzmann constant.

## B.3 Actual evapotranspiration

### B.3.1 Sublimation from snow cover

Sublimation from snow  $E_{\text{snow}}$  is taken as the minimum of the potential evaporation rate for the snow-covered fraction  $D_s$  and the supply of water in the snow cover  $W_s$ .

$$F_{\text{sublim}} = \min(D_s, W_s) \quad (\text{B.14})$$

### B.3.2 Evaporation from canopy interception reservoir

Similarly, evaporation from the canopy reservoir  $E_{\text{can}}$  is taken as the minimum of the potential evapotranspiration rate for the snow-free fraction and the supply of water in the canopy  $W_L$ .

$$E_{\text{can}} = \min(D_{\text{ns}}, W_L) \quad (\text{B.15})$$

### B.3.3 Bare soil evaporation

Bare soil evaporation  $E_{\text{bare}}$  occurs in the fraction of the snow-free area not covered by vegetation ( $1 - f_{\text{VEG}}$ ) and declines linearly within decreasing soil moisture.

$$E_{\text{bare}} = \min \begin{cases} b (1 - f_{\text{VEG}}) (D_{\text{ns}} - E_{\text{can}}) \\ W \end{cases} \quad (\text{B.16})$$

$$b = \begin{cases} 0.5 \left[ 1 - \cos \left( \pi \frac{W - (W_{\text{max}} - W_{\text{top}})}{W_{\text{top}}} \right) \right] & W \geq W_{\text{max}} - W_{\text{top}} \\ 0 & W < W_{\text{max}} - W_{\text{top}} \end{cases} \quad (\text{B.17})$$

The factor  $b$  limits soil evaporation to the water in the top 50mm of the rooting zone ( $W_{\text{top}}$ ).

### B.3.4 Transpiration

Transpiration  $E_{\text{trans}}$  is reduced by factor  $\alpha_{H_2O}$  from Eq. A.18, which is a saturating function of the available supply for transpiration  $S$  and the the atmospheric demand for transpiration ( $D_{\text{ns}} - E_{\text{can}}$ ).

$$E_{\text{trans}} = \min \begin{cases} \alpha_{H_2O} f_{\text{VEG}} (D_{\text{ns}} - E_{\text{can}}) \\ W - E_{\text{bare}} \end{cases} \quad (\text{B.18})$$

## B.4 Approximation of latent and sensible heat fluxes

The total evapotranspiration flux  $ET$  is calculated as the sum of evaporation from the canopy reservoir and bare soil, sublimation from snow, and transpiration by the vegetation.

$$\begin{aligned} ET &= E_{\text{can}} + E_{\text{bare}} + E_{\text{snow}} + E_{\text{trans}} \\ L &= \lambda ET \\ R_{\text{net}} &= f_{\text{SNOW}} R_{\text{net,s}} + (1 - f_{\text{SNOW}}) R_{\text{net,ns}} \\ H &= R_{\text{net}} - L \end{aligned} \quad (\text{B.19})$$

## APPENDIX B LAND SURFACE MODULE

The latent heat flux  $L$  is estimated by multiplying the evapotranspiration flux by the latent heat of vaporization for water  $\lambda$ . Total net radiation  $R_{\text{net}}$  is computed as the weighted combination of the net radiation over snow-covered and snow-free areas. Sensible heat  $H$  is assumed to make up the difference between the net radiation and latent heat fluxes.

## **Appendix C**

### **Model parameters and variables**

**Table C.1:** State variables and parameters of the plant growth module

Symbol	Description	Value/units
<i>Vegetation carbon pools</i>		
$C_A$	assimilates/storage carbon pool	$\text{gC m}^{-2}$
$C_L$	leaves carbon pool	$\text{gC m}^{-2}$
$C_R$	fine roots carbon pool	$\text{gC m}^{-2}$
$C_{WL}$	woody stem carbon pool	$\text{gC m}^{-2}$
$C_{WR}$	coarse roots carbon pool	$\text{gC m}^{-2}$
$C_S$	reproduction carbon pool	$\text{gC m}^{-2}$
<i>Growing conditions</i>		
$f_{\text{GROW},T}$	time-weighted temperature conditions	$^{\circ}\text{C}$
$f_{\text{GROW},W}$	time-weighted soil moisture conditions	$0 \dots 1$
$f_{\text{GERM},W}$	time-weighted soil moisture conditions for germination	$0 \dots 1$
$f_{\text{GERM}}$	0: no germination, 1: germination	
$f_{\text{GROW}}$	0: no growth, 1: growth	
$\tau_T$	response time to temperature conditions	d
$\tau_W$	response time to moisture conditions	d
<i>Allocation and Germination</i>		
$A_L$	allocation from storage to leaves	$0 \dots 1$
$A_R$	allocation from storage to fine roots	$0 \dots 1$
$A_{WL}$	allocation from storage to stem	$0 \dots 1$
$A_{WR}$	allocation from storage to coarse roots	$0 \dots 1$
$A_S$	allocation from storage to reproduction	$0 \dots 1$
$\gamma_{\text{GERM}}$	germination fraction	$\text{d}^{-1}$
<i>Turnover and Senescence</i>		
$\tau_{\text{tissue}}$	turnover times of vegetation carbon pools	d
$f_{\text{NPP}}$	time-weighted productivity conditions	$\text{gC m}^{-2} \text{d}^{-1}$
$\tau_{\text{NPP}}$	response time to productivity conditions	d
$f_{\text{SEN}}$	0: no senescence, 1: senescence	
<i>Carbon fluxes</i>		
$G_{\text{ERM}}$	germination	$\text{gC m}^{-2} \text{d}^{-1}$
$G_{\text{PP}}$	gross primary productivity	$\text{gC m}^{-2} \text{d}^{-1}$
$RES_a$	autotrophic respiration	$\text{gC m}^{-2} \text{d}^{-1}$
$N_{\text{PP}}$	net primary productivity	$\text{gC m}^{-2} \text{d}^{-1}$

**Table C.2:** Summary of the functional trait (FT) parameters. This table summarizes the parameters in the model description which define a plant growth strategy. Column 2 gives a brief description of the effect of this parameter on the plant behaviour and column 3 gives the equation in which the parameter occurs. All of these parameters range between zero and one.

Parameter	Description	Equation
$t_1$	growth response time to moisture conditions	(A.2)
$t_2$	growth response time to temperature conditions	(A.2)
$t_3$	critical temperature for growth	(A.3)
$t_4$	germination fraction	(A.4)
$t_5$	allocation to reproduction	(A.5)
$t_6$	allocation to aboveground growth	(A.5)
$t_7$	allocation to belowground growth	(A.5)
$t_8$	allocation to storage	(A.5)
$t_9$	relative allocation to aboveground structure	(A.5)
$t_{10}$	relative allocation to belowground structure	(A.5)
$t_{11}$	turnover time of structural pools	(A.6)
$t_{12}$	turnover time of leaf and fine root pools	(A.7)
$t_{13}$	senescence response time to productivity conditions	(A.8)
$t_{14}$	relative senescence aboveground	(A.9)
$t_{15}$	plant nitrogen status	(A.17)

**Table C.3:** Parameters and state variables of the interface between the land-surface module and the plant growth module

Symbol	Description	Value/units
<i>Land-surface parameters needed by land-surface module</i>		
$LAI$	leaf area index, depends on $C_L$	$\text{m}^2 \text{m}^{-2}$
$f_{\text{VEG}}$	fractional vegetation cover	0...1
$f_{\text{FOR}}$	fractional forest cover	0...1
$a_{\text{ns}}$	snow-free surface albedo	0...1
$W_{\text{MAX}}$	maximum plant available soil water storage, depending on $C_{\text{WR}}$	mm
$S$	potential supply rate for transpiration, depending on $C_{\text{R}}$	$\text{mm d}^{-1}$
<i>Conversion parameters</i>		
$SLA$	specific leaf area, depends on $\tau_L$ , converts $C_L$ to $LAI$	$\text{m}^2 \text{gC}^{-1}$
$c_{\text{WLMAX}}$	conversion factor for $C_L$ to $W_{\text{LMAX}}$	$0.2 \text{ mm m}^{-2}$
$c_{\text{FOR}}$	conversion factor for $C_{\text{WL}}$ to $f_{\text{FOR}}$	$0.002 \text{ m}^2 \text{gC}^{-1}$
$a_{\text{VEG}}$	canopy albedo	0...1
$a_{\text{SOIL}}$	bare soil albedo	0.2
$W_{\text{MAX},0}$	minimum value of $W_{\text{MAX}}$	50 mm
$c_{\text{PAW}}$	unit plant available water capacity	$\text{mm H}_2\text{O mm}^{-1} \text{ soil}$
$k$	light extinction coefficient	0.5
$c_{\text{SRL}}$	specific coarse root length, relates $C_{\text{R}}$ to $W_{\text{MAX}}$	$2250 \text{ mm gC}^{-1}$
$c_{\text{SRU}}$	specific root water uptake, relates $C_{\text{R}}$ to $S$	$0.5 \text{ mm gC}^{-1} \text{ d}^{-1}$

**Table C.4:** Variables and parameters used in net primary productivity calculations

Symbol	Description	Value/units
$h$	day length	s
$\theta$	convexity of photosynthesis-radiation curve	0.9
$\phi$	photosynthetic quantum efficiency	2.73 $\mu\text{gC J}^{-1}$
$I_a$	absorbed photosynthetically active radiation	$\text{W m}^{-2}$
$P_{\max}$	light-saturated photosynthetic rate	$\text{gC m}^{-2} \text{s}^{-1}$
$[N_L]$	canopy nitrogen concentration	$\text{gN gC}^{-1}$
$\alpha_T$	temperature limitation on productivity	0...1
$\alpha_{\text{H}_2\text{O}}$	water limitation on productivity	0...1
$c_{\text{RES,tissue}}$	growth respiration coefficient	$\text{gC gC}^{-1}$
$c_{\text{RES,N}}$	maintenance respiration coefficient	$\text{gC gN}^{-1}$
$Q_{10,\text{AR}}$	temperature sensitivity of autotrophic respiration	1.6

**Table C.5:** State variables, fluxes, and parameters of the soil carbon module

Symbol	Description	Value/units
<i>Detritus carbon pools</i>		
$C_{\text{LIT}}$	fine litter carbon pool	$\text{gC m}^{-2}$
$C_{\text{CWD}}$	woody litter carbon pool	$\text{gC m}^{-2}$
$C_{\text{SOIL}}$	soil carbon pool	$\text{gC m}^{-2}$
<i>Carbon fluxes</i>		
$\langle LIT_{\text{tissue}} \rangle$	community-aggregated litter fluxes	$\text{gC m}^{-2} \text{d}^{-1}$
$DEC_x$	decomposition fluxes from the detritus carbon pools	$\text{gC m}^{-2} \text{d}^{-1}$
$\langle GPP \rangle$	community-aggregated gross primary productivity	$\text{gC m}^{-2} \text{d}^{-1}$
$\langle RES_a \rangle$	community-aggregated autotrophic respiration	$\text{gC m}^{-2} \text{d}^{-1}$
$RES_h$	heterotrophic respiration	$\text{gC m}^{-2} \text{d}^{-1}$
$NEE$	net ecosystem exchange	$\text{gC m}^{-2} \text{d}^{-1}$
<i>Parameters</i>		
$c_{\text{lit} \rightarrow \text{atm}}$	fraction of fine litter decomposition to atmosphere	0.77
$c_{\text{cwd} \rightarrow \text{atm}}$	fraction of woody litter decomposition to atmosphere	0.2
$\tau_{\text{LIT}}$	turnover time of fine litter at 20°C	2.05 years
$\tau_{\text{CWD}}$	turnover time of woody litter at 20°C	60 years
$\tau_{\text{SOIL}}$	turnover time of soil carbon at 20°C	100 years
$Q_{10,\text{HR}}$	heterotrophic respiration coefficient	1.4

APPENDIX C MODEL PARAMETERS AND VARIABLES

**Table C.6:** Forcing, state, and flux variables of the land-surface module

Symbol	Description	Value/units
<i>Forcing variables</i>		
$P$	precipitation	mm d <sup>-1</sup>
$R_{\text{sw}\downarrow}$	downwelling shortwave radiation	W m <sup>-2</sup>
$R_{\text{lw}\downarrow}$	downward longwave radiation	W m <sup>-2</sup>
$T$	2m air temperature	°C
<i>Water pools</i>		
$W_{\text{S}}$	water stored in snow cover	mm
$W_{\text{L}}$	water intercepted in canopy	mm
$W$	water stored in rooting zone	mm
$W_{\text{SUB}}$	water stored below rooting zone	mm
<i>Water fluxes</i>		
$P_{\text{snow}}$	snowfall	mm d <sup>-1</sup>
$P_{\text{rain}}$	rainfall	mm d <sup>-1</sup>
$F_{\text{melt}}$	snow melt	mm d <sup>-1</sup>
$F_{\text{thfall}}$	throughfall	mm d <sup>-1</sup>
$F_{\text{runoff}}$	runoff	mm d <sup>-1</sup>
$F_{\text{drain}}$	drainage from rooting zone	mm d <sup>-1</sup>
$F_{\Delta W_{\text{max}}}$	flux due to change in rooting zone depth	mm d <sup>-1</sup>
$F_{\text{subdrain}}$	drainage from sub-rooting zone	mm d <sup>-1</sup>
$E_{\text{bare}}$	bare soil evaporation	mm d <sup>-1</sup>
$E_{\text{can}}$	evaporation from the canopy reservoir	mm d <sup>-1</sup>
$E_{\text{snow}}$	sublimiation from snow cover	mm d <sup>-1</sup>
$E_{\text{trans}}$	transpiration	mm d <sup>-1</sup>

**Table C.7:** Other parameters and variables of the land-surface module

Symbol	Description	Value/units
<i>Drainage parameters</i>		
$d_{\min}$	slow drainage rate	0.24 mm d <sup>-1</sup>
$d_{\max}$	fast drainage rate	2.4 mm d <sup>-1</sup>
$d$	drainage exponent	1.5
$W_{\text{SUBmax}}$	maximum storage capacity of the entire soil column	1500 mm
<i>Snow cover parameters</i>		
$a_{\text{s,min}}$	minimum snow albedo	0.4...0.8
$a_{\text{s,max}}$	maximum snow albedo	0.3...0.4
$a_{\text{s}}$	snow albedo	0.3...0.8
$W_{\text{S,crit}}$	critical snow depth	10 mm
$f_{\text{SNOW}}$	fractional snow area	0...1
<i>Evapotranspiration parameters and variables</i>		
$\epsilon$	average emissivity of land surfaces	0.97
$\sigma$	Stefan-Boltzmann constant	$5.6703 \times 10^{-8}$ W m <sup>-2</sup> K <sup>-4</sup>
$\alpha_p$	Priestly-Taylor coefficient	1.26
$\epsilon(T)$	slope of the saturation-vapour pressure curve	Pa K <sup>-1</sup>
$\Gamma$	psychrometric constant	65 Pa K <sup>-1</sup>
$\lambda$	latent heat of vaporization for water	2500 J kg <sup>-1</sup>
$R_{\text{net,s}}$	net radiation on snow-covered areas	J d <sup>-2</sup>
$R_{\text{net,ns}}$	net radiation on snow-free areas	J d <sup>-2</sup>
$D_{\text{s}}$	potential evapotranspiration from snow-covered areas	mm d <sup>-1</sup>
$D_{\text{ns}}$	potential evapotranspiration from snow-free areas	mm d <sup>-1</sup>
$W_{\text{top}}$	bare soil evaporation depth	50 mm



## Bibliography

- Ackerly, D. and Cornwell, W. K. (2007). A trait-based approach to community assembly: partitioning of species trait values into within- and among-community components. *Ecology Letters*, 10(2):135–145.
- Ainsworth, E. A. and Long, S. P. (2004). What have we learned from 15 years of free-air CO<sub>2</sub> enrichment (FACE)? A meta-analytic review of the responses of photosynthesis, canopy properties and plant production to rising CO<sub>2</sub>. *The New Phytologist*, 165(2):351–372.
- Allan, E., Weisser, W., Weigelt, A., Roscher, C., Fischer, M., and Hillebrand, H. (2011). More diverse plant communities have higher functioning over time due to turnover in complementary dominant species. *Proceedings of the National Academy of Sciences of the United States of America*, 108(41):17034–17039.
- Alton, P. B. (2011). How useful are plant functional types in global simulations of the carbon, water, and energy cycles? *Journal of Geophysical Research*, 116(G01030).
- Alvarado, V. and Bradford, K. (2002). A hydrothermal time model explains the cardinal temperatures for seed germination. *Plant, Cell & Environment*, 25(8):1061–1069.
- Arora, V. and Boer, G. (2006). Simulating competition and coexistence between plant functional types in a dynamic vegetation model. *Earth Interactions*, 10(10):1–30.
- Asner, G. P. and Alencar, A. (2010). Drought impacts on the Amazon forest: the remote sensing perspective. *The New Phytologist*, 187(3):569–578.
- Axelsson, E. and Axelsson, B. (1986). Changes in carbon allocation patterns in spruce and pine trees following irrigation and fertilization. *Tree Physiology*, 2(1-2-3):189–204.
- Baas-Becking, L. (1934). *Geobiologie of inleiding tot de milieukunde*. van Stockum and Zoon, The Hague, Netherlands.

## BIBLIOGRAPHY

- Baker, D., Law, R., Gurney, K., Rayner, P., Peylin, P., Denning, A., Bousquet, P., Bruhwiler, L., Chen, Y., Ciais, P., Fung, I., Heimann, M., John, J., Maki, T., Maksyutov, S., Masarie, K., Prather, M., Pak, B., Taguchi, S., and Zhu, Z. (2006). TransCom 3 inversion intercomparison: Impact of transport model errors on the interannual variability of regional CO<sub>2</sub> fluxes, 1988-2003. *Global Biogeochemical Cycles*, 20(GB1002).
- Balvanera, P., Pfisterer, A. B., Buchmann, N., He, J.-S., Nakashizuka, T., Raffaelli, D., and Schmid, B. (2006). Quantifying the evidence for biodiversity effects on ecosystem functioning and services. *Ecology Letters*, 9(10):1146–1156.
- Beer, C., Reichstein, M., Tomelleri, E., Ciais, P., Jung, M., Carvalhais, N., Rodenbeck, C., Arain, M. A., Baldocchi, D. D., Bonan, G., Bondeau, A., Cescatti, A., Lasslop, G., Lindroth, A., Lomas, M., Luysaert, S., Margolis, H., Oleson, K. W., Rouspard, O., Veenendaal, E., Viovy, N., Williams, C., Woodward, F. I., and Papale, D. (2010). Terrestrial Gross Carbon Dioxide Uptake: Global Distribution and Covariation with Climate. *Science*, 329(5993):834–838.
- Bloom, A. J., Chapin, F. S. I., and Mooney, H. (1985). Resource Limitation in Plants—An Economic Analogy. *Annual Review of Ecology and Systematics*, 16(1):363–392.
- Bohn, K., Dyke, J. G., Pavlick, R., Reineking, B., Reu, B., and Kleidon, A. (2011). The relative importance of seed competition, resource competition and perturbations on community structure. *Biogeosciences*, 8(5):1107–1120.
- Bonan, G. and Levis, S. (2006). Evaluating aspects of the community land and atmosphere models (CLM3 and CAM3) using a dynamic global vegetation model. *Journal of Climate*, 19(11):2290–2301.
- Bonan, G., Levis, S., Kergoat, L., and Oleson, K. W. (2002). Landscapes as patches of plant functional types: An integrating concept for climate and ecosystem models. *Global Biogeochemical Cycles*, 16(2):1–18.
- Box, E. (1996). Plant functional types and climate at the global scale. *Journal of Vegetation Science*, 7(3):309–320.
- Bruggeman, J. and Kooijman, S. A. L. M. (2007). A biodiversity-inspired approach to aquatic ecosystem modeling. *Limnology and Oceanography*, 52(4):1533–1544.
- Brutsaert, W. (1982). *Evaporation into the atmosphere*. theory, history, and applications. Kluwer Academic Publishers, Dordrecht, The Netherlands.

- Cannell, M. G. R. (1982). World forest biomass and primary production data. Academic Press, London, UK.
- Cannell, M. G. R. and Thornley, J. H. M. (1998). Temperature and CO<sub>2</sub> Responses of Leaf and Canopy Photosynthesis: a Clarification using the Non-rectangular Hyperbola Model of Photosynthesis. *Annals of Botany*, 82(6):883–892.
- Cardinale, B. J., Matulich, K. L., Hooper, D. U., Byrnes, J. E., Duffy, E., Gamfeldt, L., Balvanera, P., O'Connor, M. I., and Gonzalez, A. (2011). The functional role of producer diversity in ecosystems. *American Journal of Botany*, 98(3):572–592.
- Cavender-Bares, J., Kozak, K. H., Fine, P. V. A., and Kembel, S. W. (2009). The merging of community ecology and phylogenetic biology. *Ecology Letters*, 12(7):693–715.
- Chapin, F. S. I., BretHarte, M., Hobbie, S., and Zhong, H. (1996). Plant functional types as predictors of transient responses of arctic vegetation to global change. *Journal of Vegetation Science*, 7(3):347–358.
- Chave, J., Coomes, D., Jansen, S., Lewis, S. L., Swenson, N. G., and Zanne, A. E. (2009). Towards a worldwide wood economics spectrum. *Ecology Letters*, 12(4):351–366.
- Cohen, D. (1968). A General Model of Optimal Reproduction in a Randomly Varying Environment. *Journal of Ecology*, 56(1):219–228.
- Cornwell, W. K. and Ackerly, D. (2009). Community assembly and shifts in plant trait distributions across an environmental gradient in coastal California. *Ecological Monographs*, 79(1):109–126.
- Cox, P. (2001). Description of the TRIFFID dynamic global vegetation model. Hadley Centre, Bracknell, UK.
- Cox, P., Betts, R. A., Jones, C. D., Spall, S. A., and Totterdell, I. J. (2000). Acceleration of global warming due to carbon-cycle feedbacks in a coupled climate model. *Nature*, 408(6809):184–187.
- Cramer, W., Bondeau, A., Woodward, F. I., Prentice, I. C., Betts, R. A., Brovkin, V., Cox, P., Fisher, V., Foley, J. A., Friend, A. D., Kucharik, C., Lomas, M. R., Ramankutty, N., Sitch, S., Smith, B., White, A., and Young-Molling, C. (2001). Global response of terrestrial ecosystem structure and function to CO<sub>2</sub> and climate

## BIBLIOGRAPHY

- change: results from six dynamic global vegetation models. *Global Change Biology*, 7(4):357–373.
- Darwin, C. (1987). *Charles Darwin's Natural Selection: Being the Second Part of his Big Species Book Written from 1856 to 1858*. Cambridge University Press.
- Denman, K., Brasseur, G., Chidthaisong, A., Ciais, P., Cox, P., Dickinson, R., Hauglustaine, D., Heinze, C., Holland, E., Jacob, D., Lohmann, U., Ramachandran, S., da Silva Dias, P., Wofsy, S. C., and Zhang, X. (2007). Couplings Between Changes in the Climate System and Biogeochemistry. In Solomon, S., Qin, D., Manning, M., Chen, Z., Marquis, M., Averyt, K., Tignor, M., and Miller, H. L., editors, *Climate Change 2007: The Physical Science Basis. Contribution of Working Group I to the Fourth Assessment Report of the Intergovernmental Panel on Climate Change*. Climate Change 2007: The Physical Science Basis. Contribution of Working Group I to the Fourth Assessment Report of the Intergovernmental Panel on Climate Change, Cambridge, United Kingdom.
- Díaz, S. and Cabido, M. (2001). Vive la différence: plant functional diversity matters to ecosystem processes. *Trends in Ecology & Evolution*, 16(11):646–655.
- Díaz, S., Fargione, J., Chapin, F. S. I., and Tilman, D. (2006). Biodiversity loss threatens human well-being. *Plos Biology*, 4(8):1300–1305.
- Díaz, S., Lavorel, S., de Bello, F., Quetier, F., Grigulis, K., and Robson, T. M. (2007). Incorporating plant functional diversity effects in ecosystem service assessments. *Proceedings of the National Academy of Sciences of the United States of America*, 104(52):20684–20689.
- Doak, D. F., Bigger, D., Harding, E. K., Marvier, M. A., O'Malley, R. E., and Thomson, D. (1998). The Statistical Inevitability of Stability-Diversity Relationships in Community Ecology. <http://dx.doi.org/10.1086/286117>.
- Doney, S., Lindsay, K., Fung, I., and John, J. (2006). Natural Variability in a Stable, 1000-Yr Global Coupled Climate–Carbon Cycle Simulation. *Journal of Climate*, 19(13):3033–3054.
- Drewry, D. T., Kumar, P., Long, S., Bernacchi, C., Liang, X., and Sivapalan, M. (2010). Ecohydrological responses of dense canopies to environmental variability: 1. Interplay between vertical structure and photosynthetic pathway. *Journal of Geophysical Research-Biogeosciences*, 115(G04022).

- Dunne, K. and Willmott, C. (1996). Global Distribution of Plant Extractable Water Capacity of Soil. *International Journal of Climatology*, 16(8):841–859.
- Dutkiewicz, S., Follows, M. J., and Bragg, J. G. (2009). Modeling the coupling of ocean ecology and biogeochemistry. *Global Biogeochemical Cycles*, 23(GB4017).
- Elmqvist, T., Folke, C., Nyström, M., Peterson, G., Bengtsson, J., Walker, B., and Norberg, J. (2003). Response diversity, ecosystem change, and resilience. *Frontiers in Ecology and the Environment*, 1(9):488–494.
- Elser, J. J., Bracken, M. E. S., Cleland, E. E., Gruner, D. S., Harpole, W. S., Hillebrand, H., Ngai, J. T., Seabloom, E. W., Shurin, J. B., and Smith, J. E. (2007). Global analysis of nitrogen and phosphorus limitation of primary producers in freshwater, marine and terrestrial ecosystems. *Ecology Letters*, 10(12):1135–1142.
- Ezoe, H. (1998). Optimal dispersal range and seed size in a stable environment . *Journal of Theoretical Biology*, 190(3):287–293.
- Falge, E., Baldocchi, D. D., Tenhunen, J., Aubinet, M., Bakwin, P., Berbigier, P., Bernhofer, C., Burba, G., Clement, R., Davis, K. J., Elbers, J. A., Goldstein, A. H., Grelle, A., Granier, A., Guomundsson, J., Hollinger, D., Kowalski, A. S., Katul, G., Law, B. E., Malhi, Y., Meyers, T., Monson, R. K., Munger, J. W., Oechel, W., Paw U, K. T., Pilegaard, K., Rannik, Ü., Rebmann, C., Suyker, A., Valentini, R., Wilson, K., and Wofsy, S. (2002). Seasonality of ecosystem respiration and gross primary production as derived from FLUXNET measurements. *Agricultural and Forest Meteorology*, 113(1-4):53–74.
- Falster, D. S., Brännström, Å., Dieckmann, U., and Westoby, M. (2010). Influence of four major plant traits on average height, leaf-area cover, net primary productivity, and biomass density in single-species forests: a theoretical investigation. *Journal of Ecology*, 99(1):148–164.
- Figueira, A. M. e. S., Miller, S. D., de Sousa, C. A. D., Menton, M. C., Maia, A. R., da Rocha, H. R., and Goulden, M. L. (2008). Effects of selective logging on tropical forest tree growth. *Journal of Geophysical Research-Biogeosciences*, 113(G00B05).
- Fisher, J. B., Sitch, S., Malhi, Y., FISHER, R. A., Huntingford, C., and Tan, S. Y. (2010a). Carbon cost of plant nitrogen acquisition: A mechanistic, globally applicable model of plant nitrogen uptake, retranslocation, and fixation. *Global Biogeochemical Cycles*, 24(GB1014).

## BIBLIOGRAPHY

- Fisher, R., McDowell, N., Purves, D., Moorcroft, P., Sitch, S., Cox, P., Huntingford, C., Meir, P., and Woodward, F. I. (2010b). Assessing uncertainties in a second-generation dynamic vegetation model caused by ecological scale limitations. *The New Phytologist*, 187(3):666–681.
- Fisher, R., Williams, M., Lola da Costa, A., Malhi, Y., Lola da Costa, R. F., Almeida, S., and Meir, P. (2007). The response of an Eastern Amazonian rain forest to drought stress: results and modelling analyses from a throughfall exclusion experiment. *Global Change Biology*, 13(11):2361–2378.
- Flombaum, P. and Sala, O. E. (2008). From the Cover: Higher effect of plant species diversity on productivity in natural than artificial ecosystems. *Proceedings of the National Academy of Sciences of the United States of America*, 105(16):6087–6090.
- Foley, J. A., Levis, S., Costa, M., Cramer, W., and Pollard, D. (2000). Incorporating dynamic vegetation cover within global climate models. *Ecological Applications*, 10(6):1620–1632.
- Foley, J. A., Prentice, I. C., Ramankutty, N., Levis, S., Pollard, D., Sitch, S., and Haxeltine, A. (1996). An integrated biosphere model of land surface processes, terrestrial carbon balance, and vegetation dynamics. *Global Biogeochemical Cycles*, 10(4):603–628.
- Follows, M. J. and Dutkiewicz, S. (2011). Modeling Diverse Communities of Marine Microbes. *Annual Review of Marine Science*, 3:427–451.
- Follows, M. J., Dutkiewicz, S., Grant, S., and Chisholm, S. W. (2007). Emergent Biogeography of Microbial Communities in a Model Ocean. *Science*, 315(5820):1843–1846.
- Franklin, O. (2007). Optimal nitrogen allocation controls tree responses to elevated CO<sub>2</sub>. *The New Phytologist*, 174(4):811–822.
- Freschet, G. T., Dias, A. T. C., Ackerly, D., Aerts, R., Van Bodegom, P. M., Cornwell, W. K., Dong, M., Kurokawa, H., Liu, G., Onipchenko, V. G., Ordoñez, J. C., Peltzer, D. A., Richardson, S. J., Shidakov, I. I., Soudzilovskaia, N. A., Tao, J., and Cornelissen, J. H. C. (2011). Global to community scale differences in the prevalence of convergent over divergent leaf trait distributions in plant assemblages. *Global Ecology and Biogeography*, 20(5):755–765.

- Friedlingstein, P., Cox, P., Betts, R. A., Bopp, L., von Bloh, W., Brovkin, V., Cadule, P., Doney, S., Eby, M., Fung, I., Bala, G., John, J., Jones, C., Joos, F., Kato, T., Kawamiya, M., Knorr, W., Lindsay, K., Matthews, H. D., Raddatz, T., Rayner, P., Reick, C., Roeckner, E., Schnitzler, K. G., Schnur, R., Strassmann, K., Weaver, A. J., Yoshikawa, C., and Zeng, N. (2006). Climate–Carbon Cycle Feedback Analysis: Results from the C 4MIP Model Intercomparison. *Journal of Climate*, 19(14):3337–3353.
- Friedlingstein, P., Joel, G., Field, C. B., and Fung, I. Y. (1999). Toward an allocation scheme for global terrestrial carbon models. *Global Change Biology*, 5(7):755–770.
- Friend, A., Stevens, A., Knox, R., and Cannell, M. G. R. (1997). A process-based, terrestrial biosphere model of ecosystem dynamics (Hybrid v3.0). *Ecological Modelling*, 95:249–287.
- Fung, I. Y., Doney, S., Lindsay, K., and John, J. (2005). Evolution of carbon sinks in a changing climate. *Proceedings of the National Academy of Sciences of the United States of America*, 102(32):11201–11206.
- Garnier, E., Cortez, J., Billes, G., Navas, M., Roumet, C., Debussche, M., Laurent, G., Blanchard, A., Aubry, D., Bellmann, A., Neill, C., and Toussaint, J. (2004). Plant functional markers capture ecosystem properties during secondary succession. *Ecology*, 85(9):2630–2637.
- Grime, J. (1998). Benefits of plant diversity to ecosystems: immediate, filter and founder effects. *Journal of Ecology*, 86(6):902–910.
- Groenendijk, M., Dolman, A. J., van der Molen, M. K., Leuning, R., Arneth, A., Delpierre, N., Gash, J. H. C., Lindroth, A., Richardson, A. D., and Verbeeck, H. (2011). Assessing parameter variability in a photosynthesis model within and between plant functional types using global Fluxnet eddy covariance data. *Agricultural and Forest Meteorology*, 151(1):22–38.
- Gu, L., Baldocchi, D., Wofsy, S., Munger, J., Michalsky, J., Urbanski, S., and Boden, T. (2003). Response of a deciduous forest to the Mount Pinatubo eruption: Enhanced photosynthesis. *Science*, 299(5615):2035–2038.
- Gurney, K., Law, R., Denning, A., Rayner, P., Pak, B., Baker, D., Bousquet, P., Bruhwiler, L., Chen, Y., Ciais, P., Fung, I., Heimann, M., John, J., Maki, T., Maksyutov,

## BIBLIOGRAPHY

- S., Peylin, P., Prather, M., and Taguchi, S. (2004). Transcom 3 inversion intercomparison: Model mean results for the estimation of seasonal carbon sources and sinks. *Global Biogeochemical Cycles*, 18(GB1010).
- Haddeland, I., Clark, D. B., Franssen, W., Ludwig, F., Voß, F., Arnell, N. W., Bertrand, N., Best, M., Folwell, S., Gerten, D., Gomes, S., Gosling, S. N., Hagemann, S., Hanasaki, N., Harding, R., Heinke, J., Kabat, P., Koirala, S., Oki, T., Polcher, J., Stacke, T., Viterbo, P., Weedon, G. P., and Yeh, P. (2011). Multimodel Estimate of the Global Terrestrial Water Balance: Setup and First Results. *Journal of Hydrometeorology*, 12(5):869–884.
- Hagemann, S. and Dümenil, L. (1997). A parametrization of the lateral waterflow for the global scale. *Climate Dynamics*, 14(1):17–31.
- Hall, C., Stanford, J., and Hauer, F. (1992). The Distribution and Abundance of Organisms as a Consequence of Energy Balances Along Multiple Environmental Gradients. *Oikos*, 65(3):377–390.
- Harrison, S. P., Prentice, I. C., Barboni, D., Kohfeld, K. E., Ni, J., and Sutra, J.-P. (2010). Ecophysiological and bioclimatic foundations for a global plant functional classification. *Journal of Vegetation Science*, 21(2):300–317.
- Hartmann, D. L. (1994). *Global Physical Climatology*. International Geophysics Series. Academic Press, San Francisco, 1 edition.
- Hector, A., Schmid, B., Beierkuhnlein, C., Caldeira, M., Diemer, M., Dimitrakopoulos, P., Finn, J., Freitas, H., Giller, P., and Good, J. (1999). Plant diversity and productivity experiments in European grasslands. *Science*, 286(5442):1123–1127.
- Heinsch, F., Zhao, M., Running, S. W., Kimball, J. S., Nemani, R. R., Davis, K. J., Bolstad, P. V., Cook, B. D., Desai, A. R., Ricciuto, D. M., LAW, B. E., Oechel, W. C., Kwon, H., Luo, H., Wofsy, S. C., Dunn, A. L., Munger, J. W., Baldocchi, D. D., Xu, L., Hollinger, D. Y., Richardson, A. D., Stoy, P. C., Siqueira, M. B. S., Monson, R. K., Burns, S. P., and Flanagan, L. B. (2006). Evaluation of remote sensing based terrestrial productivity from MODIS using regional tower eddy flux network observations. *Geoscience and Remote Sensing, IEEE Transactions on*, 44(7):1908–1925.
- Hickler, T., Prentice, I. C., Smith, B., Sykes, M. T., and Zaehle, S. (2006). Implementing plant hydraulic architecture within the LPJ Dynamic Global Vegetation Model. *Global Ecology and Biogeography*, 15(6):567–577.

- Hickler, T., Smith, B., Prentice, I. C., Mjöfors, K., Miller, P., Arneth, A., and Sykes, M. T. (2008). CO<sub>2</sub> fertilization in temperate FACE experiments not representative of boreal and tropical forests. *Global Change Biology*, 14(7):1531–1542.
- Hollinger, D. Y., Ollinger, S. V., Richardson, A. D., Meyers, T. P., Dail, D. B., Martin, M. E., Scott, N. A., Arkebauer, T. J., Baldocchi, D. D., Clark, K. L., Curtis, P. S., Davis, K. J., Desai, A. R., Dragoni, D., Goulden, M. L., Gu, L., Katul, G. G., Pallardy, S. G., Paw U, K. T., Schmid, H. P., Stoy, P. C., Sukyer, A. E., and Verma, S. B. (2010). Albedo estimates for land surface models and support for a new paradigm based on foliage nitrogen concentration. *Global Change Biology*, 16(2):696–710.
- Hooper, D., Chapin, F. S. I., Ewel, J., Hector, A., Inchausti, P., Lavorel, S., Lawton, J., Lodge, D., Loreau, M., Naeem, S., Schmid, B., Setälä, H., Symstad, A., Vandermeer, J., and Wardle, D. (2005). Effects of biodiversity on ecosystem functioning: A consensus of current knowledge. *Ecological Monographs*, 75(1):3–35.
- Houghton, R. A., Hall, F., and Goetz, S. J. (2009). Importance of biomass in the global carbon cycle. *Journal of Geophysical Research-Biogeosciences*, 114(G00E03).
- Hubbell, S. P. (1979). Tree dispersion, abundance, and diversity in a tropical dry forest. *Science*, 203(4387):1299–1309.
- Hubbell, S. P. (1997). A unified theory of biogeography and relative species abundance and its application to tropical rain forests and coral reefs. *Coral Reefs*, 16(5):S9–S21.
- Ito, A. (2011). A historical meta-analysis of global terrestrial net primary productivity: are estimates converging? *Global Change Biology*, 17(10):3161–3175.
- Ives, A. R. and Carpenter, S. R. (2007). Stability and Diversity of Ecosystems. *Science*, 317(5834):58–62.
- Jackson, S. and Williams, J. (2004). Modern analogs in Quaternary paleoecology: Here today, gone yesterday, gone tomorrow? *Annual Review of Earth and Planetary Sciences*, 32:495–537.
- Johnson, I. R. and Thornley, J. H. M. (1984). A model of instantaneous and daily canopy photosynthesis. *Journal of Theoretical Biology*, 107(4):531–545.
- Jung, M., Reichstein, M., and Bondeau, A. (2009). Towards global empirical upscaling of FLUXNET eddy covariance observations: validation of a model tree ensemble approach using a biosphere model. *Biogeosciences*, 6(10):2001–2013.

## BIBLIOGRAPHY

- Jung, M., Reichstein, M., Ciais, P., Seneviratne, S. I., Sheffield, J., Goulden, M. L., Bonan, G., Cescatti, A., Chen, J., de Jeu, R., Dolman, A. J., Eugster, W., Gerten, D., Gianelle, D., Gobron, N., Heinke, J., Kimball, J., Law, B. E., Montagnani, L., Mu, Q., Mueller, B., Oleson, K. W., Papale, D., Richardson, A. D., Roupsard, O., Running, S., Tomelleri, E., Viovy, N., Weber, U., Williams, C., Wood, E. F., Zaehle, S., and Zhang, K. (2010). Recent decline in the global land evapotranspiration trend due to limited moisture supply. *Nature*, 467(7318):951–954.
- Kaduk, J. and Heimann, M. (1996). Assessing the climate sensitivity of the global terrestrial carbon cycle model SILVAN. *Physics and Chemistry of The Earth*, 21:529–535.
- Kattge, J., Díaz, S., Lavorel, S., Prentice, I. C., Leadley, P., Bönisch, G., Garnier, E., Westoby, M., Reich, P., Wright, I. J., Cornelissen, J. H. C., Violle, C., Harrison, S., van Bodegom, P., Reichstein, M., Enquist, B., Soudzilovskaia, N., Ackerly, D., Anand, M., Atkin, O., Bahn, M., Baker, T., Baldocchi, D. D., Bekker, R., Blanco, C., Blonder, B., Bond, W., Bradstock, R., Bunker, D., Casanoves, F., Cavender-Bares, J., Chambers, J. Q., Chapin, F. S. I., Chave, J., Coomes, D., Cornwell, W., Craine, J., Dobrin, B., Duarte, L., Durka, W., Elser, J., Esser, G., Estiarte, M., Fagan, W., Fang, J., Fernández-Méndez, F., Fidelis, A., Finegan, B., Flores, O., Ford, H., Frank, D., Freschet, G., Fyllas, N., Gallagher, R., Green, W., Gutierrez, A., Hickler, T., Higgins, S. L., Hodgson, J., Jalili, A., Jansen, S., Joly, C., Kerkhoff, A., Kirkup, D., Kitajima, K., Kleyer, M., Klotz, S., Knops, J., Kramer, K., Kühn, I., Kurokawa, H., Laughlin, D., Lee, T., Leishman, M., Lens, F., Lenz, T., Lewis, S., Lloyd, J., Llusià, J., Louault, F., Ma, S., Mahecha, M., Manning, P., Massad, T., Medlyn, B., Messier, J., Moles, A., Müller, S., Nadrowski, K., Naeem, S., Niinemets, Ü., Nöllert, S., Nüske, A., Ogaya, R., Oleksyn, J., Onipchenko, V., Onoda, Y., Ordoñez, J., Overbeck, G., Ozinga, W., Patiño, S., Paula, S., Pausas, J., Peñuelas, J., Phillips, O., Pillar, V., Poorter, H., Poorter, L., Poschlod, P., Prinzing, A., Proulx, R., Rammig, A., Reinsch, S., Reu, B., Sack, L., Salgado-Negret, B., Sardans, J., Shiodera, S., Shipley, B., Siefert, A., Sosinski, E., Soussana, j.-F., Swaine, E., Swenson, N., Thompson, K., Thornton, P., Waldram, M., Weiher, E., White, M., White, S., Wright, J., Yguel, B., Zaehle, S., Zanne, A., and Wirth, C. (2011). TRY – a global database of plant traits. *Global Change Biology*, 17(9):2905–2935.
- Kattge, J., Knorr, W., Raddatz, T. J., and Wirth, C. (2009). Quantifying photosynthetic capacity and its relationship to leaf nitrogen content for global-scale terrestrial biosphere models. *Global Change Biology*, 15(4):976–991.

- Kazakou, E., Vile, D., Shipley, B., Gallet, C., and Garnier, E. (2006). Co-Variations in Litter Decomposition, Leaf Traits and Plant Growth in Species From a Mediterranean Old-Field Succession. *Functional Ecology*, 20(1):21–30.
- Kleidon, A., Adams, J., Pavlick, R., and Reu, B. (2009). Simulated geographic variations of plant species richness, evenness and abundance using climatic constraints on plant functional diversity. *Environmental Research Letters*, 4(1).
- Kleidon, A., Fraedrich, K., and Low, C. (2007). Multiple steady-states in the terrestrial atmosphere-biosphere system: a result of a discrete vegetation classification? *Biogeosciences*, 4(5):707–714.
- Kleidon, A. and Mooney, H. (2000). A global distribution of biodiversity inferred from climatic constraints: results from a process-based modelling study. *Global Change Biology*, 6(5):507–523.
- Kleinen, T., Brovkin, V., and Schuldt, R. (2012). A dynamic model of wetland extent and peat accumulation: results for the Holocene. *Biogeosciences*, 9:235–248.
- Knorr, W. and Heimann, M. (1995). Impact of Drought Stress and Other Factors on Seasonal Land Biosphere CO<sub>2</sub> Exchange Studied Through an Atmospheric Tracer Transport Model. *Tellus B*, 47(4):471–489.
- Kraft, N. J. B., Comita, L. S., Chase, J. M., Sanders, N. J., Swenson, N. G., Crist, T. O., Stegen, J. C., Vellend, M., Boyle, B., Anderson, M. J., Cornell, H. V., Davies, K. F., Freestone, A. L., Inouye, B. D., Harrison, S. P., and Myers, J. A. (2011). Disentangling the Drivers of Diversity Along Latitudinal and Elevational Gradients. *Science*, 333(6050):1755–1758.
- Kraft, N. J. B., Valencia, R., and Ackerly, D. (2008). Functional Traits and Niche-Based Tree Community Assembly in an Amazonian Forest. *Science*, 322(5901):580–582.
- Kreft, H. and Jetz, W. (2007). Global patterns and determinants of vascular plant diversity. *Proceedings of the National Academy of Sciences of the United States of America*, 104(14):5925–5930.
- Krinner, G., Viovy, N., de Noblet-Ducoudré, N., Ogée, J., Polcher, J., Friedlingstein, P., Ciais, P., Sitch, S., and Prentice, I. C. (2005). A dynamic global vegetation model for studies of the coupled atmosphere-biosphere system. *Global Biogeochemical Cycles*, 19(GB1015).

## BIBLIOGRAPHY

- Laliberté, E. and Legendre, P. (2010). A distance-based framework for measuring functional diversity from multiple traits. *Ecology*, 91(1):299–305.
- Laughlin, D. C., Fulé, P. Z., Huffman, D. W., Crouse, J., and Laliberté, E. (2011). Climatic constraints on trait-based forest assembly. *Journal of Ecology*, 99(6):1489–1499.
- LeBauer, D. S. and Treseder, K. K. (2008). Nitrogen limitation of net primary production in terrestrial ecosystems is globally distributed. *Ecology*, 89(2):371–379.
- Lee, E. (2011). *Impacts of Meteorology-Driven Seed Dispersal on Plant Migration: Implications for Future Vegetation Structure under Changing Climates*. PhD thesis, Massachusetts Institute of Technology, Cambridge, Massachusetts.
- Lee, J.-E., Oliveira, R. S., Dawson, T. E., and Fung, I. (2005). Root functioning modifies seasonal climate. *Proceedings of the National Academy of Sciences of the United States of America*, 102(49):17576–17581.
- Liang, M. and Xie, Z. (2008). Improving the vegetation dynamic simulation in a land surface model by using a statistical-dynamic canopy interception scheme. *Advances in Atmospheric Sciences*, 25(4):610–618.
- Litchman, E., Klausmeier, C. A., Schofield, O. M., and Falkowski, P. G. (2007). The role of functional traits and trade-offs in structuring phytoplankton communities: scaling from cellular to ecosystem level. *Ecology Letters*, 10(12):1170–1181.
- Litton, C. M. and Giardina, C. (2008). Below-ground carbon flux and partitioning: global patterns and response to temperature. *Functional Ecology*, 22(6):941–954.
- Litton, C. M., Raich, J. W., and Ryan, M. G. (2007). Carbon allocation in forest ecosystems. *Global Change Biology*, 13(10):2089–2109.
- Loehle, C. (1998). Height growth rate tradeoffs determine northern and southern range limits for trees. *Journal of Biogeography*, 25(4):735–742.
- Luysaert, S., Inghima, I., Jung, M., Richardson, A. D., Reichsteins, M., Papale, D., Piao, S. L., Schulzes, E. D., Wingate, L., Matteucci, G., Aragao, L., Aubinet, M., Beers, C., Bernhoffer, C., Black, K. G., Bonal, D., Bonnefond, J. M., Chambers, J., Ciais, P., Cook, B., Davis, K. J., Dolman, A. J., Gielen, B., Goulden, M., Grace, J., Granier, A., Grelle, A., Griffis, T., Gruenwald, T., Guidolotti, G., Hanson, P. J., Harding, R., Hollinger, D. Y., Hutrya, L. R., Kolar, P., Kruijt, B., Kutsch, W.,

- Lagergren, F., Laurila, T., LAW, B. E., Le Maire, G., Lindroth, A., Loustau, D., Malhi, Y., Mateus, J., Migliavacca, M., Misson, L., Montagnani, L., Moncrieff, J., Moors, E., Munger, J. W., Nikinmaa, E., Ollinger, S. V., Pita, G., Rebmann, C., Roupsard, O., Saigusa, N., Sanz, M. J., Seufert, G., Sierra, C., Smith, M. L., Tang, J., Valentini, R., Vesala, T., and Janssens, I. A. (2007). CO<sub>2</sub> balance of boreal, temperate, and tropical forests derived from a global database. *Global Change Biology*, 13(12):2509–2537.
- Mahecha, M. D., Reichstein, M., Carvalhais, N., Lasslop, G., Lange, H., Seneviratne, S. I., Vargas, R., Ammann, C., Arain, M. A., Cescatti, A., Janssens, I. A., Migliavacca, M., Montagnani, L., and Richardson, A. D. (2010). Global Convergence in the Temperature Sensitivity of Respiration at Ecosystem Level. *Science*, 329(5993):838–840.
- Malcolm, J., Markham, A., Neilson, R., and Garaci, M. (2002). Estimated migration rates under scenarios of global climate change. *Journal of Biogeography*, 29(7):835–849.
- Malhi, Y., Aragao, L. E. O. C., Metcalfe, D. B., Paiva, R., Quesada, C. A., Almeida, S., Anderson, L., Brando, P., Chambers, J. Q., da Costa, A. C. L., Hutyrá, L. R., Oliveira, P., Patiño, S., Pyle, E. H., Robertson, A. L., and Teixeira, L. M. (2009). Comprehensive assessment of carbon productivity, allocation and storage in three Amazonian forests. *Global Change Biology*, 15(5):1255–1274.
- Malhi, Y., Doughty, C., and Galbraith, D. (2011). The allocation of ecosystem net primary productivity in tropical forests. *Philosophical Transactions of the Royal Society B: Biological Sciences*, 366(1582):3225–3245.
- Marks, C. O. (2007). The Causes of Variation in Tree Seedling Traits: the Roles of Environmental Selection Versus Chance. *Evolution*, 61(2):455–469.
- Marks, C. O. and Lechowicz, M. J. (2006). A holistic tree seedling model for the investigation of functional trait diversity. *Ecological Modelling*, 193(3-4):141–181.
- Masarie, K. A. and Tans, P. P. (1995). Extension and integration of atmospheric carbon dioxide data into a globally consistent measurement record. *Journal of Geophysical Research*, 100(D6):11593–11610.
- McCree, K. (1970). An equation for the rate of respiration of white clover plants grown under controlled conditions. In Setlik, I., editor, *Productivity of Photosynthetic Systems; Models and Methods*, pages 221–229. PUDOC, Wageningen.

## BIBLIOGRAPHY

- McGill, B. J., Enquist, B. J., Weiher, E., and Westoby, M. (2006). Rebuilding community ecology from functional traits. *Trends in Ecology & Evolution*, 21(4):178–185.
- McGill, B. J., Etienne, R. S., Gray, J. S., Alonso, D., Anderson, M. J., Benecha, H. K., Dornelas, M., Enquist, B. J., Green, J. L., He, F., Hurlbert, A. H., Magurran, A. E., Marquet, P. A., Maurer, B. A., Ostling, A., Soykan, C. U., Ugland, K. I., and White, E. P. (2007). Species abundance distributions: moving beyond single prediction theories to integration within an ecological framework. *Ecology Letters*, 10(10):995–1015.
- McKay, M., Conover, W., and Bechman, R. (1979). A Comparison of Three Methods for Selecting Values of Input Variables in the Analysis of Output From a Computer Code. *Technometrics*, 21(2):239–245.
- Medvigy, D., Wofsy, S. C., Munger, J. W., Hollinger, D. Y., and Moorcroft, P. R. (2009). Mechanistic scaling of ecosystem function and dynamics in space and time: Ecosystem Demography model version 2. *Journal of Geophysical Research*, 114(G01002).
- Mercado, L. M., Bellouin, N., Sitch, S., Boucher, O., Huntingford, C., Wild, M., and Cox, P. (2009). Impact of changes in diffuse radiation on the global land carbon sink. *Nature*, 458(7241):1014–1017.
- Millennium Ecosystem Assessment (2005). *Ecosystems and human well-being: Synthesis*. Island Press, Washington, D.C.
- Monsi, M. and Saeki, T. (1953). Uber Den Lichtfaktor in Den Pflanzengesellschaften Und Seine Bedeutung Fuer Die Stoffproduktion. *Japanese Journal of Botany*, 14:22–52.
- Moorcroft, P., Hurtt, G., and Pacala, S. (2001). A method for scaling vegetation dynamics: The ecosystem demography model (ED). *Ecological Monographs*, 71(4):557–585.
- Myneni, R., Hoffman, S., Knyazikhin, Y., Privette, J. L., Glassy, J., Tian, Y., Wang, Y., Song, X., Zhang, Y., Smith, G., Lotsch, A., Friedl, M., Morisette, J., Votava, P., Nemani, R. R., and Running, S. (2002). Global products of vegetation leaf area and fraction absorbed PAR from year one of MODIS data. *Remote Sensing of Environment*, 83:214–231.
- Myneni, R. B., Yang, W., Nemani, R. R., Huete, A. R., Dickinson, R. E., Knyazikhin, Y., Didan, K., Fu, R., Negrón Juárez, R. I., Saatchi, S. S., Hashimoto, H., Ichii, K., Shabanov, N. V., Tan, B., Ratana, P., Privette, J. L., Morisette, J. T., Vermote,

- E. F., Roy, D. P., Wolfe, R. E., Friedl, M. A., Running, S. W., Votava, P., El-Saleous, N., Devadiga, S., Su, Y., and Salomonson, V. V. (2007). Large seasonal swings in leaf area of Amazon rainforests. *Proceedings of the National Academy of Sciences of the United States of America*, 104(12):4820–4823.
- Naeem, S. (1998). Species redundancy and ecosystem reliability. *Conservation Biology*.
- Neilson, R., Pitelka, L., Solomon, A., Nathan, R., Midgley, G., Fragoso, J., Lischke, H., and Thompson, K. (2005). Forecasting regional to global plant migration in response to climate change. *Bioscience*, 55(9):749–759.
- Norby, R., DeLucia, E., Gielen, B., Calfapietra, C., Giardina, C., King, J., Ledford, J., McCarthy, H., Moore, D., and Ceulemans, R. (2005). Forest response to elevated CO<sub>2</sub> is conserved across a broad range of productivity. *Proceedings of the National Academy of Sciences of the United States of America*, 102(50):18052.
- Ollinger, S. V., Richardson, A. D., Martin, M. E., Hollinger, D. Y., Frohling, S. E., Reich, P. B., Plourde, L. C., Katul, G. G., Munger, J. W., Oren, R., Smith, M. L., Paw U, K. T., Bolstad, P. V., Cook, B. D., Day, M. C., Martin, T. A., Monson, R. K., and Schmid, H. P. (2008). Canopy nitrogen, carbon assimilation, and albedo in temperate and boreal forests: Functional relations and potential climate feedbacks. *Proceedings of the National Academy of Sciences of the United States of America*, 105(49):19336–19341.
- Olson, R. J., Scurlock, J. M. O., Prince, S. D., Zheng, D. L., and Johnson, K. R. (2001). NPP Multi-Biome: NPP and Driver Data for Ecosystem Model-Data Intercomparison. Data set. Technical report, Environmental Sciences Division, Oak Ridge National Laboratory, ORNL Distributed Active Archive Center for Biogeochemical Dynamics, Oak Ridge, TN USA.
- O'Malley, M. A. (2007). The nineteenth century roots of 'everything is everywhere'. *Nature Reviews Microbiology*, 5(8):647–651.
- Page, S. E., Siegert, F., Rieley, J. O., Boehm, H.-D. V., Jaya, A., and Limin, S. (2002). The amount of carbon released from peat and forest fires in Indonesia during 1997. *Nature*, 420(6911):61–65.
- Peterson, G., Allen, C. R., and Holling, C. S. (1998). Ecological Resilience, Biodiversity, and Scale. *Ecosystems*, 1(1):6–18.
- Pielou, E. C. (1966). The measurement of diversity in different types of biological collections. *Journal of Theoretical Biology*, 13:131–144.

## BIBLIOGRAPHY

- Potter, C., Randerson, J., Field, C., Matson, P., Vitousek, P., Mooney, H., and Klooster, S. (1993). Terrestrial Ecosystem Production - a Process Model-Based on Global Satellite and Surface Data. *Global Biogeochemical Cycles*, 7(4):811–841.
- Prentice, I. C., Bondeau, A., Cramer, W., Harrison, S. P., Hickler, T., Lucht, W., Sitch, S., Smith, B., and Sykes, M. T. (2007). Dynamic Global Vegetation Modeling: Quantifying Terrestrial Ecosystem Responses to Large-Scale Environmental Change. In Canadell, J. G., Pataki, D. E., and Pitelka, L. F., editors, *Terrestrial Ecosystems in a Changing World*, pages 175–192. Springer Berlin Heidelberg, Berlin, Heidelberg.
- Priestley, C. and Taylor, R. (1972). On the assessment of Surface Heat-Flux and Evaporation Using Large-Scale Parameters. *Monthly Weather Review*, 100(2):81–89.
- Prieto, I., Armas, C., and Pugnaire, F. I. (2012). Water release through plant roots: new insights into its consequences at the plant and ecosystem level. *The New Phytologist*, 193(4):830–841.
- Proulx, R., Wirth, C., Voigt, W., Weigelt, A., Roscher, C., Attinger, S., Baade, J., Barnard, R. L., Buchmann, N., Buscot, F., Eisenhauer, N., Fischer, M., Gleixner, G., Halle, S., Hildebrandt, A., Kowalski, E., Kuu, A., Lange, M., Milcu, A., Niklaus, P. A., Oelmann, Y., Rosenkranz, S., Sabais, A., Scherber, C., Scherer-Lorenzen, M., Scheu, S., Schulze, E.-D., Schumacher, J., Schwichtenberg, G., Soussana, j.-F., Temperton, V. M., Weisser, W. W., Wilcke, W., and Schmid, B. (2010). Diversity Promotes Temporal Stability across Levels of Ecosystem Organization in Experimental Grasslands. *PLoS ONE*, 5(10).
- Purves, D. and Pacala, S. (2008). Predictive models of forest dynamics. *Science*, 320(5882):1452–1453.
- Qian, T., Dai, A., Trenberth, K. E., and Oleson, K. W. (2006). Simulation of global land surface conditions from 1948 to 2004. Part I: Forcing data and evaluations. *Journal of Hydrometeorology*, 7(5):953–975.
- Quesada, C. A., Lloyd, J., Anderson, L. O., Fyllas, N. M., Schwarz, M., and Czimczik, C. I. (2009). Soils of amazonia with particular reference to the rainfor sites. *Biogeosciences Discussions*, 6(2):3851–3921.
- Quetier, F., Thebault, A., and Lavorel, S. (2007). Plant traits in a state and transition framework as markers of ecosystem response to land-use change. *Ecological Monographs*, 77(1):33–52.

- Quillet, A., Peng, C., and Garneau, M. (2010). Toward dynamic global vegetation models for simulating vegetation-climate interactions and feedbacks: recent developments, limitations, and future challenges. *Environmental Reviews*, 18:333–353.
- Raddatz, T. J., Reick, C. H., Knorr, W., Kattge, J., Roeckner, E., Schnur, R., Schnitzler, K. G., Wetzell, P., and Jungclaus, J. (2007). Will the tropical land biosphere dominate the climate-carbon cycle feedback during the twenty-first century? *Climate Dynamics*, 29(6):565–574.
- Randerson, J. T., Hoffman, F. M., Thornton, P. E., Mahowald, N. M., Lindsay, K., Lee, Y.-H., Nevison, C. D., Doney, S., Bonan, G., Stoeckli, R., Covey, C., Running, S. W., and Fung, I. Y. (2009). Systematic assessment of terrestrial biogeochemistry in coupled climate-carbon models. *Global Change Biology*, 15(10):2462–2484.
- Reich, P. B., Hobbie, S. E., Lee, T., Ellsworth, D. S., West, J. B., Tilman, D., Knops, J. M. H., Naeem, S., and Trost, J. (2006). Nitrogen limitation constrains sustainability of ecosystem response to CO<sub>2</sub>. *Nature*, 440(7086):922–925.
- Reich, P. B., Walters, M., Ellsworth, D., Vose, J., Volin, J., Gresham, C., and Bowman, W. (1998). Relationships of leaf dark respiration to leaf nitrogen, specific leaf area and leaf life-span: a test across biomes and functional groups. *Oecologia*, 114(4):471–482.
- Reich, P. B., Walters, M. B., and Ellsworth, D. S. (1997). From tropics to tundra: global convergence in plant functioning. *Proceedings of the National Academy of Sciences of the United States of America*, 94(25):13730–13734.
- Reich, P. B., Wright, I. J., and Lusk, C. H. (2007). Predicting leaf physiology from simple plant and climate attributes: a global GLOPNET analysis. *Ecological Applications*, 17(7):1982–1988.
- Reu, B., Proulx, R., Bohn, K., Dyke, J. G., Kleidon, A., Pavlick, R., and Schmidlein, S. (2010). The role of climate and plant functional trade-offs in shaping global biome and biodiversity patterns. *Global Ecology and Biogeography*, 20:570–581.
- Reu, B., Zaehle, S., Proulx, R., Bohn, K., Kleidon, A., Pavlick, R., and Schmidlein, S. (2011). The role of plant functional trade-offs for biodiversity changes and biome shifts under scenarios of global climatic change. *Biogeosciences*, 8:1255–1266.
- Robock, A. (1980). The Seasonal Cycle of Snow Cover, Sea Ice and Surface Albedo. *Monthly Weather Review*, 108(3):267–285.

## BIBLIOGRAPHY

- Roeckner, E., Arpe, K., Bengtsson, L., Christoph, M., Claussen, M., Dümenil, L., Esch, M., Giorgetta, M., Schlese, U., and Schulzweida, U. (1996). The atmospheric general circulation model ECHAM-4: Model description and simulation of present-day climate. Max Planck Institute for Meteorology, Hamburg, Germany.
- Ryan, M. (1991). A Simple Method for Estimating Gross Carbon Budgets for Vegetation in Forest Ecosystems. *Tree Physiology*, 9:255–266.
- Ryu, Y., Baldocchi, D. D., Kobayashi, H., van Ingen, C., Li, J., Black, T. A., Beringer, J., van Gorsel, E., Knohl, A., Law, B. E., and Rouspard, O. (2011). Integration of MODIS land and atmosphere products with a coupled-process model to estimate gross primary productivity and evapotranspiration from 1 km to global scales. *Global Biogeochemical Cycles*, 25(GB4017).
- Saatchi, S. S., Houghton, R. A., Alvala, R. C. D. S., Soares, J. V., and Yu, Y. (2007). Distribution of aboveground live biomass in the Amazon basin. *Global Change Biology*, 13(4):816–837.
- Samanta, A., Ganguly, S., Hashimoto, H., Devadiga, S., Vermote, E., Knyazikhin, Y., Nemani, R. R., and Myneni, R. B. (2010). Amazon forests did not green-up during the 2005 drought. *Geophysical Research Letters*, 37(L05401).
- Scheiter, S. and Higgins, S. L. (2009). Impacts of climate change on the vegetation of Africa: an adaptive dynamic vegetation modelling approach. *Global Change Biology*, 15(9):2224–2246.
- Shinozaki, K., Yoda, K., Hozumi, K., and Kira, T. (1964). A Quantitative Analysis of Plant Form-The Pipe Model Theory, 1. Basic Analysis. *Japanese Journal of Ecology*, 14(3):97–105.
- Shipley, B., Lechowicz, M., Wright, I. J., and Reich, P. B. (2006a). Fundamental trade-offs generating the worldwide leaf economics spectrum. *Ecology*, 87(3):535–541.
- Shipley, B., Vile, D., and Garnier, E. (2006b). From Plant Traits to Plant Communities: A Statistical Mechanistic Approach to Biodiversity. *Science*, 314(5800):812–814.
- Sitch, S., Huntingford, C., Gedney, N., Levy, P. E., Lomas, M., Piao, S. L., Betts, R. A., Ciais, P., Cox, P., Friedlingstein, P., Jones, C. D., Prentice, I. C., and Woodward, F. I. (2008). Evaluation of the terrestrial carbon cycle, future plant geography and climate-carbon cycle feedbacks using five Dynamic Global Vegetation Models (DGVMs). *Global Change Biology*, 14(9):2015–2039.

- Sitch, S., Smith, B., Prentice, I. C., Arneeth, A., Bondeau, A., Cramer, W., Kaplan, J. O., Levis, S., Lucht, W., Sykes, M. T., Thonicke, K., and Venevsky, S. (2003). Evaluation of ecosystem dynamics, plant geography and terrestrial carbon cycling in the LPJ dynamic global vegetation model. *Global Change Biology*, 9(2):161–185.
- Smith, T. and Huston, M. (1989). A theory of the spatial and temporal dynamics of plant communities. *Plant Ecology*, 83(1-2):49–69.
- Sonnier, G., Shipley, B., and Navas, M.-L. (2010). Plant traits, species pools and the prediction of relative abundance in plant communities: a maximum entropy approach. *Journal of Vegetation Science*, 21(2):318–331.
- Stöckli, R., Lawrence, D. M., Niu, G.-Y., Oleson, K. W., Thornton, P. E., Yang, Z.-L., Bonan, G., Denning, A. S., and Running, S. W. (2008). Use of FLUXNET in the Community Land Model development. *Journal of Geophysical Research*, 113(G01025).
- Swenson, N. G. and Weiser, M. (2010). Plant geography upon the basis of functional traits: an example from eastern North American trees. *Ecology*, 91(8):2234–2241.
- Taylor, K. (2001). Summarizing multiple aspects of model performance in a single diagram. *Journal of Geophysical Research-Atmospheres*, 106(D7):7183–7192.
- Thonicke, K., Venevsky, S., Sitch, S., and Cramer, W. (2008). The role of fire disturbance for global vegetation dynamics: coupling fire into a Dynamic Global Vegetation Model. *Global Ecology and Biogeography*, 10(6):661–677.
- Thornley, J. H. M. (1970). Respiration, Growth and Maintenance in Plants. *Nature*, 227(5255):304–305.
- Thornton, P. E., Lamarque, J.-F., Rosenbloom, N. A., and Mahowald, N. M. (2007). Influence of carbon-nitrogen cycle coupling on land model response to CO<sub>2</sub> fertilization and climate variability. *Global Biogeochemical Cycles*, 21(GB4018).
- Thum, T., Räisänen, P., Sevanto, S., Tuomi, M., Reick, C., Vesala, T., Raddatz, T., Aalto, T., Järvinen, H., Altimir, N., Pilegaard, K., Nagy, Z., Rambal, S., and Liski, J. (2011). Soil carbon model alternatives for ECHAM5/JSBACH climate model: Evaluation and impacts on global carbon cycle estimates. *Journal of Geophysical Research*, 116(G02028).

## BIBLIOGRAPHY

- Tilman, D., Lehman, C. L., and Bristow, C. E. (1998). Diversity-stability relationships: statistical inevitability or ecological consequence? *American Naturalist*, 151(3):277–282.
- Tilman, D., Reich, P. B., and Knops, J. M. H. (2006). Biodiversity and ecosystem stability in a decade-long grassland experiment. *Nature*, 441(7093):629–632.
- Van Bodegom, P. M., Douma, J. C., Witte, J. P. M., Ordoñez, J. C., Bartholomeus, R. P., and Aerts, R. (2011). Going beyond limitations of plant functional types when predicting global ecosystem-atmosphere fluxes: exploring the merits of traits-based approaches. *Global Ecology and Biogeography*.
- van der Werf, G. R., Dempewolf, J., Trigg, S. N., Randerson, J. T., Kasibhatla, P. S., Giglio, L., Murdiyarso, D., Peters, W., Morton, D. C., Collatz, G. J., Dolman, A. J., and DeFries, R. S. (2008). Climate regulation of fire emissions and deforestation in equatorial Asia. *Proceedings of the National Academy of Sciences of the United States of America*, 105(51):20350–20355.
- van der Werf, G. R., Randerson, J. T., Giglio, L., Collatz, G. J., Kasibhatla, P. S., and Arellano Jr., A. F. (2006). Interannual variability in global biomass burning emissions from 1997 to 2004. *Atmospheric Chemistry and Physics*, 6(11):3423–3441.
- Vieira, S., de Camargo, P. B., Selhorst, D., da Silva, R., Hutyra, L., Chambers, J. Q., Brown, I. F., Higuchi, N., dos Santos, J., Wofsy, S. C., Trumbore, S. E., and Martinelli, L. A. (2004). Forest structure and carbon dynamics in Amazonian tropical rain forests. *Oecologia*, 140(3):468–479.
- Vile, D., Shipley, B., and Garnier, E. (2006). Ecosystem productivity can be predicted from potential relative growth rate and species abundance. *Ecology Letters*, 9(9):1061–1067.
- Wang, A. and Price, D. T. (2007). Estimating global distribution of boreal, temperate, and tropical tree plant functional types using clustering techniques. *Journal of Geophysical Research*, 112(G01024).
- Webb, C. T., Hoeting, J. A., Ames, G. M., Pyne, M. I., and LeRoy Poff, N. (2010). A structured and dynamic framework to advance traits-based theory and prediction in ecology. *Ecology Letters*, 13(3):267–283.
- Westoby, M., Falster, D., Moles, A., Vesk, P., and Wright, I. J. (2002). Plant ecological strategies: Some leading dimensions of variation between species. *Annual Review of Ecology and Systematics*, 33:125–159.

- Westoby, M. and Wright, I. J. (2006). Land-plant ecology on the basis of functional traits. *Trends in Ecology & Evolution*, 21(5):261–268.
- Wigmosta, M., Vail, L., and Lettenmaier, D. (1994). A Distributed Hydrology-Vegetation Model for Complex Terrain. *Water Resources Research*, 30(6):1665–1679.
- Williams, J. W. and Jackson, S. T. (2007). Novel climates, no-analog communities, and ecological surprises. *Frontiers in Ecology and the Environment*, 5(9):475–482.
- Wolf, A., Field, C. B., and Berry, J. A. (2011). Allometric growth and allocation in forests: a perspective from FLUXNET. *Ecological Applications*, 21(5):1546–1556.
- Woodward, F. I., Lomas, M. R., Betts, R. A., Wagner, A., Mulligan, M., and Hewitt, C. N. (1998). Vegetation-Climate Feedbacks in a Greenhouse World. *Philosophical Transactions: Biological Sciences*, 353(1365):29–39.
- Wright, I. J., Reich, P. B., Cornelissen, J. H. C., Falster, D. S., Garnier, E., Hikosaka, K., Lamont, B. B., Lee, W., Oleksyn, J., Osada, N., Poorter, H., Villar, R., Warton, D. I., and Westoby, M. (2005). Assessing the generality of global leaf trait relationships. *The New Phytologist*, 166(2):485–496.
- Yachi, S. (1999). Biodiversity and ecosystem productivity in a fluctuating environment: The insurance hypothesis. *Proceedings of the National Academy of Sciences of the United States of America*, 96(4):1463–1468.
- Zaehle, S. and Friend, A. D. (2010). Carbon and nitrogen cycle dynamics in the O-CN land surface model: 1. Model description, site-scale evaluation, and sensitivity to parameter estimates. *Global Biogeochemical Cycles*, 24(GB1005).
- Zaehle, S., Friend, A. D., Friedlingstein, P., Dentener, F., Peylin, P., and Schulz, M. (2010). Carbon and nitrogen cycle dynamics in the O-CN land surface model: 2. Role of the nitrogen cycle in the historical terrestrial carbon balance. *Global Biogeochemical Cycles*, 24(GB1006).
- Zhao, M., Heinsch, F. A., Nemani, R. R., and Running, S. W. (2005). Improvements of the MODIS terrestrial gross and net primary production global data set. *Remote Sensing of Environment*, 95(2):164–176.
- Zhao, M., Running, S. W., and Nemani, R. R. (2006). Sensitivity of Moderate Resolution Imaging Spectroradiometer (MODIS) terrestrial primary production to the accuracy of meteorological reanalyses. *Journal of Geophysical Research-Biogeosciences*, 111(G01002).



## Acknowledgments

It is hard to believe that it has been almost 10 years, since I was sitting in the back row of Dr. Axel Kleidon's GEOG345 Introduction to Climatology course. I got a B in that class. Probably because I nodded off one too many times, no fault of the teacher, only my notoriously poor sleep habits. Something drew me back in though and I was back for more with GEOG445 Advanced Climatology . Then, it was Climate Modeling and Analysis. Then, a disasterous Undergraduate Research Project. That was my first real battle with debugging Fortran code. Fortran won that round and I never did finish quantifying atmospheric entropy production on Mars.

Nearing graduation day, Axel offered me a graduate research assistantship. I had just received another job offer doing GIS programming and the pay was much better than grad student money. But, I was hooked on this science stuff and I quickly decided money wasn't everything and told Axel I was in. Only a week or so after I started though, Axel and I went to lunch and he told me he was moving to Germany at the end of the school year to start a research group there. I wondered if I had made a mistake. It all worked out well though. And, I ended up visiting Jena the next summer to finish up my Masters thesis work, and Axel offered me a PhD position. I had to think a bit longer about that one.

I made the right choice though and it has been a great time. I'm still hooked on this science stuff. I've developed a cool model and have a dozen ideas for what to do next with it. I've co-supervised my own Masters student and seen things from the other side. I've fought many bloody battles with Fortran and won them all, eventually. I've met good friends and I married my incredible wife. I wonder what that sleepy kid in the back row of GEOG345 would think if you told him all that.

And now, I'm finally here, at the end of it all. I've made it to the top of this mountain, but I wouldn't be here without an excellent guide. You have always been supportive and inspiring. Thanks Axel.

I would also like to thank the other members of my advisory panel, Prof. Dr. Martin Claussen, Prof. Dr. Martin Heimann, and Dr. Christian Reick for their time and

## ACKNOWLEDGMENTS

guidance throughout my PhD process.

May the Force be with my fellow “Jedis”, Dr. Björn Reu and Kristin Bohn, who were there from the beginning when JeDi was just an idea sketched out on a piece of A4 during a train ride to and from Hamburg. I am particularly indebted to Dr. Darren Drewry, another “Jedi” who came along a little later, for his extensive support while writing and his patient and thorough editing.

I’m thankful to all of the members of the Biospheric Theory and Modelling Group for their constructive comments, encouraging support, and just for being cool, interesting people. Our joint seminars with the former Organismal Biogeochemistry group at the MPI-BGC and our occasional meetings with the Land Department at the MPI-M were always fruitful. I received helpful feedback and suggestions from many other colleagues as well, too many to list here without leaving someone out, but know that I’ve appreciated every day, every conversation, every coding tip, suggestion, pat on the back and open ear, every constructive criticism, many of the distractions, and even every nagging reminder of “When do you finish?”.

The countless simulations that went in to developing and debugging JeDi-DGVM would not have been possible without Dr. Peer-Joachim Koch and the rest of MPI-BGC IT department working their magic to keep the computing cluster up and running. Steffen Richter and Kerstin Sickel were also invaluable in maintaining the JeDi model code. Birgitta Wiehl, our department secretary, was incredibly helpful throughout my PhD time but most especially in those first few months in Jena, when everything seemed new, different, and bewildering.

Another big thank you goes to Dr. Antje Weitz and Cornelia Kampmann from the IMPRS-ESM office for their administrative support throughout my PhD. I also sincerely appreciate their efforts and those of so many affiliated with the school for always managing to make the ‘Jena’ students (as well as our compatriots from PIK and Kassel) feel welcome and integrated in the school. Participating in the IMPRS-ESM has been a great privilege. While the official retreat programs made for interesting albeit long days, and the knowledge gained from my coursework has proven quite useful, it was the sum of all the informal moments of getting to know and sharing ideas with the faculty, visitors, and other students that will leave the longest impression.

I’m also thankful to the Max Planck Society (and thus, ultimately, the German taxpayers) for making this PhD project possible through their financial support of the Max Planck Research Group for Biospheric Theory and Modelling.

I'm very grateful for my family back in the US, especially my parents and grandparents. You made this PhD possible. You helped shape me in to the person I am and have always encouraged me in all my pursuits, even when they took me far away to do something as crazy as a PhD.

Finally, but most importantly, I dedicate this thesis to my wife, Damiana. Words will never express my gratitude for your unceasing support and your immeasurable patience. I would not have finished this long project without you.



## **Eidesstattliche Erklärung**

Hiermit versichere ich, dass ich diese Arbeit selbständig verfasst habe und keine anderen als die angegebenen Quellen und Hilfsmittel benutzt habe.

Ryan Pavlick

